ANTI-TUMOR ACTIVITIES OF *AURICULARIA POLYTRICHA* EXTRACTS IN
HEPATOCELLULAR CARCINOMA CELL LINE (HEPG2) AND BREAST CANCER CELL
LINES (MCF-7 AND MDA-MB-231)

Miss Sunita Nilkhet

จุฬาลงกรณ์มหาวิทยาลัย
CHULALONGKORN UNIVERSITY

A Thesis Submitted in Partial Fulfillment of the Requirements

for the Degree of Master of Science in Clinical Biochemistry and Molecular Medicine

Department of Clinical Chemistry

Faculty of Allied Health Sciences

Chulalongkorn University

Academic Year 2019

ฤทธิ์ต้านมะเร็งของสารสกัดเห็ดหูหนูช้างในเซลล์มะเร็งตับเพาะเลี้ยง (HEPG2) และเซลล์มะเร็ง
เต้านมเพาะเลี้ยง (MCF-7 และ MDA-MB-231)

น.ส.สุนิตา นิลเขตร์

วิทยานิพนธ์นี้เป็นส่วนหนึ่งของการศึกษาตามหลักสูตรปริญญาวิทยาศาสตรมหาบัณฑิต
สาขาวิชาชีวเคมีคลินิกและอณูทางการแพทย์ ภาควิชาเคมีคลินิก
คณะสหเวชศาสตร์ จุฬาลงกรณ์มหาวิทยาลัย
ปีการศึกษา 2562

Thesis Title	ANTI-TUMOR ACTIVITIES OF *AURICULARIA POLYTRICHA* EXTRACTS IN HEPATOCELLULAR CARCINOMA CELL LINE (HEPG2) AND BREAST CANCER CELL LINES (MCF-7 AND MDA-MB-231)
By	Miss Sunita Nilkhet
Field of Study	Clinical Biochemistry and Molecular Medicine
Thesis Advisor	Assistant Professor SIRIPORN CHUCHAWANKUL, Ph.D.
Thesis Co Advisor	Associate Professor Alison T Ung, Ph.D.

Accepted by the Faculty of Allied Health Sciences, Chulalongkorn University in Partial Fulfillment of the Requirement for the Master of Science

-- Dean of the Faculty of Allied Health Sciences

(Associate Professor PALANEE AMMARANOND, Ph.D.)

THESIS COMMITTEE

-- Chairman

(Assistant Professor TEWIN TENCOMNAO, Ph.D.)

-- Thesis Advisor

(Assistant Professor SIRIPORN CHUCHAWANKUL, Ph.D.)

-- Thesis Co-Advisor

(Associate Professor Alison T Ung, Ph.D.)

-- Examiner

(Assistant Professor TEWARIT SARACHANA, Ph.D.)

-- External Examiner

(Warunya Arunotayanun, Ph.D.)

สุนิตา นิลเขตร์ : ฤทธิ์ต้านมะเร็งของสารสกัดเห็ดหูหนูช้างในเซลล์มะเร็งตับเพาะเลี้ยง (HEPG2) และเซลล์มะเร็งเต้านมเพาะเลี้ยง (MCF-7 และ MDA-MB-231). (ANTI-TUMOR ACTIVITIES OF *AURICULARIA POLYTRICHA* EXTRACTS IN HEPATOCELLULAR CARCINOMA CELL LINE (HEPG2) AND BREAST CANCER CELL LINES (MCF-7 AND MDA-MB-231)) อ.ที่ปรึกษาหลัก : ผศ. ดร.ศิริพร ชื้อชวาลกุล, อ.ที่ปรึกษาร่วม : รศ. ดร.Alison T Ung

มะเร็งเป็นโรคที่มีอัตราการเกิดสูงในแต่ละปี แม้ว่าในปัจจุบันมีการพัฒนายาและวิธีการรักษาที่หลากหลาย แต่ผลข้างเคียงจากการใช้ยาต้านมะเร็งในผู้ป่วยทำให้การศึกษาสารออกฤทธิ์ที่ให้ผลข้างเคียงน้อยยังเป็นที่ต้องการในปัจจุบัน งานวิจัยชิ้นนี้ต้องการศึกษาฤทธิ์ของเห็ดหูหนูช้าง (*Auricularia polytricha*) และสารประกอบออกฤทธิ์ของเห็ดหูหนูช้างต่อเซลล์มะเร็งเพาะเลี้ยงของมนุษย์ ได้แก่ มะเร็งตับชนิด HepG2 มะเร็งเต้านมชนิด MCF-7 และ MDA-MB-231 ผู้วิจัยได้ทำการสกัดสารจากเห็ดด้วยเอทานอลด้วยวิธี Sohxlet (APE) และสกัดสารด้วยเฮกเซนด้วยวิธี Maceration (APH) จากการศึกษาสารประกอบโดยวิธี GC-MS พบว่าใน APH มี Ergosterol มากกว่าใน APE ถึงสองเท่า การแยกสารสกัด APH โดยวิธี PREP-LC และ TLC ได้ส่วนประกอบทั้งหมด 4 fraction ได้แก่ F1 F2 F3 และ Ergosterol และเมื่อวิเคราะห์คุณลักษณะของ Ergosterol จาก APH และสารมาตรฐาน Ergosterol โดยวิธี HLPC ได้ผลว่า Ergosterol จากทั้งสองแหล่งมีคุณลักษณะเดียวกัน ในการทดสอบฤทธิ์ต่อการรอดชีวิตของเซลล์มะเร็งด้วย APE APH และ Doxorubicin ซึ่งเป็นยาต้านมะเร็ง โดยการตรวจวัดด้วย MTT ใน HepG2 MCF-7 และ MDA-MB-231 ที่เวลา 24 ชั่วโมง พบว่า APH ยับยั้งการรอดชีวิตของเซลล์มะเร็งได้มากกว่า APE โดยมีค่า IC_{50} ที่ 0.06 ± 0.02 0.06 ± 0.02 และ 0.06 ± 0.01 mg/ml ตามลำดับ และ Ergosterol ยับยั้งการรอดชีวิตของเซลล์มะเร็งได้ดีที่สุดในบรรดา 4 fraction ที่แยกได้จาก APH นอกจากนี้ผู้วิจัยได้ทดสอบการออกฤทธิ์ของสารผ่านกลไกต่างๆ ของเซลล์มะเร็ง ได้แก่ Apoptosis Cell cycle Migration และ Invasion assay พบว่า APH 50 µg/ml และ Ergosterol 25 µM กระตุ้นการเกิด Apoptosis ยับยั้ง Migration และ Invasion ได้ ในขณะที่ APH และ Erogsterol ไม่ยับยั้ง Cell cycle จากการศึกษาทาง Molecular docking ระหว่างสาร Ergosterol และเอนไซม์ gelatinase A (MMP-2) ซึ่งเป็นเอนไซม์ที่เกี่ยวข้องกับการรุกรานของเซลล์มะเร็ง พบว่าให้ผลการจับเอนไซม์ที่ -32.7324 kcal/mol โดยมีการจับที่ Active site ของ MMP-2 สรุปได้ว่า APH และ Ergosterol มีฤทธิ์ยับยั้งมะเร็ง และสามารถนำไปสู่การพัฒนายาต้านมะเร็งจากสารสกัดเห็ดหูหนูช้างและ Ergosterol ต่อไป

สาขาวิชา	ชีวเคมีคลินิกและอณูทางการแพทย์	ลายมือชื่อนิสิต ....
ปีการศึกษา	2562	ลายมือชื่อ อ.ที่ปรึกษาหลัก ....
		ลายมือชื่อ อ.ที่ปรึกษาร่วม ....

5976674837 : MAJOR CLINICAL BIOCHEMISTRY AND MOLECULAR MEDICINE

KEYWORD: Auricularia polytricha, Antitumor activity, Apoptosis

Sunita Nilkhet : ANTI-TUMOR ACTIVITIES OF *AURICULARIA POLYTRICHA* EXTRACTS IN HEPATOCELLULAR CARCINOMA CELL LINE (HEPG2) AND BREAST CANCER CELL LINES (MCF-7 AND MDA-MB-231). Advisor: Asst. Prof. SIRIPORN CHUCHAWANKUL, Ph.D. Co-advisor: Assoc. Prof. Alison T Ung, Ph.D.

Cancer is the disease that happens to occur in a high number of new cases each year. Even the choice of treatment is developing, but the adverse effects on cancer therapeutic drugs still challenging. To investigate the antitumor activities of *Auricularia polytricha* (AP) mushroom extract and active compounds, human cancer cell lines such as Hepatocellcular (HepG2) and Breast cancer cell lines (MCF-7 and MDA-MB-231) were interested. The crude hexane extract of AP (APH) and crude ethanol extract of AP (APE) were prepared by maceration and Soxhlet extraction, respectively. Both APE and APH were investigated for their compound compositions by GC-MS. We found that APH contains almost twice the quantity of ergosterol (ER) compared to APE. The separation of APH was conducted by HPLC to check the characteristic of ER in APH. Moreover, four compound fractions (F1, F2, F3, and ER) were separated by PREP-LC with TLC screening. Cell viability assay after 24 hours treatment of the cancer cells with APH APE and Doxorubicin (an antitumor drug) using MTT were observed. We found that APH exerted a higher effect on all cancer cell lines (HepG2, MCF-7, and MDA-MB-231) by showing IC_{50} at 0.06 ± 0.02, 0.06 ± 0.01 and 0.02 ± 0.01 mg/mL, respectively. Moreover, apoptosis, cell cycle, migration and invasion assay were tested with APH (12, 25 and 50 µg/ml) and ER (6, 12 and 25 µM). The results showed that the high doses of APH and ER induced apoptosis, migration and invasion. However, both APH and ER could not significantly induce cell cycle arrest. In addition, *in silico* study of ER as a major compound found in the extract and gelatinase (MMP-2) as the enzyme that involves an invasion process was performed. The result displayed the mild binding of ER to MMP-2 (-32.7324 kcal/mol) with key interactions in the active site of MMP-2. We concluded that APH and ER revealed the antitumor activities leading to the future development for drug discovery of this edible mushroom and ergosterol.

Field of Study:	Clinical Biochemistry and	Student's Signature ....
	Molecular Medicine	
Academic Year:	2019	Advisor's Signature ....
		Co-advisor's Signature ....

ACKNOWLEDGEMENTS

Sunita Nilkhet

TABLE OF CONTENTS

จุฬาลงกรณ์มหาวิทยาลัย

CHULALONGKORN UNIVERSITY

LIST OF TABLES

จุฬาลงกรณ์มหาวิทยาลัย

CHULALONGKORN UNIVERSITY

LIST OF FIGURES

CHAPTER I INTRODUCTION

Cancer is the result of mutations in the deoxyribonucleic acid (DNA) that cause cells to grow uncontrollably, spread to the other organs and caused complications (1). The occurrences of cancers around the world are on the increase. The risk factors of the disease are related to sex, age, race, family history, infections, or hormonal changing (2). In 2018, Global cancer statistics (GLOBOCAN) showed that breast cancers remain the highest number of cancer cases in females around the world (3, 4). While liver cancer, especially in Asia, tends to be the highest incidence of diseases among men, with a high lethal rate when compared to other diagnosed cancer cases (4, 5). The conventional cancer treatments are including surgery, radiation, chemotherapy, hormone therapy, and targeted drug therapy (6). However, the most concerns in these treatments are the multidrug resistance, recurrent of cancers, and adverse side effects of cancer drugs that resulted in an inferior quality of life and a low chance of survival in patients (7).

Current cancer drugs used in chemotherapy were designed to mostly target cancer cells; however, to some degree, they also affected the healthy cells. The discovery of safer drugs with potent antitumor activity has been a challenging endeavor to date (8, 9). Alternative medicine becomes a new option for cancer patients not only because of the practical outcome in cancer remission; however, more importantly, it may also promote therapeutic effect without the adverse side effect (10).

Natural products, which derived from plants, fungi, bacteria, or animals, have been known as valuable sources of compounds to be developed into therapeutic drugs. There is a remarkable similarity in physicochemical properties between natural products and FDA-approved drugs (11). The drug discovery from natural products were either as

a pure isolated compound or in a mixture of compounds. The combination effects of the mixture of natural products could also provide therapeutic outcome (12).

Mushroom extracts were shown to be good sources of natural products for investigating anticancer effects in cell-based studies and clinical trials (13, 14). For example, Polysaccharide-K (PSK) derivatives from Turkey tail mushroom (*Trametes versicolor)* were tested against several cancer types such as colon cancer cell lines (HT29 and SW480), promyelomonocytic leukemia cell line (HL 60) and monocytic cell line (U937) (15). These derivatives were shown, in clinical trial phase I, to have the immunomodulation in cancer patients by improving the immune system and prolonging the survival rate of patients (16, 17). *Ganoderma lucidum* or *Lingzhi* mushroom is a well-known medicinal mushroom used in Chinese and Japanese traditional medicine. The extracts from the mushroom were shown to have cytotoxicity against cancer cells and immunomodulatory effects in patients. Cell-based studies revealed that the extracts are acting as the inhibitors of cell proliferation, cell migration and cell invasion. The extracts also killed cancer cells by promoting apoptosis, anti-inflammation and anti-angiogenesis (18, 19).

Auricularia polytricha (AP) is an edible mushroom from the *Auriculariaceae* family. This mushroom has been used as traditional medicine and as an essential ingredient in Asia and in Thai cooking. The previous studies of AP were showed to have antidiabetes (20), antibiotics (21), immunomodulation (22), antioxidants (23) and antitumor activity. The antitumor activity of AP has been tested in several cancer cell lines such as Human lung cancer cell line A549 in induced cell cycle arrest at G0/G1 phase (24) and triggered apoptosis on human colon cancer cell line (COLO-205) (25). Surveying of the literature reveals limited research into the systematic anticancer investigation of AP. To date, polysaccharides isolated from AP has investigated for

anticancer activity and targeted mechanisms in limited number of cancers. The further study of AP in other cell lines and mechanism of actions is worthwhile conducting.

To achieve this goal, we aim to investigate the anticancer activity of the AP crude extracts and its fractions against the hepatocellular cell line (HepG2) and breast cancer cell lines (MCF-7 and MDA-MB-231). The determination of the mechanism divided into *in vitro* and *in silico*. The *in vitro* study, apoptosis assay used annexin V-FITC and propidium iodide dual staining to observe the early and late stages of apoptosis induction. While DNA contents stained by Propidium iodine to determine the cell cycle arrest in different cell phases. Both assays were carried out by the flow cytometry. To look into the other inhibitions on cancer, migration, and invasion have been tested in cancer cells by using wound-healing assay and transwell invasion assay. Furthermore, *in silico* study such as a molecular docking has become a tool to predict the possible circumstances of AP purified-compound binds to MMP-2 as the inhibitors in which this enzyme is one of the important main enzymes involved in the metastasis of cancer in extracellular matrix (ECM) degradation on tumor site. The results of this project will be invaluable data for cancer drug discovering and value-adding to AP.

1.1   Research objectives

1.1.1   To investigate the antitumor activity of *Auricularia polytricha* extracts in cancer cell lines.

1.1.2   To examine the ability of *Auricularia polytricha* extracts in apoptosis induction, cell cycle arrest, migration, and invasion inhibition in cancer cell lines.

1.1.3   To predict the binding energy between phytochemical compounds in *Auricularia polytricha* extract and MMP-2 enzyme by Molecular docking (*in silico*).

1.2   Research hypothesis

1.2.1   *Auricularia polytricha* extract could be the potential source for cancer drug development.

1.2.2   *Auricularia polytricha* has the ability of apoptosis induction, cell cycle arrest, migration, and invasion inhibition in cancer cell lines.

1.2.3   *Auricularia polytricha* isolated compounds show the possibility of MMP-2 enzyme binding in molecular docking study.

1.3 Conceptual framework
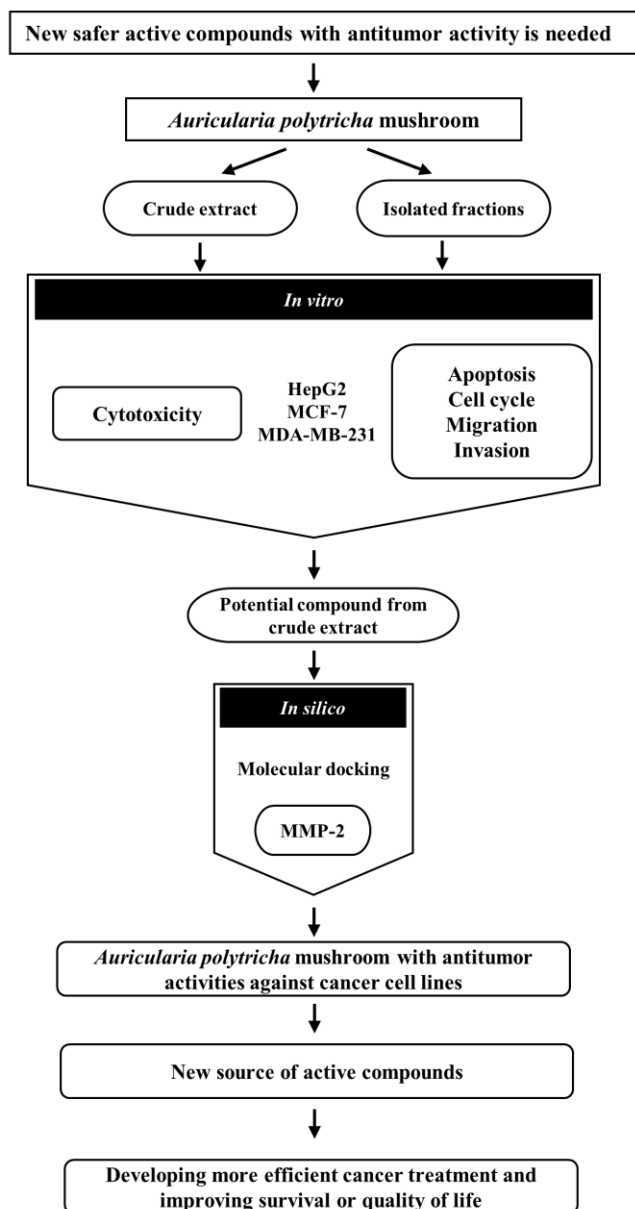
Figure 1   Conceptual framework.

CHAPTER II LITERATURE REVIEW

2.1 Cancer incidence

Cancer is the result of mutations in the deoxyribonucleic acid (DNA) that cause cells to grow uncontrollably and spread to the other organs and caused complications (1). The incidence of cancer worldwide that recorded in 2018 from Global Cancer Statistic (GLOBOCAN), the number of cancer cases worldwide detected on-trend (4).

2.1.1 Cancer epidemiology

The epidemiology of the disease has been recorded the diagnosed cancer cases, treatments, prognosis, and survival rates categorized by sexes, countries, and cancer types. The prevalence of cancer cases bases on both sexes resulted in lung cancer, and breast cancer ranked first with 11.6% worldwide. However, the statistical record has not only in the incidence but also reflected the mortality in each type of cancer. Breast cancer in female and lung cancer in men is dominant and followed by colorectum cancer and liver cancer shown to have a high mortality rate in cancer patients **Figure 2**. Countries or continents presented in the human development index (HDI) regions as the risk factors are related to the environmental and lifestyle factors (4).

High HDI or developed countries showed a less mortality rate in some cancer types such as lung cancer, breast cancer, prostate cancer, and colorectum cancer, whereas Low HDI or developing countries showed a high mortality rate in many diseases. However, liver cancer showed the similarity between the incidence and mortality in both high and low HDI groups due to the geological widespread of infectious risk in liver cancer plays an essential role for disease controlling and progression (4, 26) **Figure 3**.
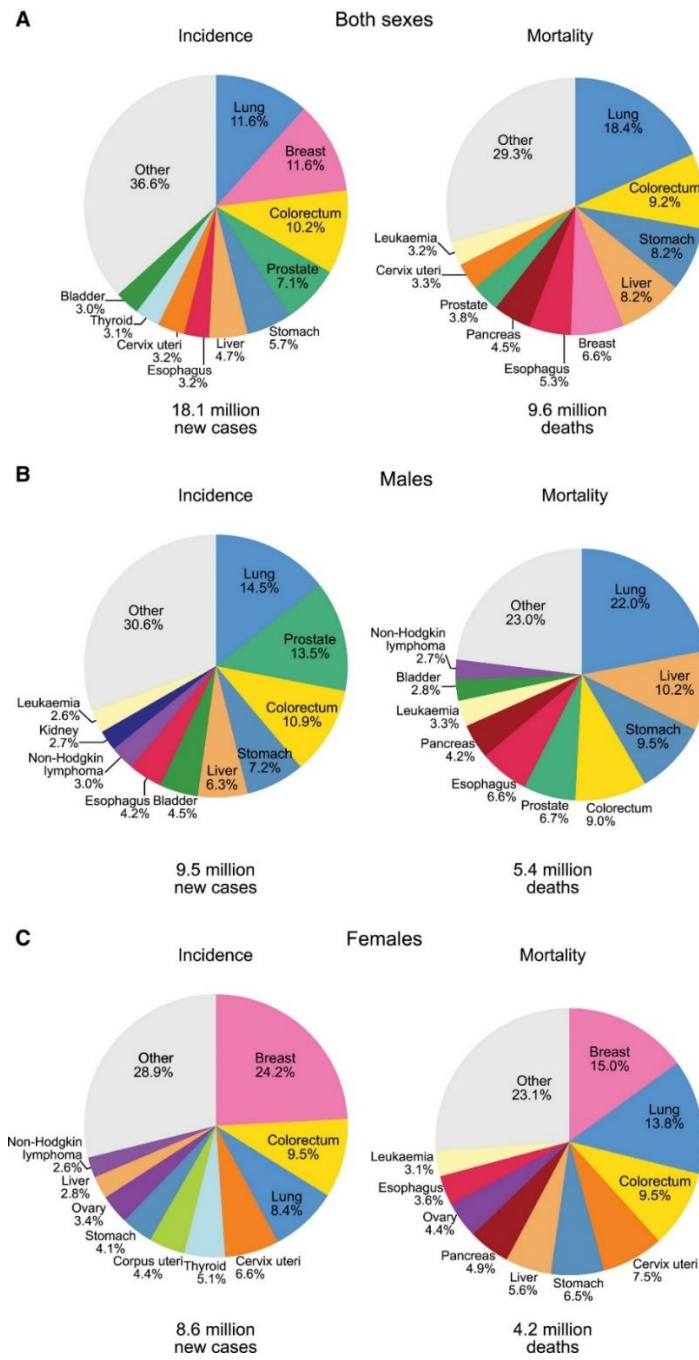
Figure 2   Pie charts present the distribution of cancer cases and mortality by GLOBOCAN 2018

A

High/Very high HDI   Low/Medium HDI

Male

Lung	40.4 / 34.1	11.8 / 11.0
Prostate	37.5 / 8.0	11.4 / 6.3
Colorectum	30.3 / 12.8	8.4 / 5.7
Stomach	20.0 / 14.3	6.6 / 5.9
Liver	16.5 / 14.8	8.5 / 8.3
Oesophagus	11.0 / 9.5	5.5 / 5.2
Bladder	12.1 / 3.6	3.6 / 2.0
Lip, oral cavity	3.9 / 1.5	8.7 / 5.0
Non-Hodgkin lymphoma	7.8 / 3.2	4.3 / 3.2
Leukaemia	7.5 / 4.5	4.0 / 3.2
Kidney	8.1 / 3.2	1.8 / 1.1
Pancreas	7.3 / 6.7	1.7 / 1.6
Brain, nervous system	5.0 / 3.8	2.4 / 2.2
Larynx	3.6 / 1.7	3.6 / 2.3
Thyroid	4.5 / 0.3	1.2 / 0.4

Age–standardized (W) rate per 100,000, male

B

High/Very high HDI   Low/Medium HDI

Female

Breast	54.4 / 11.6	31.3 / 14.9
Cervix uteri	10.4 / 4.1	18.2 / 12.0
Colorectum	20.9 / 8.5	5.9 / 3.8
Lung	19.1 / 14.3	4.6 / 4.2
Thyroid	15.5 / 0.5	3.1 / 0.5
Corpus uteri	11.1 / 2.0	3.3 / 1.2
Ovary	7.0 / 3.8	5.7 / 4.0
Stomach	8.6 / 6.1	3.6 / 3.2
Liver	5.5 / 5.1	3.5 / 3.4
Non-Hodgkin lymphoma	5.6 / 2.0	2.9 / 1.9
Leukaemia	5.3 / 2.9	3.0 / 2.4
Oesophagus	3.7 / 3.1	3.0 / 2.7
Pancreas	5.1 / 4.7	1.4 / 1.3
Brain, nervous system	4.0 / 2.8	1.7 / 1.4
Kidney	4.2 / 1.3	1.1 / 0.6

Age–standardized (W) rate per 100,000, female

Incidence ▮ Mortality ▮

Figure 3   The incidence and mortality Age-standardized rates in high/very-high human development index (HDI) versus low/medium HDI regions both in men and women by GLOBOCAN 2018.

2.1.2   Risk factors

Risk factors for cancer development are divided into endogenous and exogenous factors. Endogenous factors such as genetics, family history, hormonal changing, or aging could trigger the abnormality of cells and result in the uncontrollable division of cells. Previous studies, Indicated the breast cancer patient that carried the mutation in *BRCA1* and *BRCA2* genes about 40% develop breast cancer after 70-year-old (27). Tumor suppressor gene such as *TP53* also plays a vital role in cancer development, especially in activating invasion, metastasis, proliferation, and survival of cancer cells (28). Aging and hormonal changing are the primary keys from the reproductive system that involve in sex steroid hormone that could promote the aggressiveness of cell signaling (29). In recent decades, risk factors could be from harmful pollutions, UV radiations, Infectious diseases, diets, and obesity (30).

The industrial and modern lifestyles in this generation result to be more consume artificial substances than the old age. Tobacco ranked first as the risk factor for lung cancer accounted for almost 90% of lung cancer deaths (31). While in liver cancer, Hepatitis virus B and C (HBV and HCV) demonstrated as the leading causes of liver cancer development from inflammation as risk as to liver damage and liver cirrhosis from alcohol consumption. However, the prevalence of liver cancer showed a correlation with hepatitis viruses widespread in Asia (32). The same goes for cervical cancer as the Human papillomavirus (HPV) is the leading risk for disease development in a high prevalence of infection (33, 34).

Breast cancer is gained attention due to the high incidence in women has involved in both endogenous and exogenous factors. The endogenous risks are from the reproductive and hormonal system unbalancing after menopause or long-term conceptive pill-taking render the cycle of mensuration (35). Nonetheless, the family

history reported increasing the chance to develop breast cancer in first-degree relatives like a mother or siblings about two-fold higher than other women. Lifestyles in high-fat diets and physically inactive are also crucial for disease induction (36).

2.2 Cancer progression and prognosis

The early step of cancer progression begins with the constantly genetic instability of the somatic mutation resulting in cell proliferation and expansion of the new clone and more aggressive cells. The cell alteration in size, shape, and polarity in the epithelial origin known as epithelial-mesenchymal transition (EMT). Invasion and metastasis as the signature of cancer behaviors have two functions in basement membrane invasion, which are ECM degradation and cytoskeleton motility. The basement membrane mainly formed by collagen IV and laminin to support the structure of tissue (37, 38) **Figure 4**.
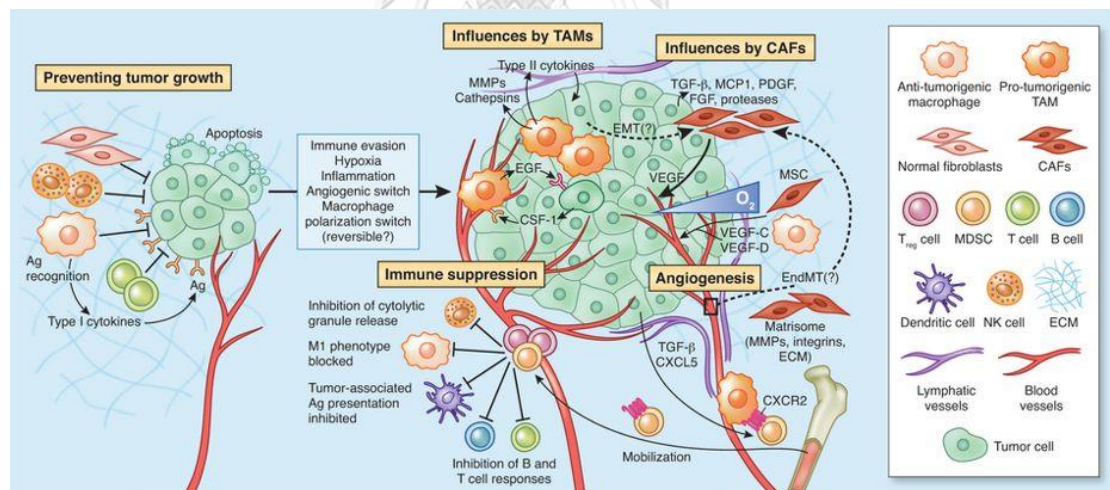
Figure 4   The progression of cancer (38).

2.3 Targeted therapies and treatments

2.3.1   Hallmark of cancers

The hallmarks of diseases involve in many regulations that alter healthy cell behaviors such as sustaining proliferative signaling, evading growth suppressors,

activating invasion and metastasis, enabling replicative immortality, inducing angiogenesis, and resisting cell death **Figure 5**. The main idea for drug development in cancers is to dysregulate these pathways of disease (39).
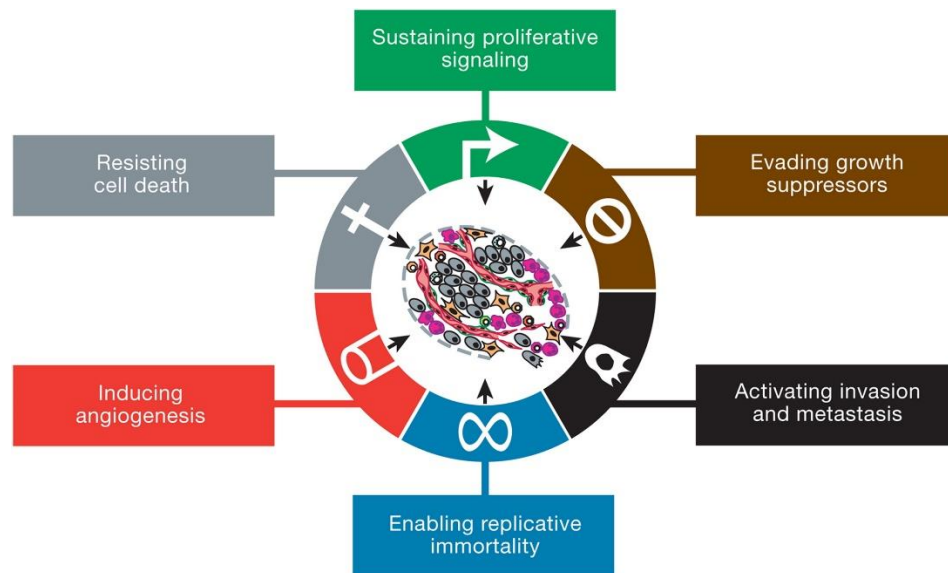
Figure 5   Hallmarks of cancer. (39)

2.3.1.1 Sustaining proliferative signaling

The proliferative signaling in cancer involves many pathways that resulted in cell cycle and cell growth activation. The growth factor ligand produced from cancer cells and activated the cancer cells in autocrine proliferative or secreted from the supporting cell around the tumor site triggers the downstream cascade. For example, the ERK MAPK pathway continuous stimulation as the result of growth factor receptor overexpression (EGFR) and growth factor overproduction, such as transforming growth factor-alpha (TGF-α). The FDA-approved cancer drug in a MAPK pathway inhibitor such as Sorafenib (40). Moreover, in the PI3K/AKT/mTOR pathway has been studied in their signaling cascades owing to the negative-feedback activator PTEN has lost their

function from the promoter methylation. Therefore, the AKT/PKB signal transducer regulated the PI3K hyperactivation in cancer cells, Everolimus, which is the drug that inhibits the mTOR, the mediator in the PI3K pathway (41) **Figure 6**.
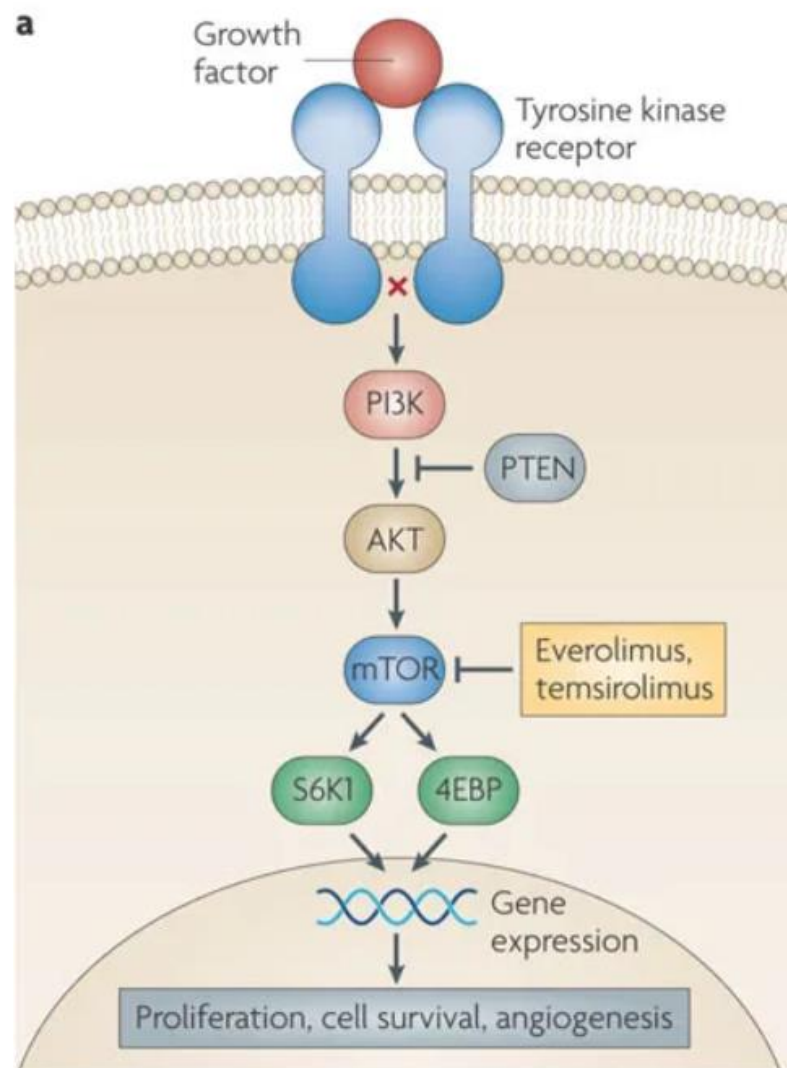
Figure 6   The inhibitors toward the PI3K proliferative signaling pathways (41).

2.3.1.2 Evading growth suppressors

The evading growth suppressor in cancer cells has been reported about two tumor suppressor genes, like retinoblastoma-associated (RB) and TP53 proteins, as they involve in cell proliferation and division. RB acts as the gatekeeper in the cell cycle in the G1 phase to allow cells to enter the S phase. While TP53 operates several roles,

such as protein checkpoint in G1 and G2 arrest, and promotes apoptosis (39). Interestingly, the current drug targeting in the cell cycle is the cell cycle checkpoint inhibitor, such as Cyclin-dependent kinase 4/6 inhibitor (palbociclib and ribociclib). Due to each phase of cell cycle require the checkpoint protein and cyclins expression such as in G1 step, the appearance of Cyclin D, CDK2/4/6 increase and allow DNA synthesis to occur in S phase, so the selective inhibitor towards the CDKs leads to the cell cycle arrest in the G1 phase of cancer cells (42) **Figure 7**.
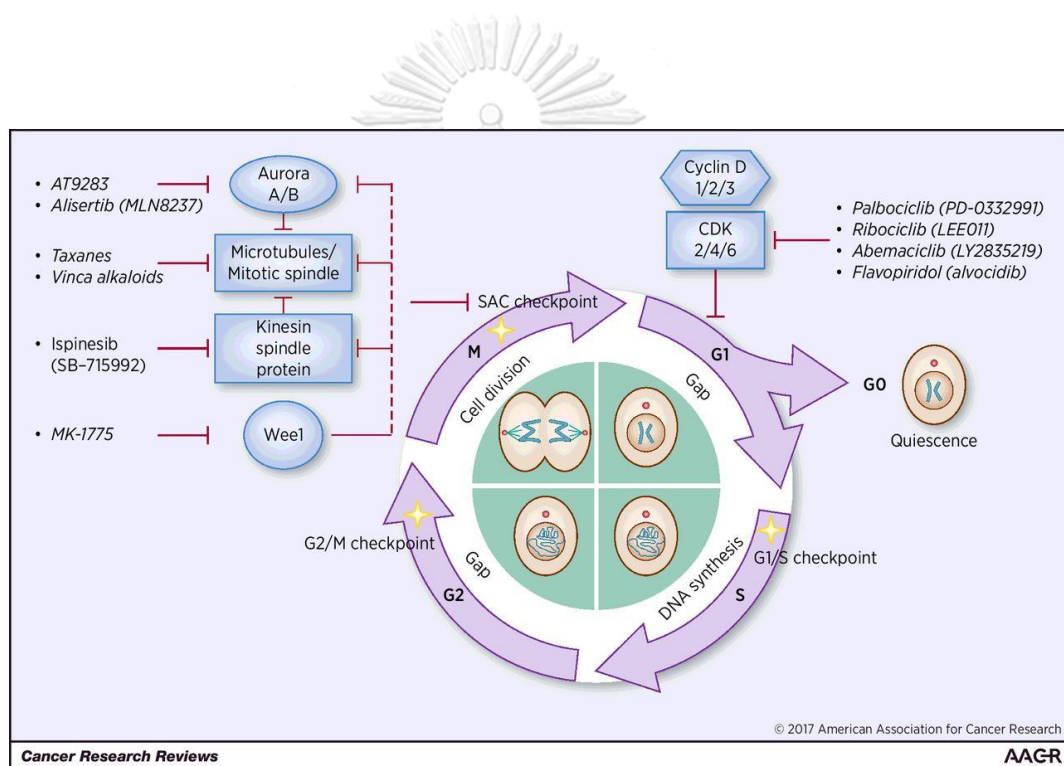
Figure 7   the cell cycle inhibitors in cancer cells (42).

2.3.1.3 Resisting cell death

Apoptosis is divided into two main pathways, which are an extrinsic pathway and Intrinsic pathway **Figure 8**. Extrinsic pathways contained death ligands and death receptors such as type 1 TNF receptor (TNFR1) and the intra-cellular inducer such as TNF related to receptor-associated death domain (TRADD), Fas-associated death domain (FADD) and Caspase-8. Cleaved caspase-8, an active form of caspase-8, acts

as the initiator of the extrinsic pathway and activates the common path with caspase-3 activation. While in the intrinsic pathway, the mitochondria played essential roles in genetic damage and oxidative stress stimulations. Mitochondrial permeability increases, and cytochrome-C releases into the cytoplasm as a result of the Bcl-2 family, which operates both pro-apoptosis (Bax) and anti-apoptosis (Bcl-2) functions. Cytochrome-C activates cleaved caspase-9 and the common pathway activation. In the common pathway, caspase-3 activation and breaks DNA and protein with morphological changes. Chromatin condensation and retraction of pseudopods with Phosphatidylserine (PS) flipped out to the outer membrane as the apoptosis marker. The loss of membrane integrity allows the organelle releasing and called phagocyte to engulf the apoptotic cells (43). The detection of apoptosis could be performed by staining the PS outside the cell membrane by Annexin V dye and counterstained the DNA content by propidium iodide as the early apoptosis occur the PS flipping phenomenon and the late apoptosis the integrity of cells is loss and DNA content could be detected (44).

Cancer cells resist apoptosis programming by disrupted the balancing between pro-apoptotic and anti-apoptotic proteins. Dysregulation of Inhibitor of apoptosis proteins (IAPs) and TP53 abnormality, which not only defect the cell cycle arrest in cells but also reflect the apoptosis induction in cancer cells due to the lack of DNA damage sensor and tumor could activate the anti-apoptotic protein in Bcl-2 (39, 45).
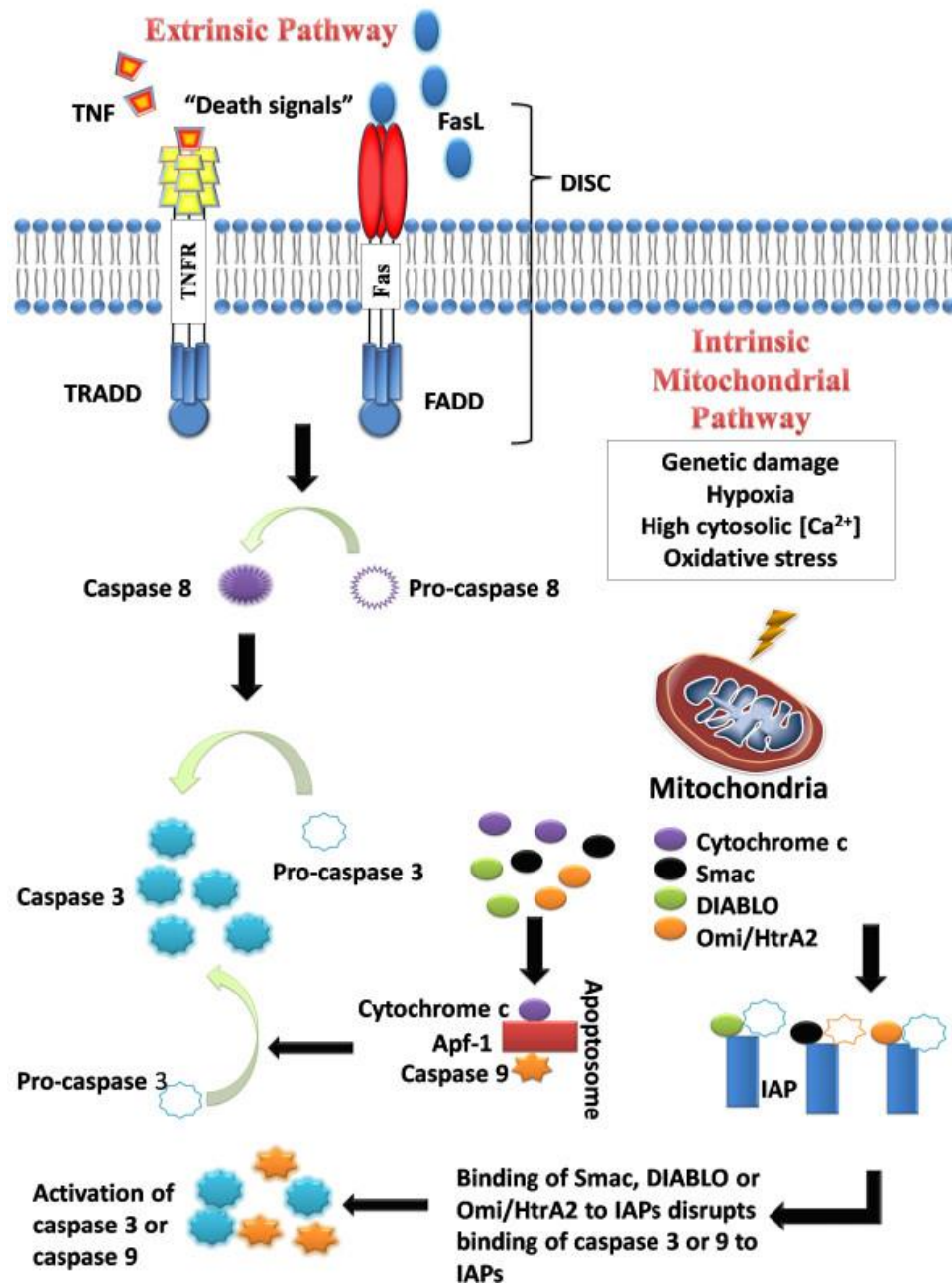
Figure 8   The mechanism of extrinsic and intrinsic pathways in apoptosis (43).

2.3.1.4 Enabling replicative immortality

Telomerase, a cellular reverse transcriptase that adds new DNA to telomeres at the end of chromosomes to help to protect telomere's lengths. Each round of cell division, the telomeric DNA shortening is a normal phenomenon, and when the shortening reach crisis, the senescence of cell occurs and results in DNA-damaged signaling to apoptosis activation. However, cancer cells can evade senescence or apoptosis by high expression of telomerase enzyme and extend the telomeric DNA repeats (46).

2.3.1.5 Activating invasion and metastasis

The extracellular matrix (ECM) also played an essential role in cancer progression due to the ability of matrix metalloproteinases enzymes (MMPs) to digest the ECM around the tumor site. MMPs also related to the VEGF, which also activating invasion and metastasis. Therefore, the MMPs enzyme showed the correlation between MMPs activation and upregulate the progression of cancer. Previous studies in invasive type of cancer such as breast cancer cell line demonstrated the overexpression of MMP-2 and MMP-9 subtypes or gelatinase A and B, respectively (47).

2.3.1.6 Inducing angiogenesis

The inducing angiogenesis as one of the hallmarks of cancer is involved in various factors such as Vascular endothelial growth factor (VEGF) and Platelet-derived endothelial growth factor (PD-EGF) that could activate the angiogenesis of tumor to infiltrate into circulation and spread to the secondary site or metastasis (45, 47) **Figure 9**.
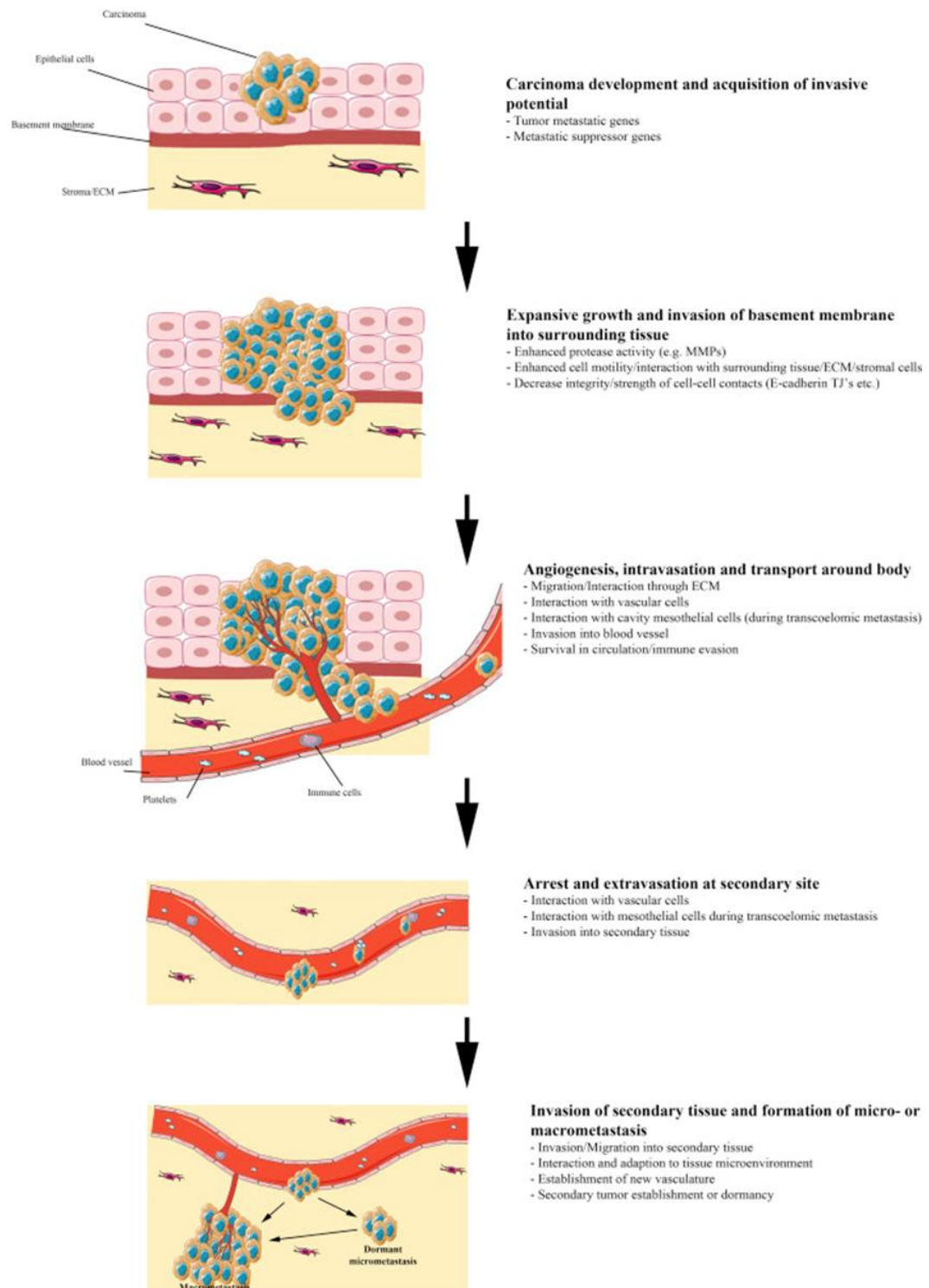
Figure 9 The process of invasion, metastasis, and angiogenesis of cancer cells (47).

2.3.2 Treatments

Treatments in the present are developing in many ways depends on the progression and prognosis of diseases. Types and stages of cancer are the main concern for the physician to offer treatments towards patients. Surgery and chemotherapy are commonly used in cancer patients, together with radiation and hormone therapy. Within the past ten years, cancer immunology gained popularity due to the concept of modulating self-immune cells to attack cancer cells (7).

As also mentioned in hallmarks of cancer, those regulations of abnormal cells have required the multiple targeted drug to attenuate the capacity of cancer cells. Therefore, the mechanism-guided combination will be an effective method for cancer treatments in humans (45, 48).

2.3.3 Adverse effects

The adverse effects of chemotherapeutic drugs both in the long-term and short-term, have been reported in Nausea and vomiting as well as gastrointestinal side-effects. The cause of oral mucositis leads to ulcers and pain. Central and peripheral neurotoxicity could be found in platinum-based agents, proteasome, and angiogenesis inhibitors. All of these effects resulted in the poor quality of life and less effective treatment. Minimizing toxicity and promoting efficiency will be a worthy challenge (49, 50).

2.4 Mushroom and cancer

The novel finding of active compounds and derivatives from natural products provides excellent outcomes for cancer treatments in isolated remedies, or cancer drug combination resulted in cell proliferation, pro-survival system, or the alteration of a cancer signaling pathway, which could be solved by computational methods and

biological tests. Mushroom, as a part of natural products, studies also shown antitumor activity and potential drug development (51, 52).

2.4.1 Mushroom and antitumor effects

Many mushrooms have been reported about their antitumor activities, such as the crude ethyl acetate extract of Antrodia cinnamomea showed the anti-angiogenesis against VEGF in human liver cancer cells (53). The methanolic extract of *Calvatia gigantea* showed the apoptosis induction and cell cycle arrest in human lung cancer cell line (A549) (54). Moreover, a *lectin* from Clitocybe nebularis (55) and the polysaccharides of mushrooms such as *Ga*noderma lucidum (56), Inonotus obliqus (57), and Lentinus edodes (15) have been reported about their anti-proliferative and apoptosis induction in several cancer cell lines as listed in **Table 1**.

Table 1   Mushroom extracts and anti-tumor activity.

Mushroom	Fraction/ active compound	Models	Mechanisms	Ref
Antrodia cinnamomea	Ethyl acetate extract	Human liver cancer cell	inhibits VEGF and anti-angiogenesis	(53, 58)
Calvatia gigantea	methanolic extract	human lung cancer cell line (A549)	induced cell cycle arrest and apoptosis	(54)
Clitocybe nebularis	lectin	Human pro-monocytic lymphoma cell line (U937) and Mo-T and Jurkat human leukemic T cell lines	Antiproliferation effect on leukemic cell lines.	(55)
Ganoderma lucidum	Ganopoly® polysaccharide	human tumor CaSki, SiHa, Hep3B, HepG2,	Cytotoxicity and apoptosis induction	(56)

Mushroom	Fraction/ active compound	Models	Mechanisms	Ref
		HCT116 HT29, and MCF7 cells		
Inonotus obliqus	Polysaccharide	Human neurogliocytoma cells	downregulated Bcl-2 and upregulated Caspase-3	(57)
Lentinus edodes	Polysaccharide	Human hepatocellular carcinoma cell	upregulated caspase-3 and caspase-8	(59)
Trametes versicolor	Polysaccharide K (PSK)	Colon cancer cell lines (HT29 and SW480), Promyelomonocytic leukemia cell line (HL 60) and monocytic cell line (U937)	Induced apoptosis with caspase-3 upregulation	(15)

2.4.2   Auricularia spp.

Mushroom extracts in the *Auriculariacieae* family have been studied in their antitumor activities. The dichloromethane fraction from *Auricularia auricula-judae* found to have the antitumor effect in bronchoalveolar and gastric cancer cells resulted in the downregulation of Bcl-2 expression and increased the p53 protein expression (60). Moreover, the water extract and ethanolic extract of *Auricularia auricula-judae* showed the cell growth inhibition in the monocytic leukemia cell line (U937) (61), Sarcoma 180, lung cancer cell line (NCI H358), and human gastric cancer cell line (SNU 1) (62). As well as *Auricularia polytricha*, or called a wood ear mushroom, the close species to *Auricularia auricula-judae* has been examined its antitumor effect as an apoptosis

inducer in MCF-7, colon (COLO-205), and kidney (ACHN) cancer cell lines (63). Furthermore, because of both *Auricularia* spp. contained a large proportion of carbohydrates such as polysaccharides, so the active component in this part has been prioritized for further study. Polysaccharides fractions from the ethanolic and water extracts of *Auricularia auricula-judae* have been investigated and found the active compound, which is Beta-glucans the well-known polysaccharides for their immunomodulation and antitumor activity. AA polysaccharides complexed with cisplatin and folic acid targeted cervical cancer cells in apoptosis induction and resulted in the upregulation of Cax, cytochrome-c, and caspase-3 and decreased bcl-2 protein (64). *Auricularia polytricha* polysaccharides (AAP) also showed the antitumor effects in intrinsic apoptosis pathway induction and cell cycle arrested at the G0/G1 phase on lung cancer cell line (A549) (24). The briefed information of *Auricularia* spp. activities were listed in **Table 2**.

Table 2   Auricularia spp. and their antitumor effect.

Mushroom	Fraction/ active compound	Models	Mechanisms	Ref
Auricularia auricula-judae	Dichloromethane	Bronchoalveolar and gastric cancer cells	Apoptosis (downregulation of Bcl-2 expression and p53 overexpression)	(60)
	Ethanolic	Monocytic cell line (U937)	Cell viability	(61)
	Ethanolic	Sarcoma 180, NCI H358, and SNU 1 cell lines	Cell viability	(62)

Mushroom	Fraction/ active compound	Models	Mechanisms	Ref
	Polysaccharides/ folic acid, AAP and cisplatin complexes	Cervical cancer	Apoptosis (Bax, cytochrome-c, and caspase-3 and downregulation of bcl-2, increase mitochondria membrane potential)	(64)
Auricularia polytricha	Polysaccharides	Breast (MCF-7), colon (COLO-205), and kidney cell lines (ACHN)	Intrinsic apoptosis and G0/G1 cell cycle arrest (decreased expression of cyclin A, cyclin D and CDK2, as well as the increased expression of p21 and p53	(63)
	water	lung cancer cell line (A549)	Cell viability, colony formation inhibition, DNA fragmentation, and apoptosis	(24)

2.4.3 *Auricularia polytricha*

Auricularia polytricha (AP), also known as Cloud ear mushroom or Wood ear mushroom, generally found in Asia. The properties of this mushroom are composed of gelatinizing texture in brown fruit body and ear shape **Figure 10** (65). The AP has been used as traditional medicine and food preparation. The natural compounds and nutrients of AP have been reported. The aqueous fraction of AP showed an anti-inflammatory effect with decreased pro-inflammatory cytokines such as tumor necrosis factor -α and interleukin-6 (23). The AP polysaccharides have been evaluated. Its antioxidant and phenolic compounds found that gallic acid and vanillic acid exerts the antioxidative activity of AP (20).

Furthermore, the polysaccharides also showed the hepatoprotective effect against carbofuran-induced rats and paracetamol-induced toxicity rats as well. The AP polysaccharides balanced the oxidative stress in exercise-induced oxidative stress in mice (66). The antihyperchloresterolemic impact has been studied in cell models and in vivo models and resulted in reducing blood cholesterol levels (67) in **Table 3**.

Figure 10   Auricularia polytricha mushroom (65).

Table 3   Auricularia polytricha active compound studies.

Active compounds	Models	Mechanism	Ref
Aqueous extract	Forty-six-week-old, male Sprague-Dawley rats	Decreased tumor necrosis factor-α and interleukin-6 expression	(23)
Polysaccharide-peptides	human hepatoma HepG2 cells *in vitro* and an animal model of fatty liver disease	Reduced lipid deposits in cells, blood, and the liver increased cellular antioxidant activity and viability and protected the liver against injury.	(66)
Polysaccharides	Male Wistar rats with body weights (BW)	Antioxidative levels (Gallic acid and Vanillic acid)	(20)
Soluble polysaccharide	Sprague-Dawley (SD) rats	a decrease of AST, ALT, ALP, LDH, TB, TG and cholesterol in the paracetamol-induced toxicity	(67)

2.5 Molecular modeling

Computational-aided drug design or CADD is a tool to study the drug interaction in silico to classify the potential compounds towards the disease targets. CADD is an

inexpensive and effective tool due to the convenience in time and instruments, which required only the compound characteristics and the molecular simulations (68). In the present, the most well-known database for protein structure is the Research Collaboratory for Structure Bioinformatics or RCSB (www.rcsb.org), which integrated the 3D structure information of proteins and organized structures into the protein data bank ID (PBD ID) for each complex. Most of them were received from X-ray crystallography and Nuclear magnetic resonance (NMR) techniques (69). The structure from the database needed to be processed after downloaded in the molecular simulation, such as removing water molecules, adding polar hydrogen, or modifying binding pocket. For predicting the drug interaction in molecular simulation, CADD was classified into two groups composed of Ligand-based drug discovery (LBDD) and Structure-based drug discovery (SBDD) (70).

Ligand-based drug discovery (LBDD), active compounds were known with or without targeted proteins; this method could still be used. The common structural features and the quantitative structure-activity relationship (QSAR) were calculated to predict the compound activity in vivo (71). Whereas Structure-Based drug discovery (SBDD) is the predictive method between the known target protein and candidate drugs allow the software to dock the ligand into the protein target and score the binding energy or conformations (72). Molecular docking, as described in brief earlier, the excellent protein structure for direct docking obtained from x-ray crystallization or NMR and the resolution should less than $2°A$. The CDOCKER (CHARMm-based DOCKER) simulation in Discovery Studio software is the method that used the simulated-annealing-based algorithm to generate the full ligand flexibility. Gib and force field was conducted, and the top ranking of the ligand-protein docking pose (lowest energy) referred to the best affinity of the complex (73).

In this study, the molecular modeling was computed to predict the ligand-protein interaction between active compounds from *Auricularia polytricha* extract and matrix metalloprotease-2 (MMP-2), which has been studied the invasion inhibitory effects *in silico*, *in vitro,* and *in vivo* with natural derivatives before. The first report about the human MMP-2 structure was published in (PDB ID 1QIB) about the protein and a hydroxamate inhibitor complex (74). Then, the study of this protein was carried on until the latest of the structure research in the human MMP-2 catalytic domain was modified to MMP-2 complexed with beta-amyloid precursor protein-derived inhibitor (PDB ID 3AYU) with the resolution at 2°A which is meet the criteria for structure selection (75).
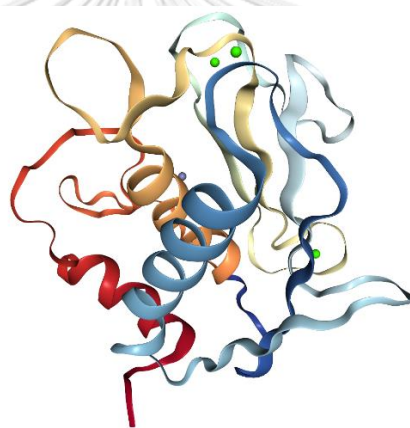
Figure 11   the MMP-2 complex with (PBD ID 1QIB).
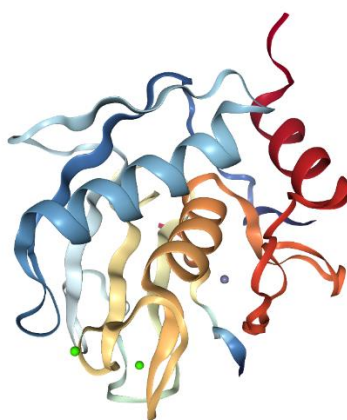
Figure 12   the MMP-2 complex with APP-IP (PBD ID 3AYU).

2.6 Cell models

2.6.1   Hepatocellular carcinoma cell lines (HepG2)

American Type Culture Collection (ATCC), as the organization of collect, stores, and distributes human and animal cell lines, have been described and categorizes characteristics and information in each cell type. HepG2 cells (ATCC® HB-8065) are human hepatocellular carcinoma-derived cell lines and widely used for hepatocellular carcinoma studies in vitro. The morphology of HepG2 cells is attached to cells with the vacuole-like inside of the cell could be observed. The high density of cells or confluent colony-forming could be seen in **Figure 13**.
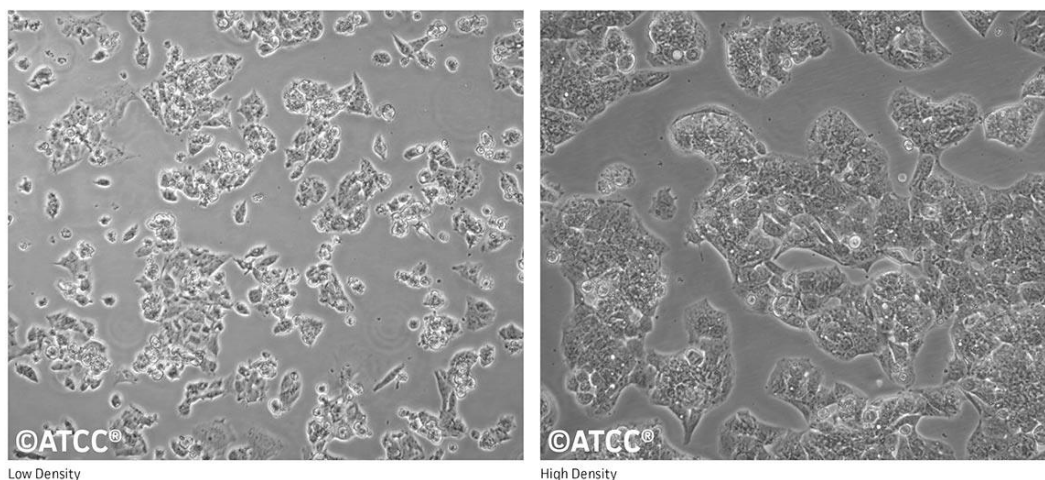
Figure 13   HepG2 cells morphology from ATCC

2.6.2   Breast cancer cell lines (MCF-7 and MDA-MB-231)

Breast cancer cell lines are provided with various expressions of receptors and characteristics. In this study, the breast cancer cell type with estrogen and progesterone receptors positive (MCF-7) is selected for an antitumor activity to investigate the

susceptibility of candidate compounds to these receptors. The morphology of MCF-7 is adherent cells with clumping at the confluent **Figure 14** (76). In contrast, the triple-negative breast cancer cell (MDA-MB-231) is the absence of all three primary receptors on the cell surface, which are the estrogen receptor, progesterone receptor, and human epidermal growth factor receptor 2 **Figure 15**. Therefore, the invasiveness of MDA-MB-231 exerted more than MCF-7 and reported the high expression of MMP-2 and MMP-9 levels could provide the information for invasion inhibition and cytotoxicity towards breast cancer compared to MCF-7 (77).

ATCC Number: **HTB-22**
Designation: **MCF-7**

Low Density — Scale Bar = 100μm
High Density — Scale Bar = 100μm
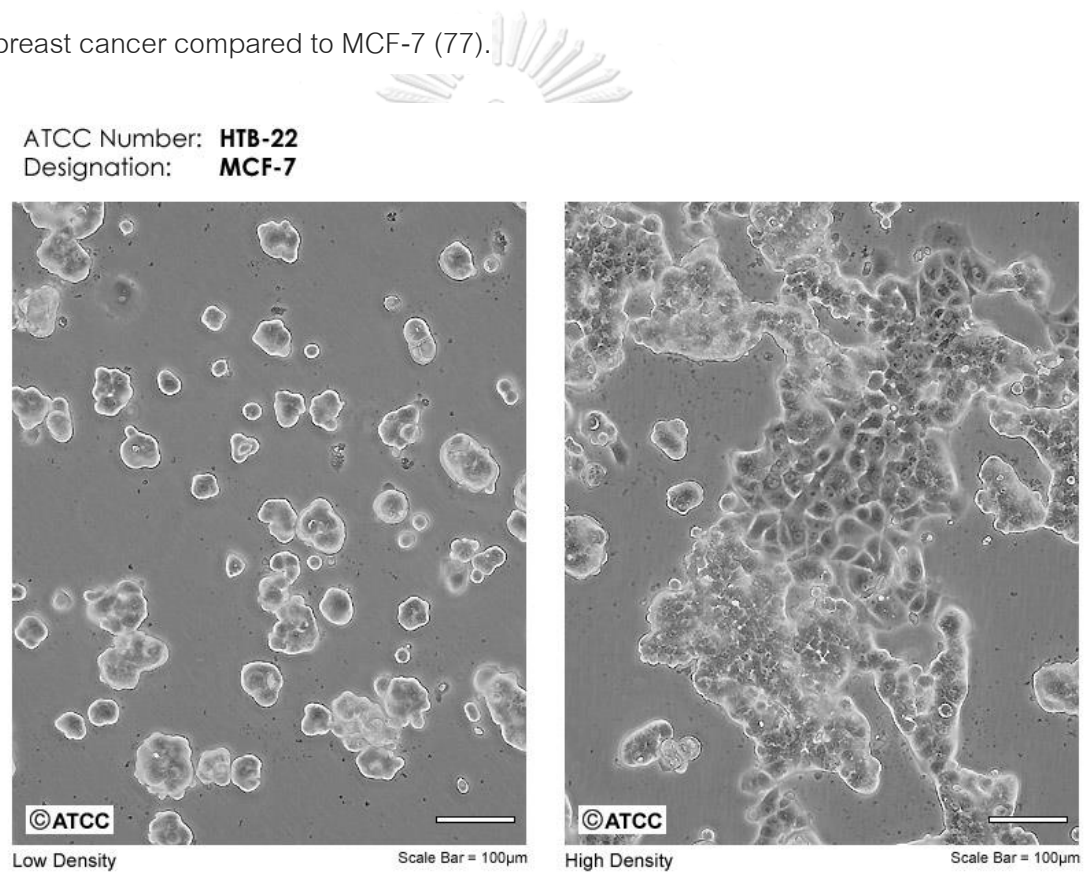
Figure 14 The morphology of the MCF-7 cell line (ATCC® HTB-22).

ATCC Number: **HTB-26** ™
Designation: **MDA-MB-231**
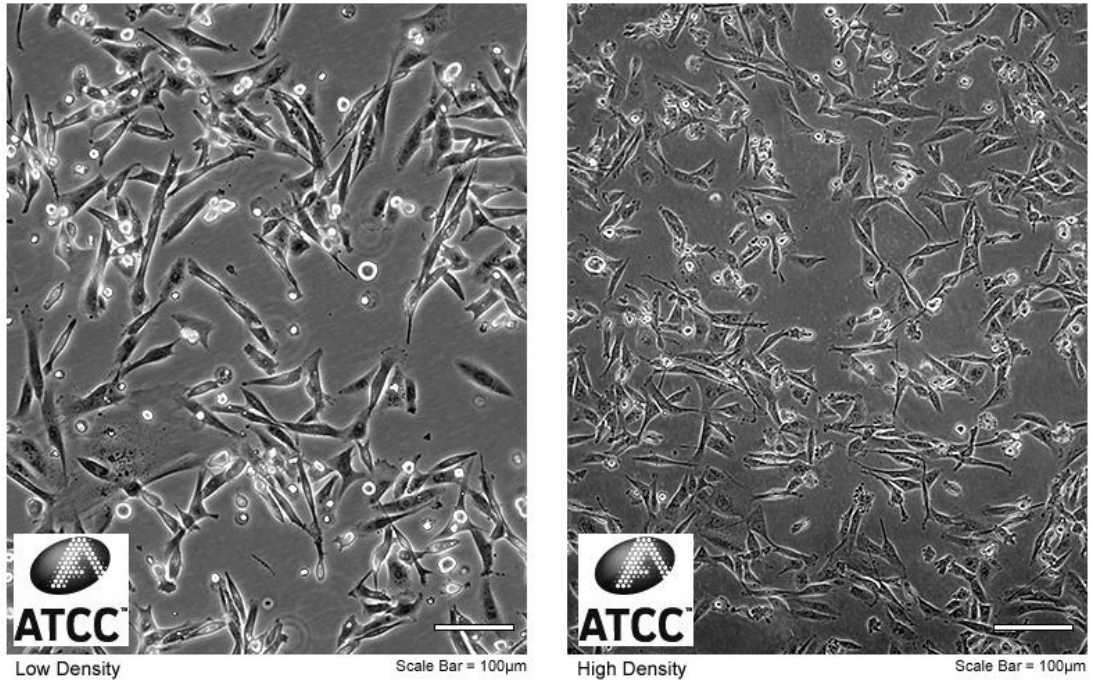
Figure 15 The morphology of the MDA-MB-231 cell line (ATCC® HTB-26).

CHAPTER III MATERIALS AND METHODS
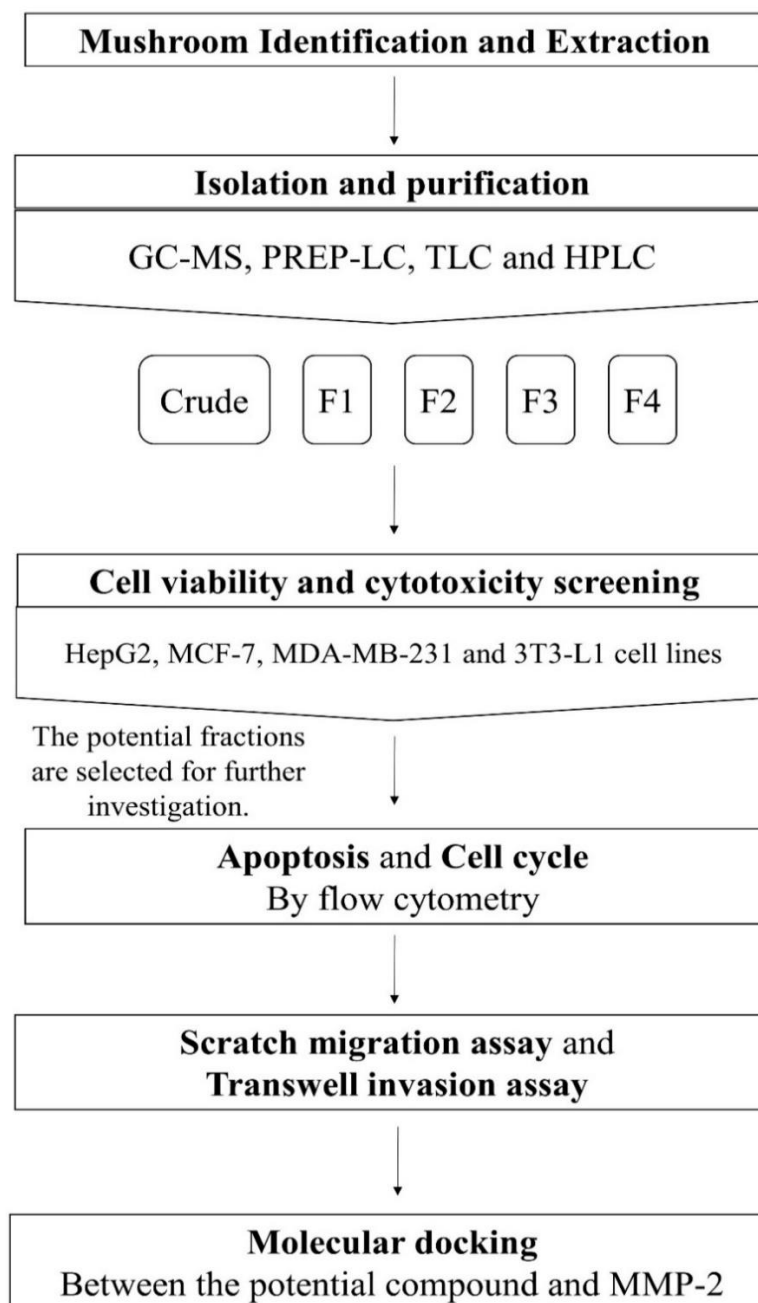
Figure 16   The experimental workflow.

3.1 Chemicals

Hexane, ethyl acetate, and acetonitrile were purchased from Honeywell, USA. Dulbecco's Modified Eagle's Medium (DMEM), Phosphate Buffered Saline, Trypsin 0.25% (v/v), and Fetal Bovine Serum (FBS) were purchased from HyClone, USA. 3-(4,5-Dimethyl-2-thiazolyl)-2,5-diphenyl-2H-tetrazolium bromide (MTT), Ergosterol, and Propidium iodide were purchased from Sigma-Aldrich, *Germany*. FITC Annexin V Apoptosis Detection Kit with PI was purchased from BioLegend, USA. Dimethyl sulfoxide (DMSO) was purchased from RCI Labscan, Thailand. Caspase-3 (8G10), Beta-actin (13E5), and secondary antibody (7074) were purchased from Cell Signaling Technology, USA. Bradford protein assay and was purchased from Bio-Rad Laboratories, USA.

3.2 Mushroom identification

The mushroom was purchased from Chang Daeng mushroom farm in Samutprakarn province, Thailand. Mushroom fruiting bodies were sterilized by immersing in 70% alcohol in a laminar hood. A small piece of the inner tissue was picked and placed on a potato dextrose agar (PDA) medium and incubated at 25°C for seven days, followed by single colony isolation during the subculture process. Total genomic DNA was extracted from 50 mg fruiting body of each sample using Cetyl Trimethyl Ammonium Bromide (CTAB) DNA extraction method. The sequence data were compared with the known *ITS1* and *ITS4* sequences the PCR protocol for *ITS* amplification was listed in **Table 4**; *ITS1* Sequence (5'TCCGTAGGTGAACC TGCGG3') and *ITS4* Sequence (5'TCCTCCGCTTA TTGATATGC 3'). *ITS* sequences of samples were operated by Bioneer sequencing service (Bioneer Corporation Korea) and the sequences extracted from the GenBank (www.ncbi.blast.lnm.nih.gov) with BLAST Basic

Local Alignment Tool (BLAST Query) alignment were generated, and highest score alignment was considered closely related sequences.

Table 4   The PCR protocol for ITS region amplification.

Step	Temperature (°C)	Time (sec)
1. Initial denaturation	94	180
2. Denaturation	94	30
3. Annealing	55	30
4. Extension	72	90
Repeat step 2 to 4 for 30 cycles		
5. Final extension	72	600

3.3   Mushroom extraction

Dried *Auricularia polytricha* (AP) was crushed and blended into powder by a blender (Philips, Japan) and weighted at ratio 1:10 to absolute ethanol (Merck, Germany). The Soxhlet extractor was used to extract the mushroom for 24 hours. After the extraction, the extract was evaporated by the Laborota 4011 rotary evaporator (*Heidolph*, Germany) at 50°C with speed 80 rpm. Until the extract reduced to around 10 mL, and the solvent was concentrated by the miVac Quattro concentrator (GeneVac, UK) at 50°C. The extract was stored at -20°C until used. Percent yield was calculated using this formula.

$$\% \text{ Yield} = \frac{\text{The crude extract (g)}}{\text{Crude powder (g)}} \times 100$$

The hexane extract of *Auricularia polytricha* (APH) from the previous study (Sillapachaiyaporn et al., 2019) obtained by the maceration method also included in this project.

3.4   Isolation and Purification
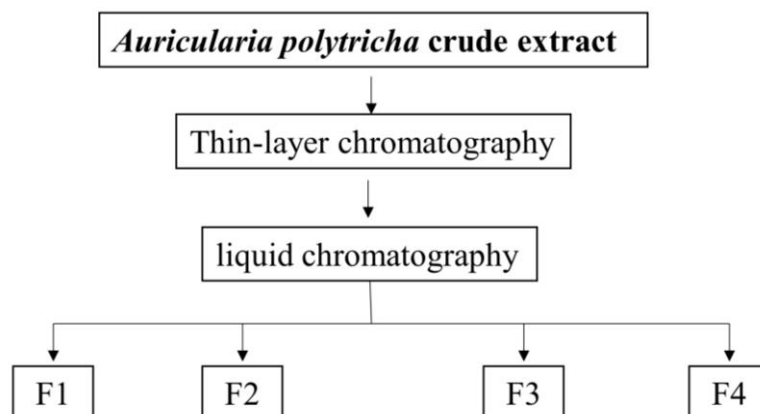
Figure 17   Diagram for AP crude extract isolation

3.4.1   Thin-Layer Chromatography (TLC)

The APH mixture was dissolved in ethyl acetate and spotted on the TLC silica plate for 1-2 mm diameters. After drying, TLC plates were run on different mobile phases (hexane: ethyl acetate from 100: 0, 90: 10, 80: 20, 70: 30, 60: 40, 50: 50) and observed bands under UV at 245 and 365 nm. Then Retention factor (R_f) was calculated with the distance between compounds and the solvent front.

$$\text{Retention factor } (R_f) = \frac{\text{Distance traveled by compound (cm.)}}{\text{Distance traveled by the solvent front (cm.)}}$$

3.4.2 Preparative Liquid Chromatography (PREP-LC)

The APH crude extract was purified by Reveleris ®PREP-LC (*Büchi*, *Switzerland*) with the normal stationary phase cartridge using hexane: ethyl acetate system generated by Navigator software in the machine with the TLC R_f values three

components mode output (**Table 5**). The fractionations were screened by TLC plates using hexane: ethyl acetate mobile system (80:20).

Table 5　　　The gradient table of hexane: ethyl acetate system was generated by the Navigator® software.

Steps	Min	Solvents	% 2nd
1	0.0	AB	0
2	1.0	AB	0
3	8.3	AB	10
4	16.7	AB	14
5	7.0	AB	14
6	0.0	AB	100
7	2.0	AB	100

3.4.3　　Gas Chromatography-Mass spectrometry (GM-MS)

APH crude extract was dissolved in ethyl acetate, and GC-MS was done by using Agilent 19091P-M15 with column HP-PLOT Al203 (50.0m x 320 µm x 8.00 µm). The sample was analyzed using split ratio 15 :1, 1.5 ml/min of He flow rate with an oven temperature of 50°C to 220°C (2 min) at 7°C/min, then 270°C (5 min) at 7°C/min, followed by 290°C at 5 °C/min. The chromatogram and peaks were compared to the NIST MS search 2.0 Data analysis.

3.4.4   High-Performance Liquid Chromatography (HPLC)

The HPLC result was done by UHPLC VANQUISH (Thermo scientific) on reverse-phase Eclipse XDB C-18 column. The gradient flow was designed in water/acetonitrile (95:5) and (5:95) with a flow rate at 1 mL/min and UV wavelength detected at 254 nm. The purified ergosterol fraction was prepared at the concentration of 100 ppm in acetonitrile as same as the standard ergosterol (Sigma-Aldrich, Merck) and the spiked sample.

3.5   Cell line maintenance and harvesting

The hepatocellular carcinoma cell line (HepG2), the breast cancer cell line (MCF-7), and the triple-negative breast cancer cell line (MDA-MB-231) were maintained in DMEM media supplemented with 10% fetal bovine serum. Cells were incubated at 37°C and 5% CO_2 in a humidified condition until the cultures reach confluence.

For cell harvesting, cells were washed with PBS without calcium and magnesium. Trypsinization was performed using 0.25% trypsin incubated with the cells for 5 min in the 37°C incubator. Then, cells were washed and collected into a conical tube and spin down at 25°C in refrigerated centrifuge with 1500 rpm for 5 min.

3.5.1   Cell viability assay

Cells were plated at a density of 5×10^3 cells/well for 100 μl in a completed DMEM medium supplemented with 10% fetal bovine serum and incubated overnight at 37°C with 5% CO_2 in a humidified condition. Then, they were incubated with various treatments. In all conditions, the final concentration of FBS and dimethyl sulfoxide (DMSO) were 5% and 0.1%, respectively. DMSO at 0.1% was a solvent control. After 24, 48, and 72 hours, 5 mg/ml of 3-(4, 5-dimethyl thiazolyl-2)-2, 5-diphenyltetrazolium bromide (MTT) was added into each well, and the plate was put back into the incubator

for 3 hours for color development. Then, the plates were read out at 550 nm by a microplate reader, an EnSpire™ 2300 multilabel plate (Perkin Elmer, USA). The cell viability was calculated in the percentage of cell viability. Sigma Plot calculated the half-maximum inhibitory concentration (IC50).

$$\text{Cell viability (\%)} = \frac{\text{Absorbance of treatment}}{\text{Absorbance of control cell}} \times 100$$

3.5.2 Cytotoxicity testing

The mouse embryonic fibroblast cell line (3T3-L1) was used to determine the cytotoxicity of the extract against the healthy cell (78, 79). The toxicity of cells was performed as described in the cell viability assay.

3.6 Apoptosis induction and cell cycle arrest

3.6.1 Apoptosis assay

Cells at 1×10^5 cells per well were seeded into a 6-well plate. After overnight incubation, the cells were treated with various treatments for 24 hours. Cells were harvested by trypsinization and resuspended in binding buffer. Annexin V-FITC and Propidium iodide (PI) was added to 100 µL of cell suspension and incubated for 20 min in the dark at room temperature. At the end of the incubation period, 400 µL of binding buffer was added up into the tubes. Cells were then analyzed by a BD FACS Calibur flow cytometer (Becton Dickinson, USA). The Annexin V dye positive cells were counted as apoptosis-induced cells and compared to control cells.

3.6.2 Cell cycle assay

Cells at 1×10^5 cells per well were seeded in a 6-well plate and incubated overnight. The culture medium was replaced with serum-free DMEM for serum starvation

24 hours before testing. Cells were harvested and stained with 500 µl of propidium iodide solution (0.1%, v/v) Triton X-100; 10 µg/mL propidium iodide; 100 µg/mL DNase-free RNase A (500 U/ml) in PBS) and incubated for 30 min at room temperature. The cell cycle analysis was evaluated by a BD FACS Calibur flow cytometry (Becton Dickinson, USA). The DNA contents at different phases (G0/G1, S, and G2/M) were compared to control cells.

3.7 Migration and invasion assays

3.7.1 Migration assay or wound healing assay

Cells in completed DMEM medium supplemented with 10% fetal bovine serum were plated into 12-well microplate and plated in 5% CO_2 incubator at 37°C in a humidified condition until reaching the confluent Then, the serum-free DMEM was added for cell starvation for 24 hours. A 200 µL sterile-pipette tip was used to created straight lines in cultured wells. The wells were washed twice with pre-warmed PBS and replaced with various concentrations of treatment prepared in 5% FBS in DMEM. The inverted-light microscope photographed the baseline control for pre and postmigration. Cell migration depends on the invasiveness of cell lines. We measured the cell migration at 0, and 6 for MDA-MC-231 cells while MCF-7 and HepG2 cells monitored 0 and 24 hours for five random fields. The width of the wound was calculated using ImageJ software compared to DMSO control cells using the formulation below.

$$\% \text{ of wound closure} = [(\text{at} = 0 \text{ h} - \text{at} = \Delta \text{ h})/\text{at} = 0 \text{ h}] \times 100\%$$

3.7.2 Transwell invasion assay

Transwell invasion assays were performed using the 24-well modified Boyden chambers containing membrane filter inserts with 8-µm pores (Falcon, USA). Inserts were pre-coated with 50 µL of diluted Matrigel (Corning, USA) at a 1:8 ratio in serum-

free DMEM and solidified in the incubator for an hour. To evaluate the cell invasion by transwell invasion assay, cells were seeded at 200 µl of 5×10^4 cells/well, and various treatments were treated in the inserts while the lower compartment was filled with 10% FBS in DMEM as the chemoattractant. The assay was determined after 24 hours. Cotton swabs removed the non-invaded cells in the inserts. The invaded-cells attached to the bottom of the insert were fixed in 100% methanol for 20 min. Cells were washed with PBS and stained with 0.1% crystal violet for 20 min. After re-washing with PBS and air drying, chambers were photographed under the Observer A1 inverted microscope (ZEISS, Germany) at 50x magnification for five random fields.

3.8   Molecular modeling

The computational study was carried out by using BIOVIA Discovery Studio 4.5 software (Accelrys Inc., San Diego, CA, USA). The software was used for visualization, preparation of protein and ligand structures, and docking simulation. The building and optimizing of molecules were performed in the "Small Molecules" module. The docking simulations study was done using the CDOCKER method available in DS 4.5 was used this study (73). The parameters for the docking study were adapted as that suggested by the software.

3.8.1.   Protein preparation

The crystal structure of matrix metalloproteinase 2 (MMP-2, PDB ID: 3AYU) co-crystallized with a peptide (APP-IP) inhibitor was downloaded from the Protein Data Bank database (75). The crystal structure (PDB ID: 3AYU) was chosen as the template for molecular docking study due to its high resolution (R = 2 Å) of the X-ray structure, which defines the high quality and accuracy of the enzyme structure.

The MMP-2 crystal structure was prepared by first removing the original ligand peptide (APP-IP) inhibitor. All crystallographic water molecules in each protein were kept, and the missing hydrogen atoms were added. The protein structure was optimized using the CHARMm forcefield in the "Prepare Protein" module. All visualizing and processing in protein preparation were generated by BIOVIA Discovery Studio 4.5.

3.8.2. Ligand preparation

APP-IP ligand from the original complex of MMP-2 was selected, ergosterol and sterol compound 49, and other inhibitors were drawn using ChemDraw (80, 81) and the corresponding MDL-SD file (*SDF) files were imported into Discovery Studio and converted to the 3D structures. The compounds were minimized to the lowest possible energy using the CHARMm force field in the Small Molecules module. Conformations of all the compounds were generated using the 'best conformer generation' to ensure the best coverage of conformational space was considered, the maximum number of formations was set to 200, and the minimum energy threshold for the compounds was equal to 20 kcal/mol. The default setting was used for the rest of the parameters.

3.8.3. Protein and ligand docking

In CDOCKER studies, the protein was kept rigid while the ligands were as allowed to be flexible during calculation and refinement, and a final minimization step is used to refine the docked poses. The CDOCKER method uses the CHARMm forcefield, and the parameters were set as default, allowing for 10 Top Hits and 10 Random Conformations to occur. The CDOCKER method scored the ligands using the CDOCKER Energy and –CDOCKER Interaction Energy functions in the CDOCKER module. These functions calculate the energy values using the Gibb's Free Energy (ΔG) of the interaction between the ligand and receptor with the highest score determined as the best possible ligand. The higher scores with most top negative ΔG would indicate

favorable ligand-protein interactions.

MMP2 protein and the docking method were validated to ensure the structural integrity of binding pocket and connectedness of the technique, by re-docking the APP-IP ligand into the protein to approve the default parameters. Once the process has been verified, the ergosterol and sterol compound 49 were docked to predict their binding energy and conformations.

3.9   Statistical analysis

All experiments were performed in triplicates. The results were shown as the mean ± Standard Deviation (SD). One-way analysis of variance (ANOVA) analyzed the significant results using SPSS 16.0 software and GraphPad prism followed by a *post hoc* Dunnett's test with * *p* value < 0.05 and ** *p* value < 0.01 were considered as significant results.
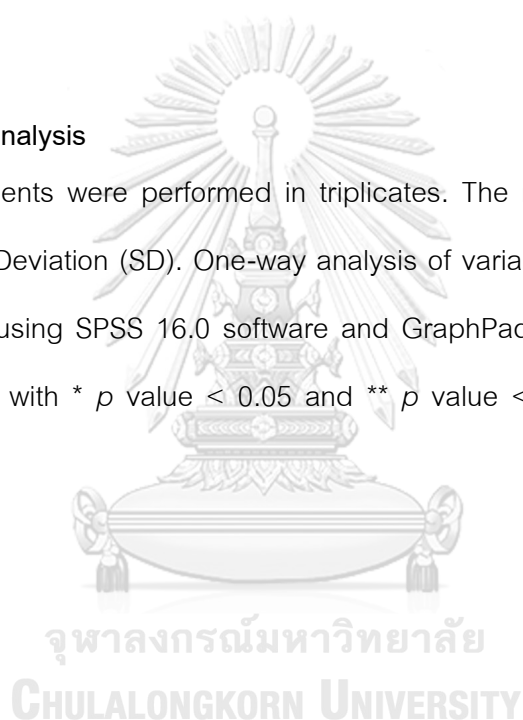
CHAPTER IV RESULTS

4.1 Mushroom identification

Mushroom DNA samples from the mycelium of *Auricularia polytricha* (AP) were extracted and amplified in the *ITS* region. The sequencing was analyzed and showed a nucleotide sequence from the *ITS1* and *ITS4* nucleotide regions (**Table A1, Figure A1 and A2**). The DNA sequence was alignment using the Basic Local Alignment Search Tool (BLAST) search. BLAST is an algorithm that can be used to map by comparing the query biological information such as DNA sequence with a database of sequences. The BLAST analysis showed that the DNA sequences AP in both the *ITS1* and *ITS4* regions are almost closely aligned with that found in the database, as shown in **Table 6**.

Figure 18   The mycelium of mushroom cultivation on potato-dextrose agar (PDA) plates.

Table 6 the BLAST alignment result from mushroom *ITS* amplification.

#	Description	Max Score	Total Score	Query Cover	Ident	Accession
ITS1	*Auricularia polytricha* strain 4328 18S ribosomal RNA gene, partial sequence; internal transcribed spacer 1, 5.8S ribosomal RNA gene, and internal transcribed spacer 2, complete sequence; and 28S ribosomal RNA gene, partial sequence	1048	1048	98%	99.48%	KY345416.1
ITS4	*Auricularia polytricha* strain 610723MF0009 small subunit ribosomal RNA gene, partial sequence; internal transcribed spacer 1, 5.8S ribosomal RNA gene, and internal transcribed spacer 2, complete sequence; and large subunit ribosomal RNA gene, partial sequence	1026	1026	97%	99.13%	KY950445.1

4.2 Mushroom extraction

The ethanol extracts of AP by Soxhlet extraction (APE) and Hexane extract by maceration (APH) percentage yields (%) were calculated based on their weights of crude powder. The percentage of yields in APE found to be 1.493 %, while APH showed 0.36% of yield, as shown in **Table 7**

Table 7   The yield (%) of AP crude extracts

Crude extracts	Yield (%)
APE	1.50
APH	0.36

4.3   Mushroom purification

4.3.1   Gas Chromatography-Mass Spectrometry

The hexane extract (APH) by maceration from AP, in our previous study or the ethanol extract by Soxhlet extraction (APE), was individually dissolved in ethyl acetate and performed GC-MS to determine the chemical components in the extracts. The analytical data of APE and APH are summarized in **Tables 8 and 9**. While the GC chromatograms of APE and APH are presented in **Figure 19** and **Figure 20**, respectively. The GC-MS result from APE and APH showed that ergosterol was the presence in both extracts. However, ergosterol and ergosterol-related compound peaks showed at a retention time of 40.312 (0.97%) and 40.897 (13.79%) minutes, which accounted for approximately 15% of the total peak areas in APE. Whereas ergosterol and ergosterol-related compounds in APH were found at a retention time of 39.91 (3.41%), 40.483 (30.39%), and 40.731 (2.48%) minutes with approximately 36% of combined peak areas in APH.

Palmitic acid, Linoleic acid, and Stearic acid were found to be the presence in APE and APH. However, the percentages of these three fatty acids are comparatively higher in APE than those found in APH (Table 1 and 2).

Also, there are differences in chemical components found in APE and APH. Compounds highlighted in green (Table 1) were only found in APE. While compounds highlighted in purple (Table 2) were only found in APH.
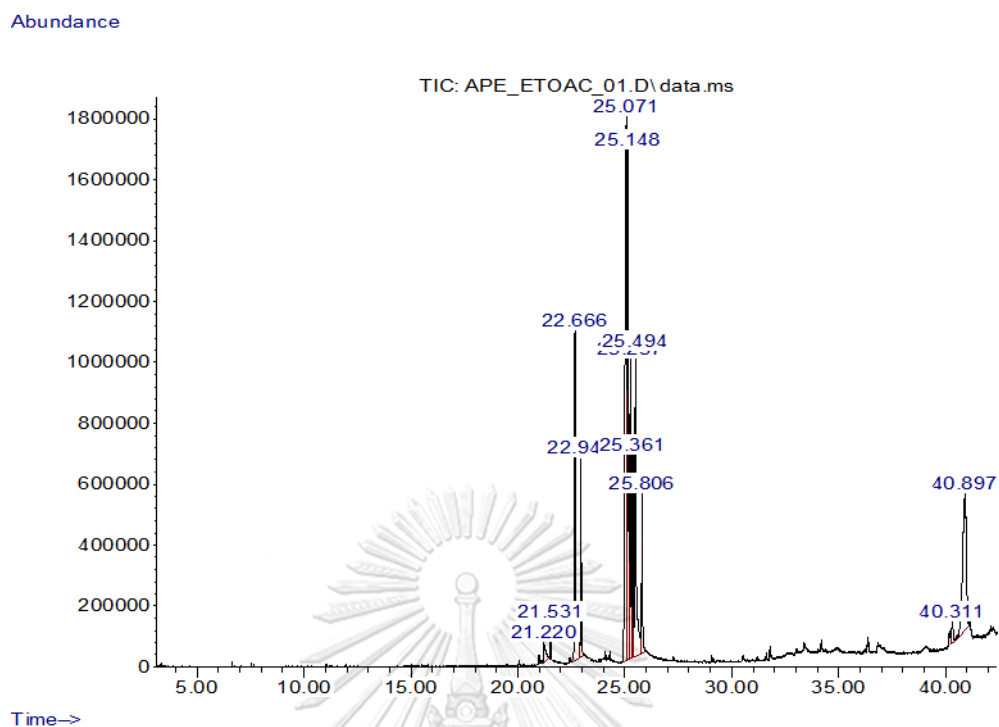
Figure 19   The GC-MS result of the ethanol (APE) extract of AP

Table 8   The GC-MS profile of APE crude extract.

RT (min)	% Area of total	Predicted compound
21.22	1.14%	Pentadecanoic acid
21.53	0.56%	Pentadecanoic acid, ethyl ester
22.666	10.98%	Palmitic acid
22.949	3.54%	Hexadecenoic acid, ethyl ester
25.072	27.62%	Linoleic acid
25.148	13.65%	trans-13-Octadecenoic acid
25.258	7.95%	9,12-Octadecadienoic acid, ethyl ester
25.362	5.23%	Ethyl Oleate
25.494	10.60%	Stearic acid
25.806	3.99%	Octadecanoic acid, ethyl ester

RT (min)	% Area of total	Library best matched
40.312	0.97%	Ergosterol
40.897	13.79%	Ergosterol
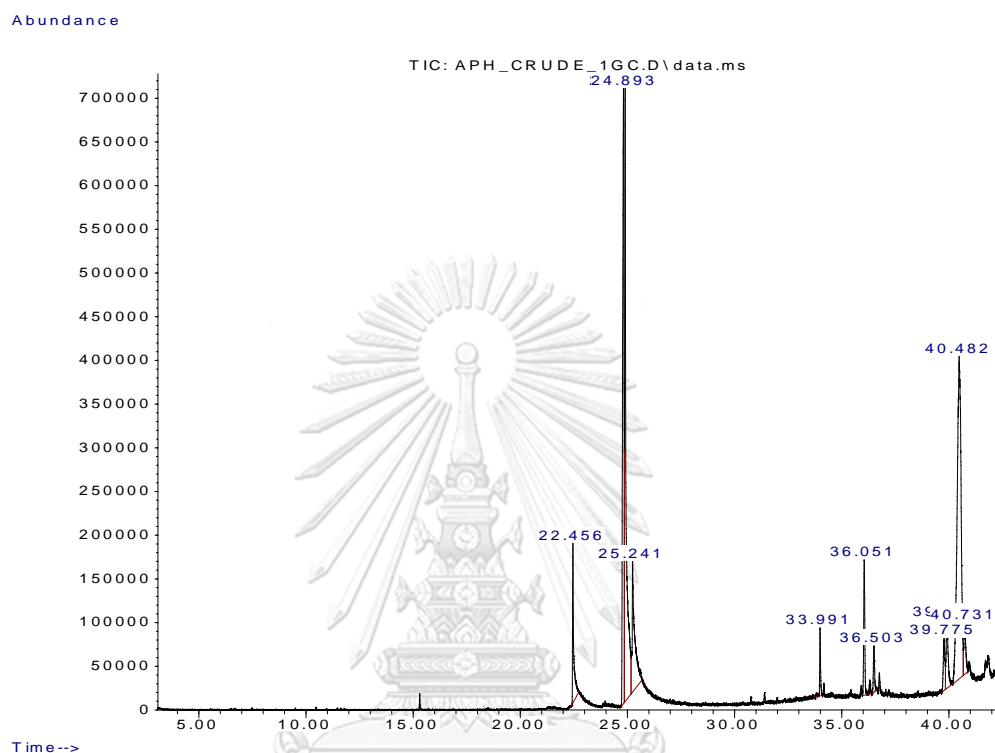
Figure 20   The GC-MS result of the hexane extract of AP

Table 9   The GC-MS profile of APH crude extract.

RT (min)	% Area of total	Library best matched
22.457	4.36%	Palmitic acid
24.813	19.51%	Linoleic acid
24.892	22.84%	Oleic Acid
25.24	8.47%	Stearic acid
33.992	1.54%	Decanedioic acid, bis(2-ethylhexyl) ester
36.05	3.65%	9(11)-Dehydroergosteryl benzoate
36.502	1.38%	Anthiaergostan-5,7,9,16,22-penten
39.775	1.99%	Anthiaergostan-5,7,9,22-tetraen-3-ol

39.91	3.41%	Ergosterol
40.483	30.39%	Ergosterol
40.731	2.48%	Ergosterol

4.3.2 Thin Layer Chromatography (TLC)

The APH crude extract was dissolved in hexane and spotted on the TLC silica plate and developed using a mixed (hexane: ethyl acetate) solvent system, with incremental of polarity. The UV detector at 254 and 365 nm was used to visualize components in APH to reveal four spots. The four spots are referring to F1, F2, F3, and F4 in the order of their polarity. R_f values of each component were calculated. The TLC results showed that the best mobile phase of hexane and ethyl acetate for APH mixture was 80: 20 (hexane: ethyl acetate) (**Figure A3**). All four fractions of the APH mixture appeared and separated in the middle of TLC plates. F1, F2, F3 and F4 R_f values at 80: 20 ratios were 0.95, 0.64, 0.52 and 0.31, respectively. Moreover, other solvent ratios also showed the R_f values and used as a gradient system further purification, and the proper solvent ratios were between 90:10 to 60:40 as listed in (**Table 10**).

Table 10 The R_f values of APH crude extract by TLC.

Solvent ratio	R_f values			
Hexane: Ethyl acetate	F1	F2	F3	F4
100: 0	base-line = 0			
90: 10	0.89	0.35	0.23	0.12
80: 20	0.95	0.64	0.52	0.31
70: 30	0.98	0.83	0.72	0.54
60: 40	0.93	0.83	0.73	0.58

4.3.3   Preparative Liquid Chromatography (PREP-LC)

APH crude (350 mg) was dissolved in hexane for sample preparation. Then the normal stationary phase 24g-cartridge was used in hexane and ethyl acetate system as generated by Navigator software in the machine based on the TLC R_f values (Three components) input. UV detectors at 254 and 365 nm was used to detect the separated fractions. The fractions were collected in the automated fraction collector, and their profile is shown in Figure **21A and 21B**. The pattern of compounds presented in each tube was further analyzed by TLC and shown in **Figure 22**. PREP-LC could separate the total 350 mg of APH mixture and resulted in F1 (71 mg), F2 (23 mg.), F1+F2 (10.8 mg.), F2+F3 (55 mg.), F3+F4 (33.3 mg) and F4 (10 mg) as listed in **Table 11**.

Peak #	Strat Tray : Vial	End Tray : Vial
1	1 : 4	1 : 4
2	1 : 9	1 :9
3	1 : 10	1 : 15
4	1 : 16	1 : 16
5	1 : 17	1 : 17
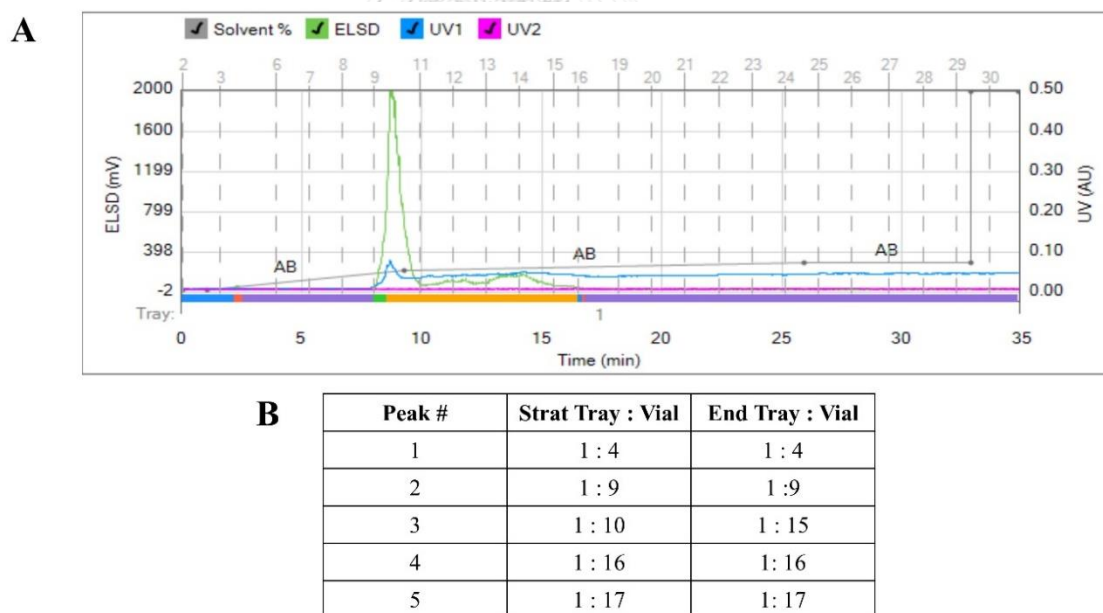
Figure 21   The APH crude mixture separated by Reveleris® PREP-LC.

(A) The chromatogram ; (B) the vial mapping table from the APH separation.
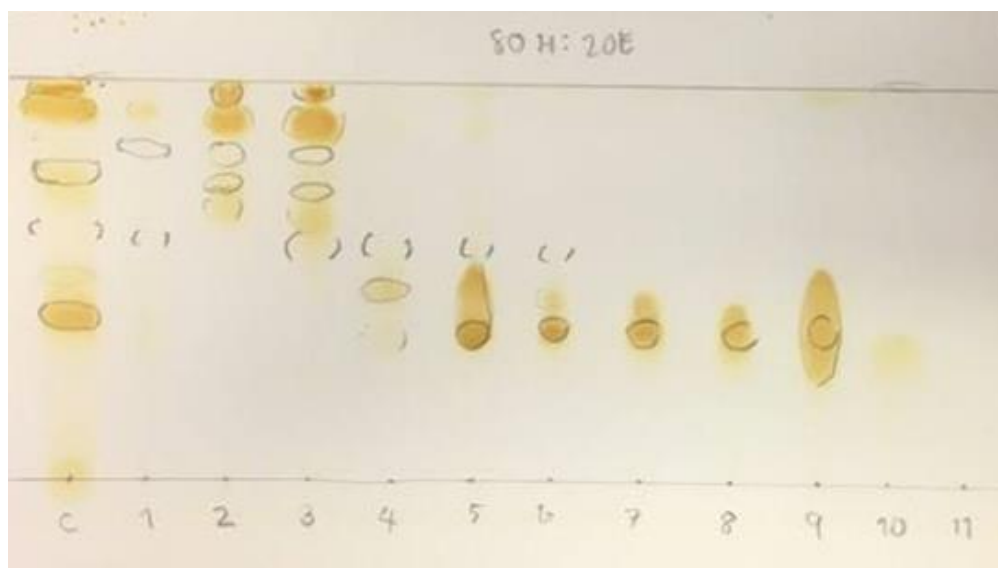
Figure 22 The screened PREP-LC fractions of APH mixture on TLC plates with hexane and ethyl acetate (80: 20) mobile system.

Table 11 The summary of APH fractions separated by PREP-LC.

Fractions	Weight (mg)
F1	71
F2	23
F1+F2	10.8
F2+F3	55
F3+F4	33.3
F4	10

4.3.4 Ergosterol-purified fraction authentication by HPLC

Retention time and characteristics of chromatograms were used to determine the identity of each compound. For instance, the first confirmation of ergosterol was done by correlating the purified-peak with the peak of the authentic ergosterol standard. A second confirmation of ergosterol was done by spiking the purified-ergosterol analyst

with the authentic ergosterol. HPLC chromatograms of the three analyses are shown in Figures 24A-24C. The districted peak of the purified-ergosterol was detected at the retention time of 16.223 min (72.2 mAU) (**Figure 23A**). The peaks for Standard Ergosterol appeared at 16.197 min (41.6 mAU) (**Figure 23B**). While the peaks for the Spiked sample of ergosterol-purified fraction and standard appeared at the same retention time at 16.183 min (33.9 mAU) (**Figure 23C**). Therefore, the purified-ergosterol fraction from APH using Preparative LC was successful separated and is the same as the ergosterol standard purchased from Sigma-Aldrich.
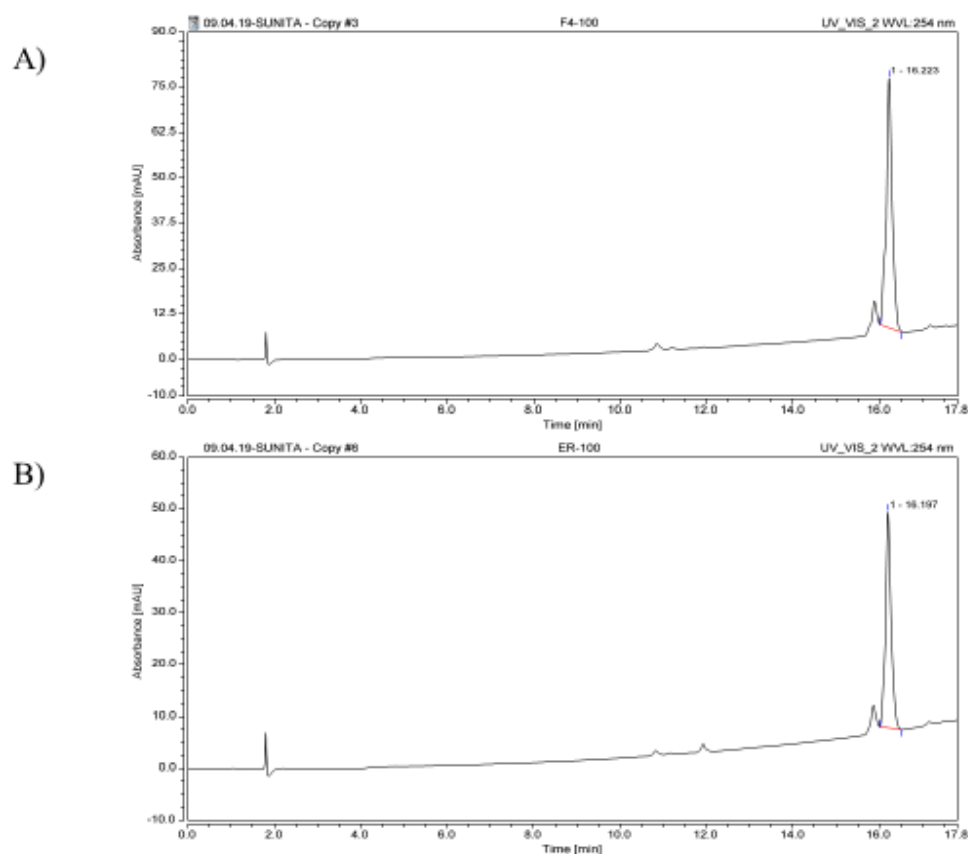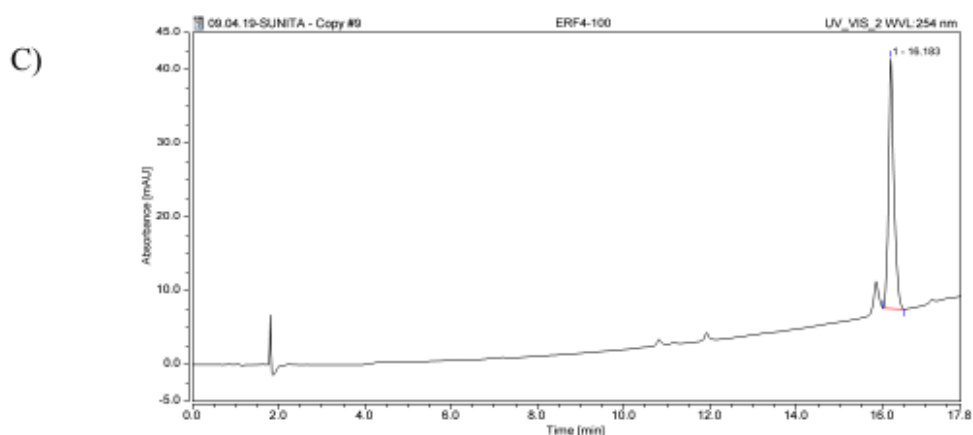
Figure 23 HPLC chromatogram of Ergosterol.

(A) HPLC Chromatogram of the purified-ergosterol fraction of AP at 100 ppm; (B) Standard Ergosterol at 100 ppm; C) Spiked sample of ergosterol-purified fraction and standard.

4.4. Antiproliferative screening on cancer cell lines

4.4.1 Antiproliferative screening of APE and APH

The antiproliferative screening on cancer cell lines was performed in Hepatocellular carcinoma cell line (HepG2), Breast cancer cell lines (MCF-7 and MDA-MB-231). The concentration range for testing with APE and APH is 0.03 – 1.00 mg/mL, while the positive controld drug (DOX) was 0.06 – 2.00 nM. The cells were treated with either APE, APH, or DOX for 24, 48 and 72 hours. At 24 hours, the IC_{50} values were determined and resulted showed that APH exerted more active effected on all cancer cell lines than APE (HepG2, MCF-7, and MDA-MB-231) with IC_{50} at 0.06 ± 0.02, 0.06 ± 0.01 and 0.02 ± 0.01 mg/mL, respectively. Whereas, the IC_{50} values of APE in HepG2, MCF-7 and MDA-MB-231 cell lines at 24 hours showed the doses at 0.59 ± 0.14, 0.25 ± 0.33, and 0.03 ± 0.00 mg/mL shown in **Figure 24, 25, and 26**, respectively. The determined IC_{50} values at 48 hours and 72 hours also showed significantly inhibited cell

survival, as shown in **Table 12**. Therefore, APH was selected to study in their isolated fractions and further investigation on antitumor effect.

Table 12 The IC_{50} values of APE, APH, and DOX against HepG2, MCF-7, and MDA-MB-231 cell lines.

Treatments		Time		
		24 h	48 h	72 h
HepG2	APE (mg/ml)	$0.59 \pm 0.14^{**}$	$0.28 \pm 0.07^{**}$	$0.18 \pm 0.02^{**}$
	APH (mg/ml)	$0.06 \pm 0.02^{**}$	$0.07 \pm 0.01^{**}$	$0.06 \pm 0.00^{**}$
	DOX (µM)	$0.48 \pm 0.06^{**}$	$0.29 \pm 0.03^{**}$	$0.14 \pm 0.01^{**}$
MCF-7	APE (mg/ml)	$0.25 \pm 0.33^{**}$	$0.11 \pm 0.03^{**}$	$0.08 \pm 0.03^{**}$
	APH (mg/ml)	$0.06 \pm 0.01^{**}$	$0.12 \pm 0.05^{**}$	$0.08 \pm 0.01^{**}$
	DOX (µM)	$0.46 \pm 0.07^{**}$	$0.28 \pm 0.05^{**}$	$0.24 \pm 0.03^{**}$
MDA-MB-231	APE (mg/ml)	$0.03 \pm 0.00^{**}$	$0.02 \pm 0.01^{**}$	$0.05 \pm 0.00^{**}$
	APH (mg/ml)	$0.02 \pm 0.01^{**}$	$0.02 \pm 0.00^{**}$	$0.02 \pm 0.03^{**}$
	DOX (µM)	> 2.00	$0.64 \pm 0.14^{**}$	$0.39 \pm 0.12^{**}$
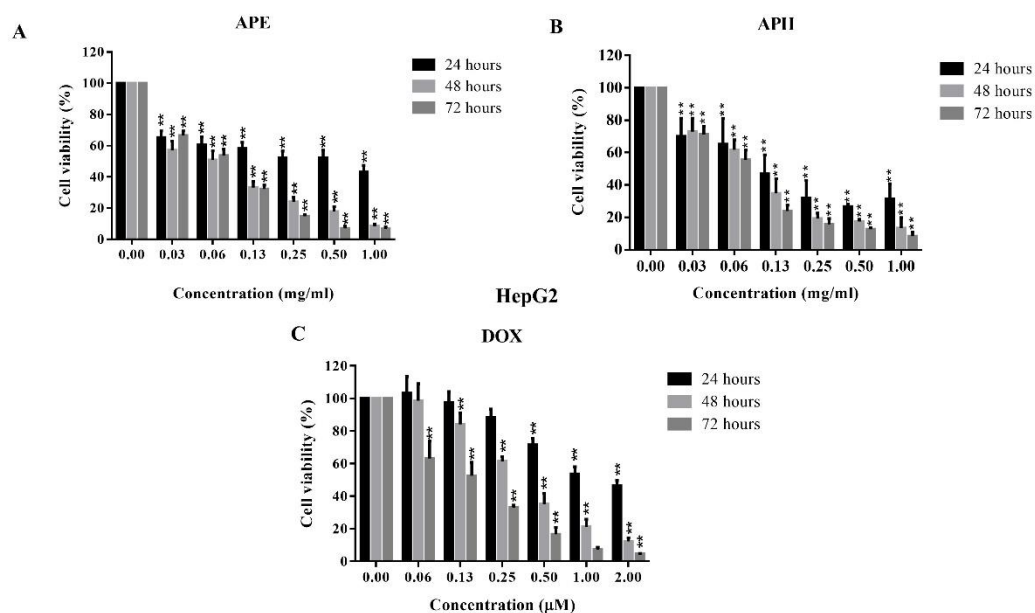
Figure 24   The HepG2 cell viability after APE, APH, and DOX treatments.

(A) APE, (B) APH, and (C) DOX treatments at 24, 48, and 72 hours. Data are shown in mean ± SD (n = 3 independent experiments). Dunnett's one-way ANOVA analysis with * p value < 0.05 and ** p value < 0.01 were considered significant, compared to the vehicle control (0.1% DMSO).
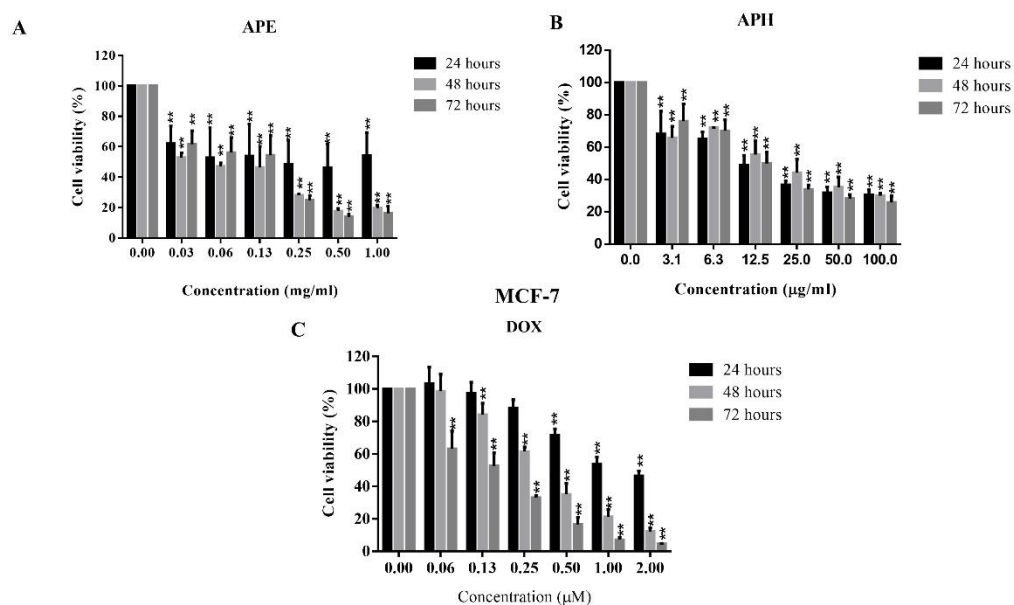
Figure 25   The MCF-7 cell viability after APE, APH, and DOX treatments.

(A) APE, (B) APH, and (C) DOX treatments at 24 hours. Data shown in mean ± SD (n = 3 independent experiments). Dunnett's one-way ANOVA analysis with * p value < 0.05 and ** p value < 0.01 were considered significant, compared to the vehicle control (0.1% DMSO).
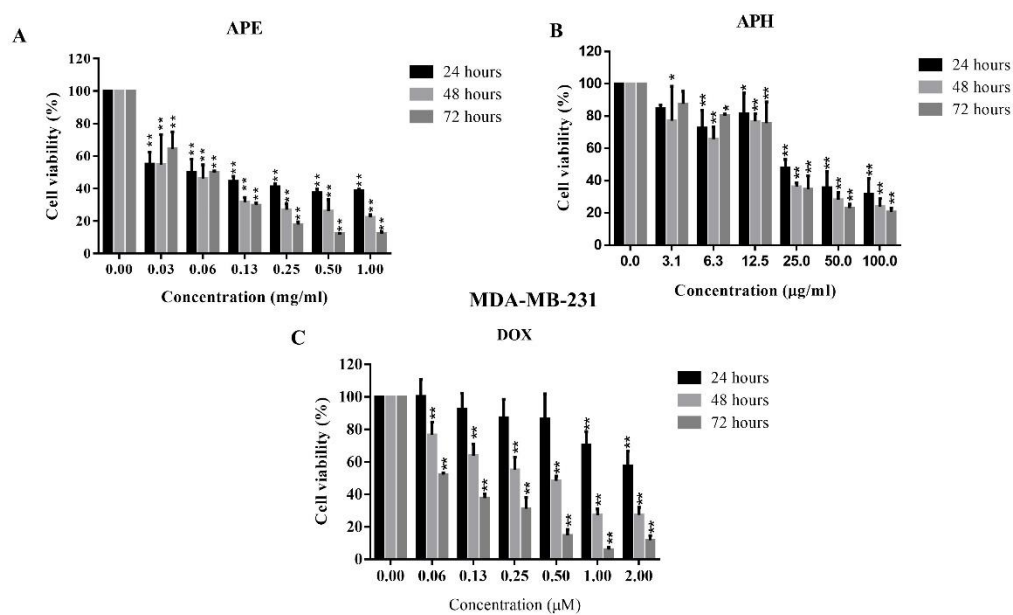
Figure 26   The MDA-MB-231 cells after APE, APH, and DOX treatments.
(A) APE, (B) APH, and (C) DOX treatments at 24, 48, and 72 hours. Data are shown in mean ± SD (n = 3 independent experiments). Dunnett's one-way ANOVA analysis with * p value < 0.05 and ** p value < 0.01 were considered significant, compared to the vehicle control (0.1% DMSO).

4.4.2   The isolated fractions of APH inhibit cancer cell growth

The four isolated fractions of APH (F1, F2, F3, and Ergosterol) were individually tested for cell growth inhibition on breast cancer cell lines (MCF-7 and MDA-MB-231) (**Figure 27 and 28**). After 48 hours of incubation, ergosterol (F4, ER) showed growth inhibition on MCF-7 and MDA-MB-231 cells with the IC_{50} valued at 48 hours were 24.49 ± 17.94 and 6.55 ± 2.59 μM, respectively, as shown in **Table 13**. Ergosterol was also

tested with HepG2 cells. However, IC_{50} value was higher than 50 μM, the highest possible concentration of ER solubilized in the tested solvent **(Figure 29)**. Therefore, further investigation for the effect of APH and ER for antitumor activities was focusing on MCF-7 and MDA-MB-231. Therefore, we tested ER at 6, 12, and 25 μM, while APH tested at 12, 25 and 50 μg/ml.

Table 13 The IC_{50} values of ergosterol treatments on HepG2, MCF-7, and MDA-MB-231 cell lines.

Treatments		Time		
		24 h	48 h	72 h
Ergosterol (μM)	HepG2	> 50	> 50	> 50
	MCF-7	> 50	$24.49 \pm 17.94^{**}$	$17.67 \pm 8.80^{**}$
	MDA-MB-231	$> 50^{**}$	$6.55 \pm 2.59^{**}$	> 50
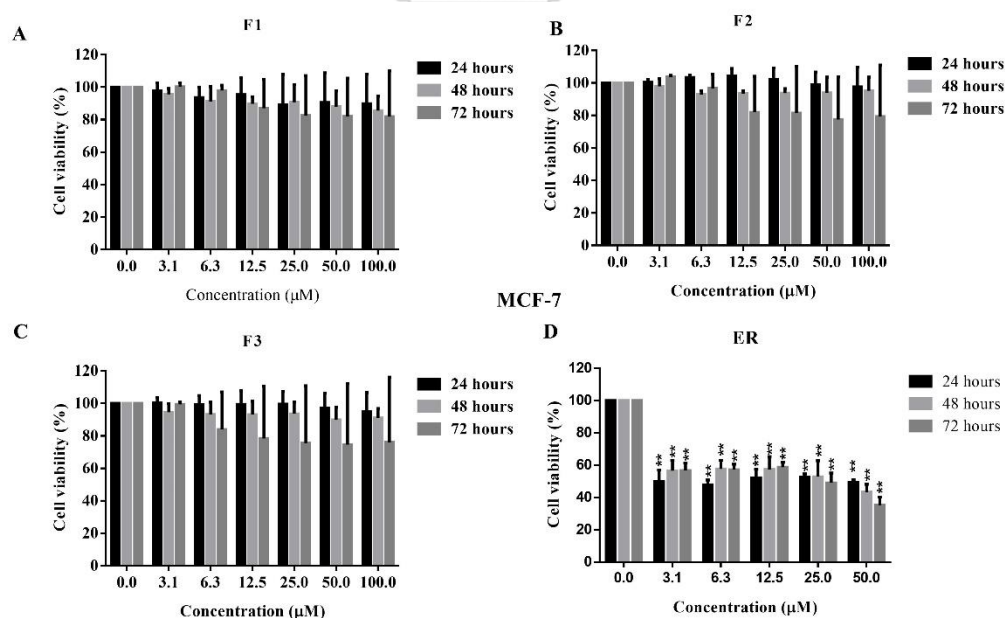
Figure 27 The MCF cell viability after F1, F2, F3 and ER treatments.

(A) F1, (B) F2, (C) F3, and (D) F4 or Ergosterol treatments at 24, 48, and 72 hours.

Data are shown in mean ± SD (n = 3 independent experiments). Dunnett's one-way ANOVA analysis with * *p* value < 0.05 and ** *p* value < 0.01 were considered significant, compared to the vehicle control (0.1% DMSO).
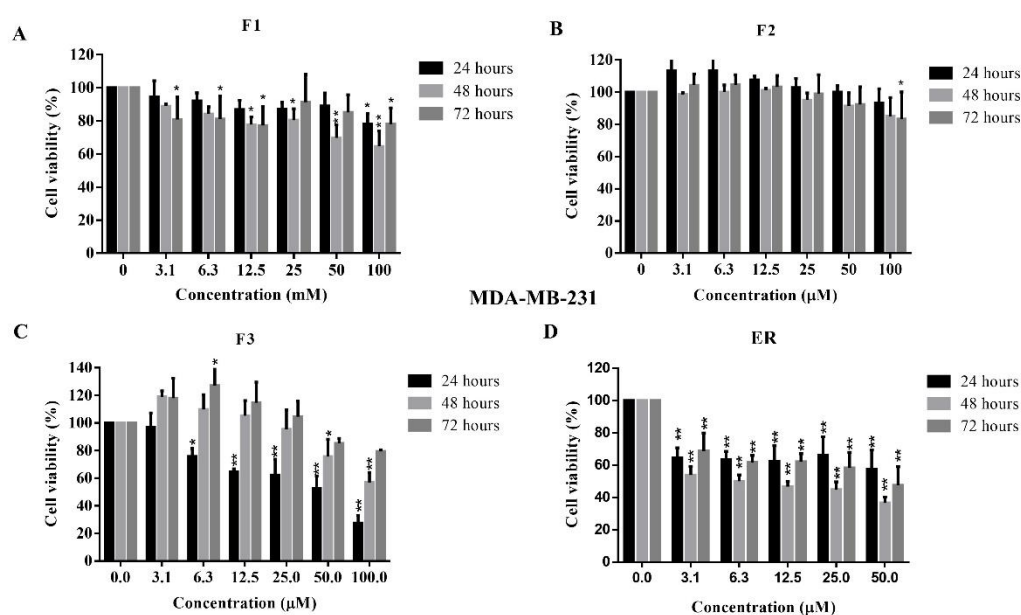
Figure 28   The MDA-MB-231 cell viability with F1, F2, F3 and ER treatments.
A) F1, (B) F2, (C) F3, and (D) F4 or Ergosterol treatments at 24, 48, and 72 hours. Data are shown in mean ± SD (n = 3 independent experiments). Dunnett's one-way ANOVA analysis with * p value < 0.05 and ** p value < 0.01 were considered significant, compared to the vehicle control (0.1% DMSO).
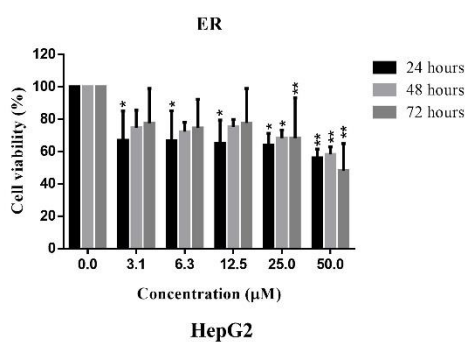
Figure 29   The HepG2 cell viability after ER treatment.

Data are shown in mean ± SD (n = 3 independent experiments). Dunnett's one-way ANOVA analysis with * p value < 0.05 and ** p value < 0.01 were considered significant, compared to the vehicle control (0.1% DMSO).

4.4.3   Cytotoxicity test on 3T3-L1 cell line

The cytotoxicity of treatments (APH, Ergosterol, Doxorubicin, and Batimastat) was performed on mouse fibroblast 3T3-L1 cell line. The results indicated that APH has no toxicity against the 3T3-L1 at 24 hours incubation. However, APH showed inhibition of 3T3-L1 cell growth with the IC_{50} at 54.18 ± 4.01 and 29.47 ± 7.38 µg/ml after 48 hours and 72 hours, respectively. While ergosterol time showed IC_{50} values toxicity at 13.53 ± 0.51 µM and 23.54 ± 3.14 µM after 24 h and 48 h, respectively. However, ergosterol after 72 hours incubation time, Doxorubicin, and Batimastat were unable to be determined IC_{50} values as shown in **Table 14** and **Figure 30**.

Table 14   The IC_{50} values of APH, ER, Batimastat, and DOX treatments on the 3T3-L1 cell line.

Treatments		24 h	Time 48 h	72 h
3T3-L1	APH (µg/ml)	> 100	54.18 ± 4.01[**]	29.47 ± 7.38[**]
	ER (µM)	13.53 ± 0.51[**]	23.54 ± 3.14[**]	> 50
	DOX (nM)	> 0.5	> 0.5	> 0.5
	BB (µM)	> 10	> 10	> 10
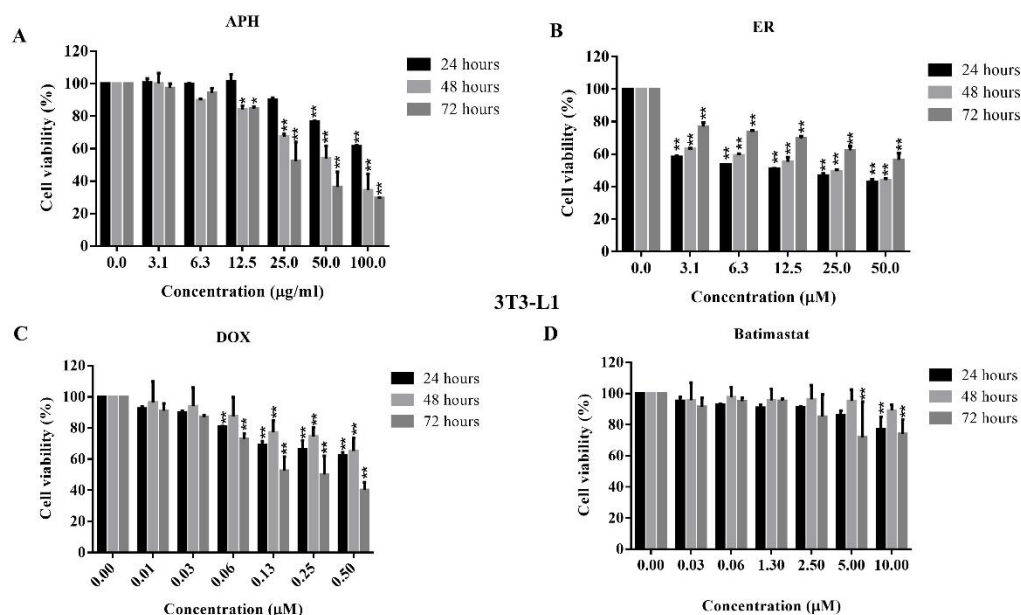
Figure 30   The 3T3-L1 cell viability with APH, ER, DOX, and BB treatments.
(A) APH, (B) ER, (C) DOX, and (D) Batimastat treatments for 24, 48, and 72 hours. Data are shown in mean ± SD (n = 3 independent experiments). Dunnett's one-way ANOVA analysis with * p value < 0.05 and ** p value < 0.01 were considered significant, compared to the vehicle control (0.1% DMSO).

4.5   AP extracts and ergosterol induced apoptosis on cancer cell lines

The study of apoptosis induction on HepG2 cell line was carried out by compared the annexin V positive cells between the APE (0.03,0.13 and 0.50 mg/ml), APH (0.03,0.13 and 0.50 mg/ml), and DOX (0.03,0.13 and 0.50 μM) treatments to the vehicle control, which was the 0.1% DMSO control. The results from HepG2 cells showed that APE was induced apoptosis at 0.13 (39.88 ± 1.95%) and 0.50 mg/ml (43.78 ± 0.00%) while APH was induced apoptosis at 0.50 mg/ml (50.24 ± 0.00%). DOX as the positive control also showed the percentage of apoptosis at 48.25 ± 0.00% as shown in **Table 15** and **Figure 31**. This showed that APH at same amount with APE showed more apoptosis effect to HepG2 cells., Ergosterol was excluded from apoptosis and cell cycle

assays due to the low sensitive towards HepG2 cell which could not determine the IC_{50} value from the cell viability.

On the other hand, apoptosis results from MCF-7 and MDA-MB-231 cell lines were carried out by annexin V-FITC/PI. The annexin V positive cells or apoptotic cells induced by the APH, ER, and DOX and vehicle control (0.1% DMSO) treatments were compared. After the 24hours-incubation, The ER (6, 12, and 25 µM) showed a dose-dependent manner result in MDA-MB-231 at 7.71 ± 2.14, 22.73 ± 11.59, and 37.21 ± 2.59 %, respectively. While in MCF-7 -MB-231 cells with ER showed significant results in all concentrations but not in dose-dependent. Moreover,.APH (12, 25, and 50 µg/ml) showed the significant results in all concentrations as well as DOX at 125 and 250 nM in both MCF-7 (**Figure 32**) and MDA-MB-231 cell lines (**Figure 33)** Summuarized data were shown in **Table 16**.

In summary, APE, APH and DOX was induced early apoptosis in HepG2 cells. Moreover, APH, ER and DOX were also significantly induced early apoptosis in all three cancer cell lines (HepG2, MCF-7 and MDA-MB-231).

Table 15   The percentage of apoptosis-induced cells with APE, APH, and DOX treatments on HepG2 cell line.

Treatments		HepG2		
		Early	Late	Annexin V
DMSO		3.76 ± 1.90	11.5 ± 3.42	15.65 ± 12.45
APE	0.03 mg/ml	5.64 ± 3.93	14.06 ± 3.07	15.70 ± 11.02
	0.13 mg/ml	7.34 ± 5.08	17.06 ±7.78	39.88 ± 1.95[*]
	0.50 mg/ml	9.02 ± 4.14	25.57 ± 2.56	43.78 ± 0.00[**]
APH	0.03 mg/ml	16.66 ± 890	5.00 ± 2.12	21.66 ± 12.93
	0.13 mg/ml	17.48 ± 3.42	6.66 ± 1.59	24.14 ± 13.05

	0.50 mg/ml	34.19 ± 6.41[*]	10.86 ± 8.01	50.24 ± 0.00[**]
	0.03 µM	13.48 ± 7.24	12.64 ± 4.68	32.46 ± 6.85
DOX	0.13 µM	7.85 ± 4.86	14.43 ± 2.25	35.42 ± 6.41
	0.50 µM	9.49 ± 3.30	27.42 ± 11.98	48.25 ± 0.00[**]

จุฬาลงกรณ์มหาวิทยาลัย

CHULALONGKORN UNIVERSITY
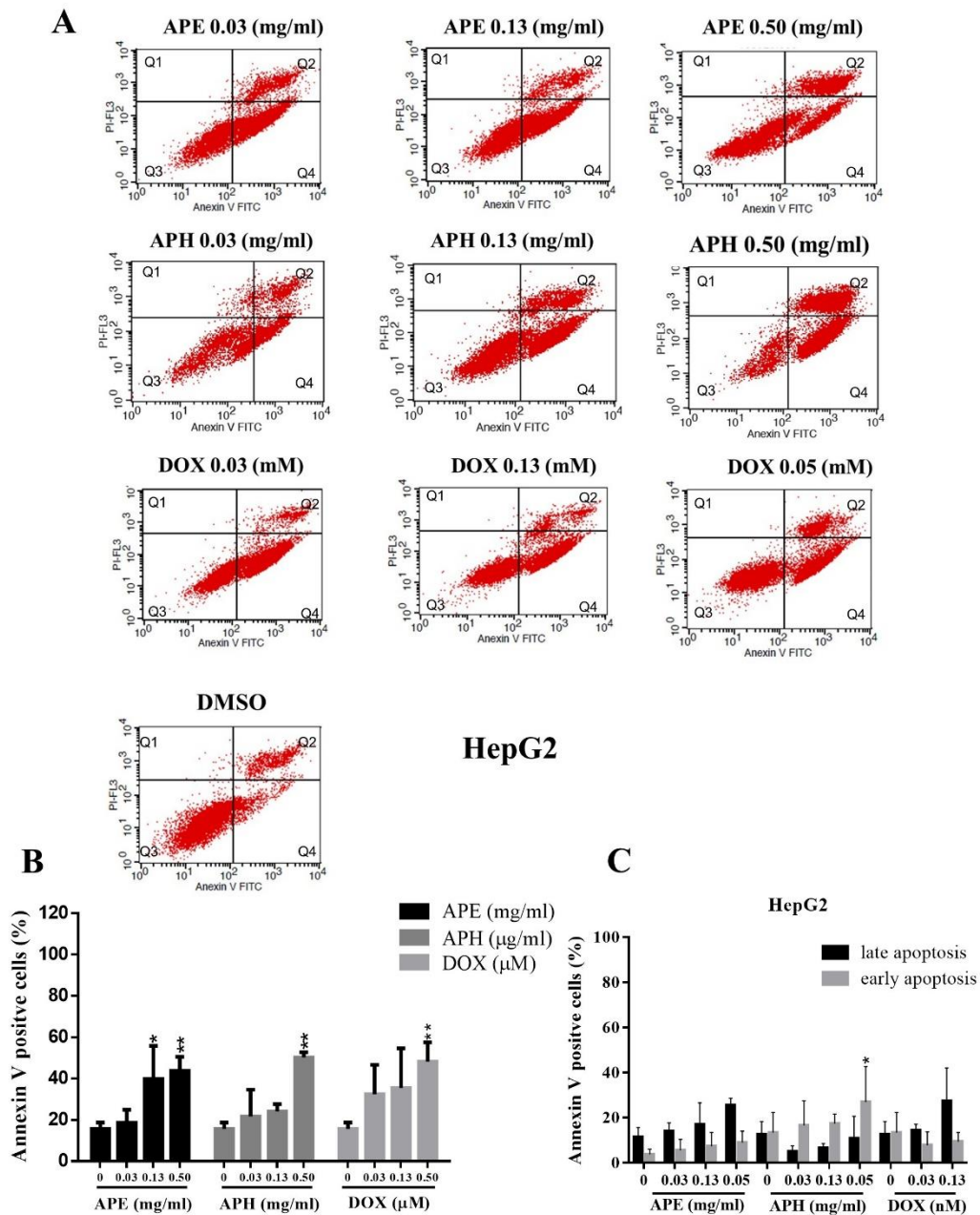
Figure 31   The HepG2 Annexin V positive cells with APE, APH, and DOX treatments.

(A) The results from the flow cytometry after 24 hours. Q1 = dead or necrosis cells, Q2 = late apoptosis cells, Q3 = live cells, and Q4 = early apoptosis cells. (B) Population of apoptotic cells. (C) Population of early and late apoptotic cells. The results were carried out in mean ± SD (n = 3 independent experiments). Dunnett's one-way ANOVA analysis

with * *p* value < 0.05 and ** *p* value < 0.01 were considered significant, compared to the vehicle control (0.1% DMSO).

Table 16   The apoptosis-induced cells with APH, ER, and DOX treatments

Treatments		MCF-7			MDA-MB-231		
		Early	Late	Annexin V	Early	Late	Annexin V
DMSO control		1.52 ± 0.60	5.23 ± 1.00	6.75 ± 1.30	1.96 ± 0.93	2.95 ± 0.28	4.91 ± 0.99
ER (µM)	6	25.73 ±12.64**	4.95 ± 1.78	30.68±8.8*	5.3± 2.54**	2.36 ± 5.35	7.71 ± 2.14
	12	35.07 ± 9.29**	3.41 ± 1.39	38.48 ±6.45**	19.22 ± 14.29**	3.51 ± 0.09	22.73 ± 11.59**
	25	26.64 ± 2.87**	4.74 ± 0.42	31.38 ± 2.00*	33.52 ± 2.35**	3.69 ± 0.83	37.21 ± 2.59
APH (µg/ml)	12	32.12 ± 1.92**	2.9 ± 0.26	35.02 ± 1.36*	31.77 ± 0.09**	2.07 ± 0.20	33.96 ± 0.33
	25	33.51 ± 2.27**	3.29 ± 0.42	36.8 ±2.19*	36.90 ± 0.38**	2.41 ± 0.17	38.91 ± 0.49**
	50	30.51 ± 2.71**	5.46 ± 1.77	35.97 ± 3.65*	31.10 ± 0.65**	2.12 ± 0.27	33.15 ± 0.70
DOX (nM)	125	31.39 ± 3.70**	3.99 ± 0.09	35.37 ± 3.09*	38.86 ± 1.46**	3.11 ± 0.60	41.99 ± 0.73**
	250	36.00 ± 0.79**	3.49 ± 0.46	36.49 ± 1.02**	41.84 0.99**	1.77 ± 0.02	43.91 ± 1.07**

จุฬาลงกรณ์มหาวิทยาลัย
CHULALONGKORN UNIVERSITY
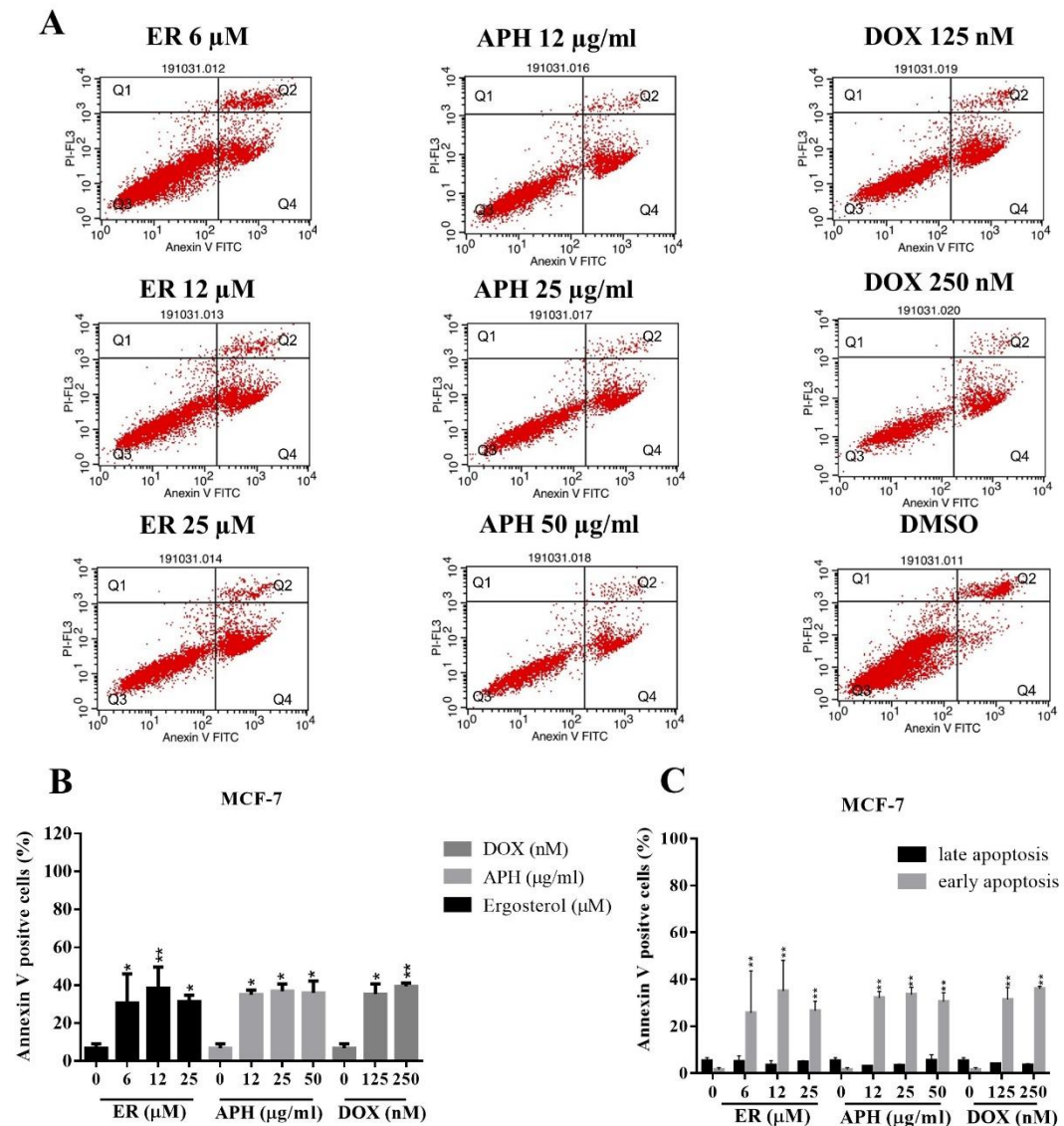
Figure 32 The MCF-7 Annexin V positive cells with APH, ER, and DOX treatments. (A) The results from the flow cytometry after 24 hours. Q1 = dead or necrosis cells, Q2 = late apoptosis cells, Q3 = live cells, and Q4 = early apoptosis cells. (B) Population of apoptotic cells. (C) Population of early and late apoptotic cells. The results were carried out in mean ± SD (n = 3 independent experiments). Dunnett's one-way ANOVA analysis with * p value < 0.05 and ** p value < 0.01 were considered significant, compared to the vehicle control (0.1% DMSO).
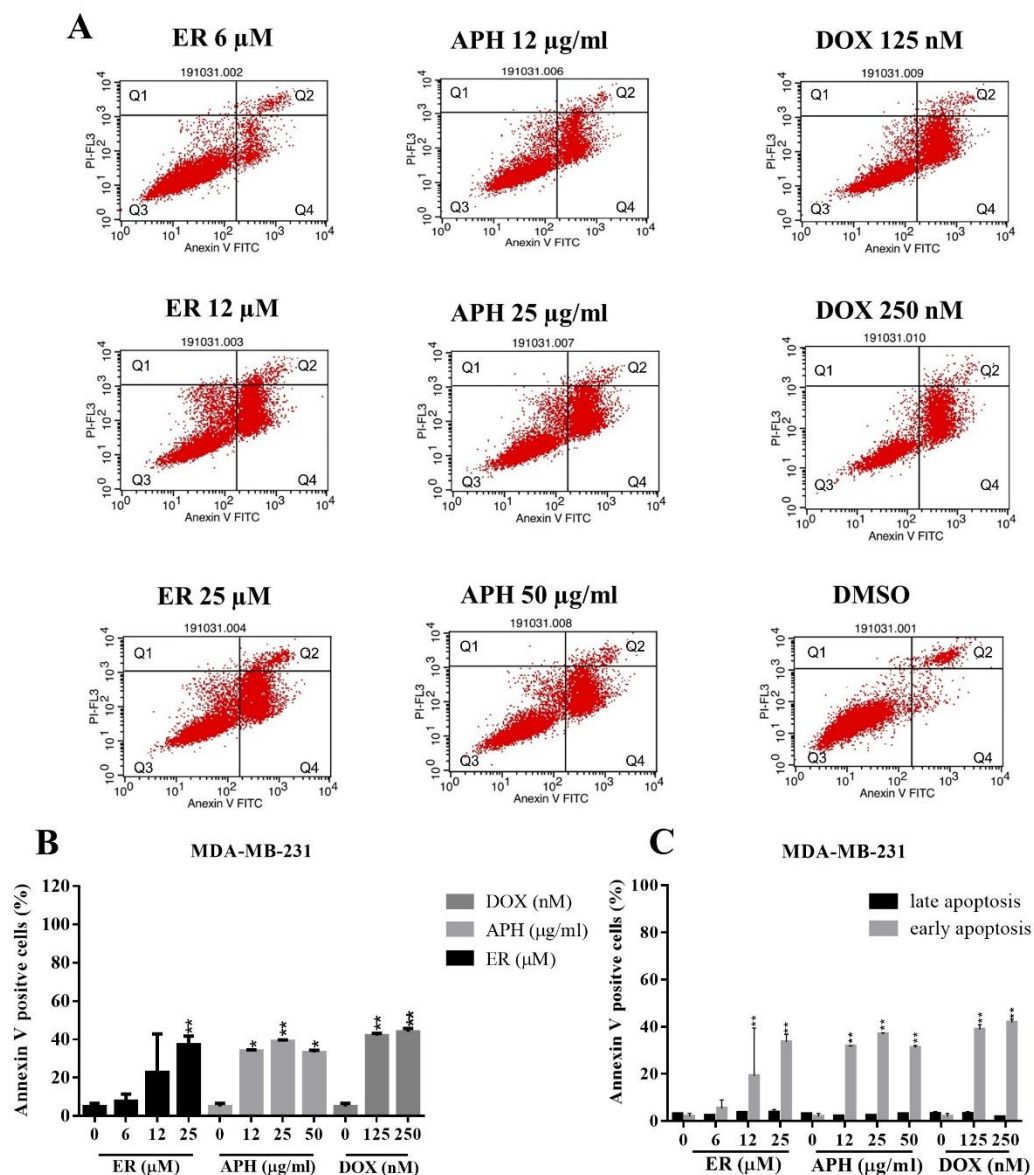
Figure 33   The MDA-MB-231 Annexin V positive cells with APH, ER, and DOX treatments.

(A) The results from the flow cytometry after 24 hours. Q1 = dead or necrosis cells, Q2 = late apoptosis cells, Q3 = live cells, and Q4 = early apoptosis cells. (B) Population of apoptotic cells. (C) Population of early and late apoptotic cells.The results were carried out in mean ± SD (n = 3 independent experiments). Dunnett's one-way ANOVA analysis with * p value < 0.05 and ** p value < 0.01 were considered significant, compared to the vehicle control (0.1% DMSO).

4.6 AP extracts and ergosterol could not arrest the cell cycle in cancer cell lines

The cell cycle arrest capacity of AP extracts and Ergosterol determined by DNA content staining by propidium iodide, and the cell population in each phase was compared to the vehicle control cells. In HepG2 cell line, the IC_{50} values at 72 hours of APE (0.20 mg/ml) and APH (0.06 mg/ml) were selected for cell cycle arrest study and DOX at 0.50 µM was selected as a positive control. We observed at 24, 48 and 72 hour and found that APE and APH treatments showed no inhibition to the cell cycle process at all time points excepted DOX that showed the inhibition at the G2/M phase for 24 hours as shown in **Figure 34**.

This result from HepG2 cell line leading us to focus on the dose-dependent manners of APH and Ergosterol in MCF-7 and MDA-MB-231 cell lines. So, after that the cell cycle assay were performed at concentration that covered the IC_{50} value at 24 hours. As shown in **Figures 35 and 36**, APH showed slightly induced cell cycle arrest on MCF-7 and MDA-MB-231 cells at the G0/G1 in a dose-dependent manner. While ergosterol showed no significantly different from vehicle control, both cell lines used doxorubicin as the positive control at the G2/M phase.

Therefore, the cell cycle assay with APE and APH treatments showed no significant in HepG2 cells. Besides, APH and Ergosterol in MCF-7 and MDA-MB-231 cells also showed no arrest to the cell cycle assay.
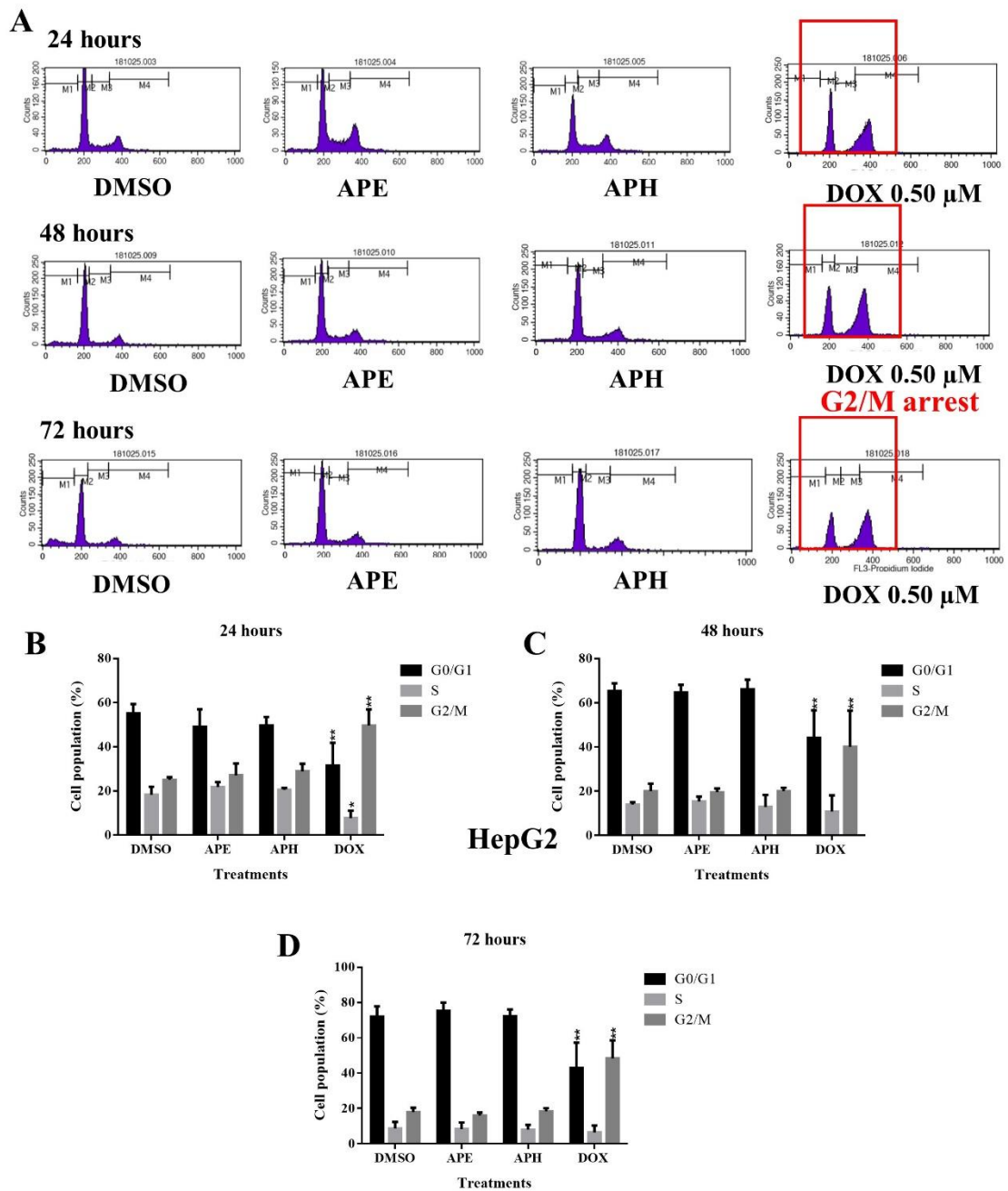
Figure 34   The HepG2 cell cycle population with APE, APH, and DOX treatments.

(A) the cell cycle histogram after 24, 48 and 72 hours. (B), (C), and (D) Population of cells in each phase at 24, 48, and 72 hours, respectively. The results were carried out in mean ± SD (n = 3 independent experiments). Dunnett's one-way ANOVA analysis with * p value < 0.05 and ** p value < 0.01 were considered significant, compared to the vehicle control (0.1% DMSO).
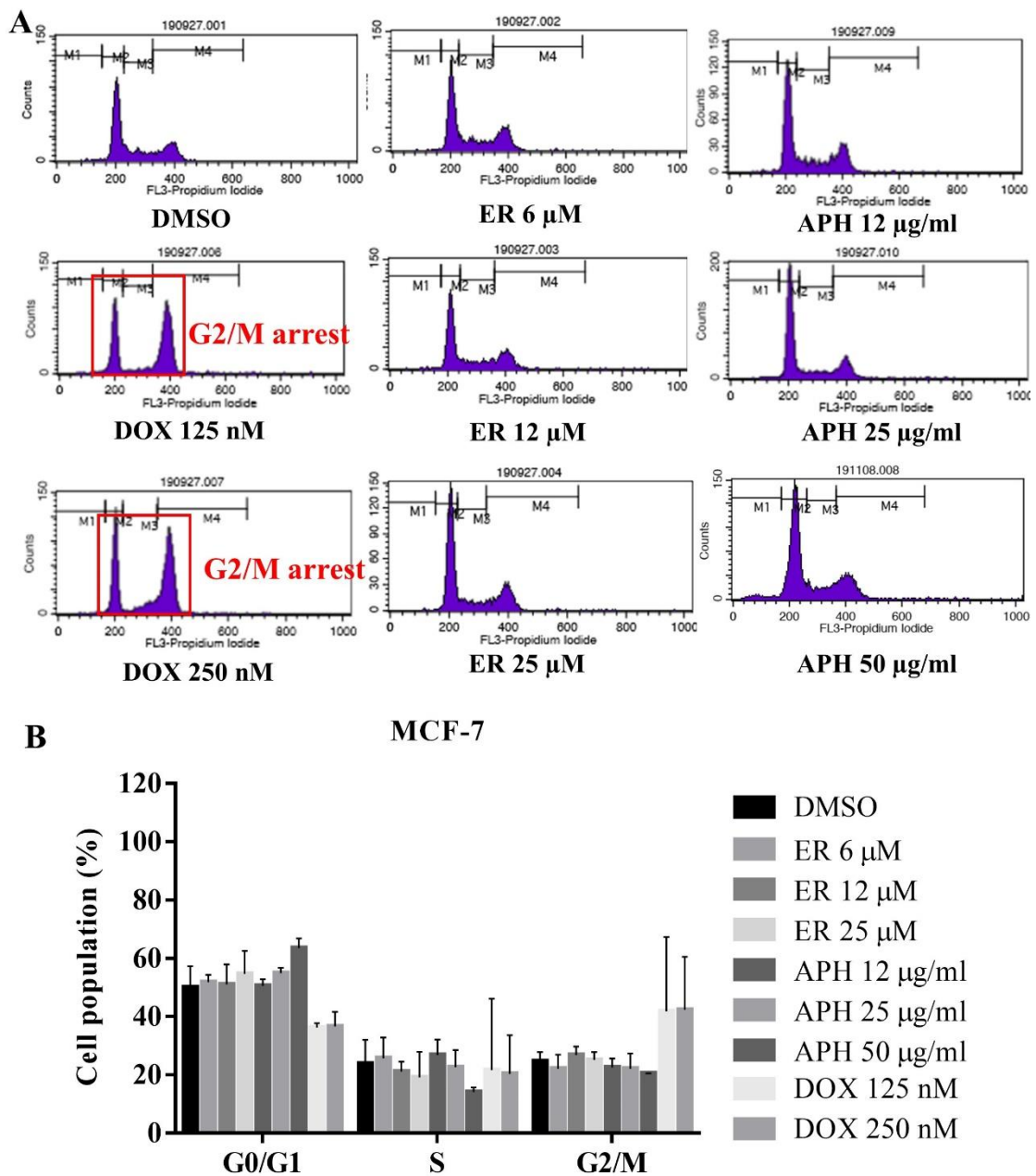
Figure 35   The MCF-7 cell cycle population with APH, ER, and DOX treatments. (A) the cell cycle histogram after 24, 48 and 72 hours. (B), (C), and (D) Population of cells in each phase at 24, 48, and 72 hours, respectively. The results were carried out in mean ± SD (n = 3 independent experiments). Dunnett's one-way ANOVA analysis with * p value < 0.05 and ** p value < 0.01 were considered significant, compared to the vehicle control (0.1% DMSO).
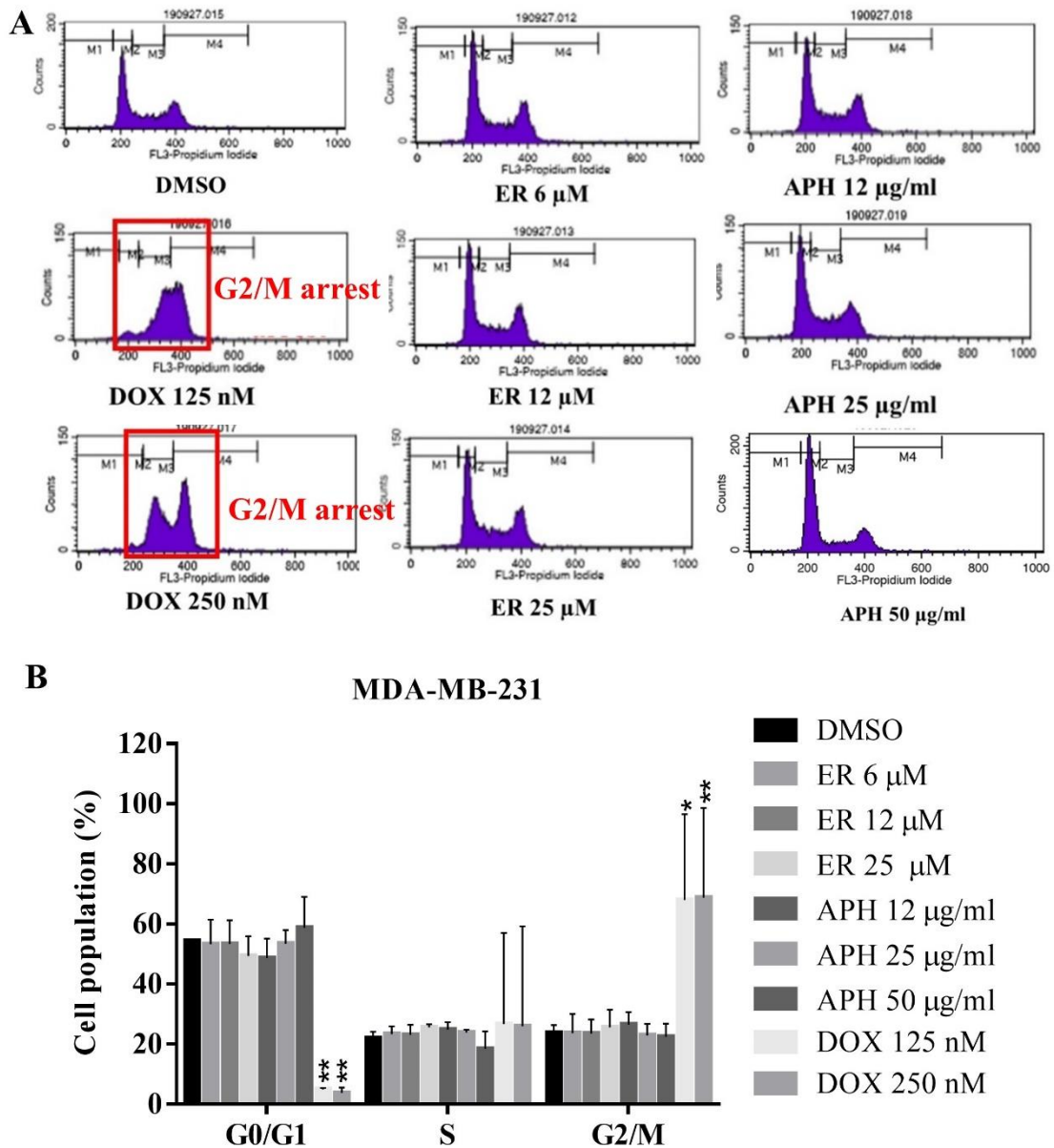
Figure 36   The MDA-MB-231 cell cycle with APH, ER, and DOX treatments.

(A) the cell cycle histogram after 24, 48 and 72 hours. (B), (C), and (D) Population of cells in each phase at 24, 48, and 72 hours, respectively. The results were carried out in mean ± SD (n = 3 independent experiments). Dunnett's one-way ANOVA analysis with * p value < 0.05 and ** p value < 0.01 were considered significant, compared to the vehicle control (0.1% DMSO).

4.7   Migratory inhibition effect of APH and ergosterol on cancer cell lines

The ability of APH to inhibit cancer cell migration was tested on HepG2 and MCF-7 with 24 hours incubation times. Whereas, MDA-MB-231 was determined the migration rate at 6 hours. The shorter migration time was used because of MDA-MB-231 higher growth rate. Batimastat (BB), known as the MMP-2 and MMP-9 metalloproteinase inhibitor, and has been known to be used in migration and invasion assay as a positive control. In this study, Batimastat was used at a concentration of 10 µM.

The results showed that at high dose APH (50 µg/ml) and ER (25 µM) inhibited the wound closure more than low doses as described in **Table 17** in all cell lines, as showed in **Figure 37,38, and 39**.

Table 17   The percentage of wound closure after APH, ER, and BB treatments.

Treatments	Wound closure (%)		
	HepG2 (24 h.)	MCF-7 (24 h.)	MDA-MB-231 (6 h.)
DMSO	7.51 ± 5.31	40.26 ± 3.85	52. 80 ± 2.68
BB 10 µM	11.49 ± 8.25	11.60 ± 5.65**	46.61 ± 4.96
ER 12 µM	19.98 ± 6.51	16.81 ± 3.21**	49.02 ± 1.24
ER 25 µM	9.32 ± 6.77	8.99 ± 3.63**	46.17 ± 5.72
APH 25 µg/ml	18.39 ± 10.52	55.72 ± 2.11**	55.07 ± 4.25
APH 50 µg/ml	13.12 ± 7.40	10.60 ± 3.85**	39.60 ± 2.94*
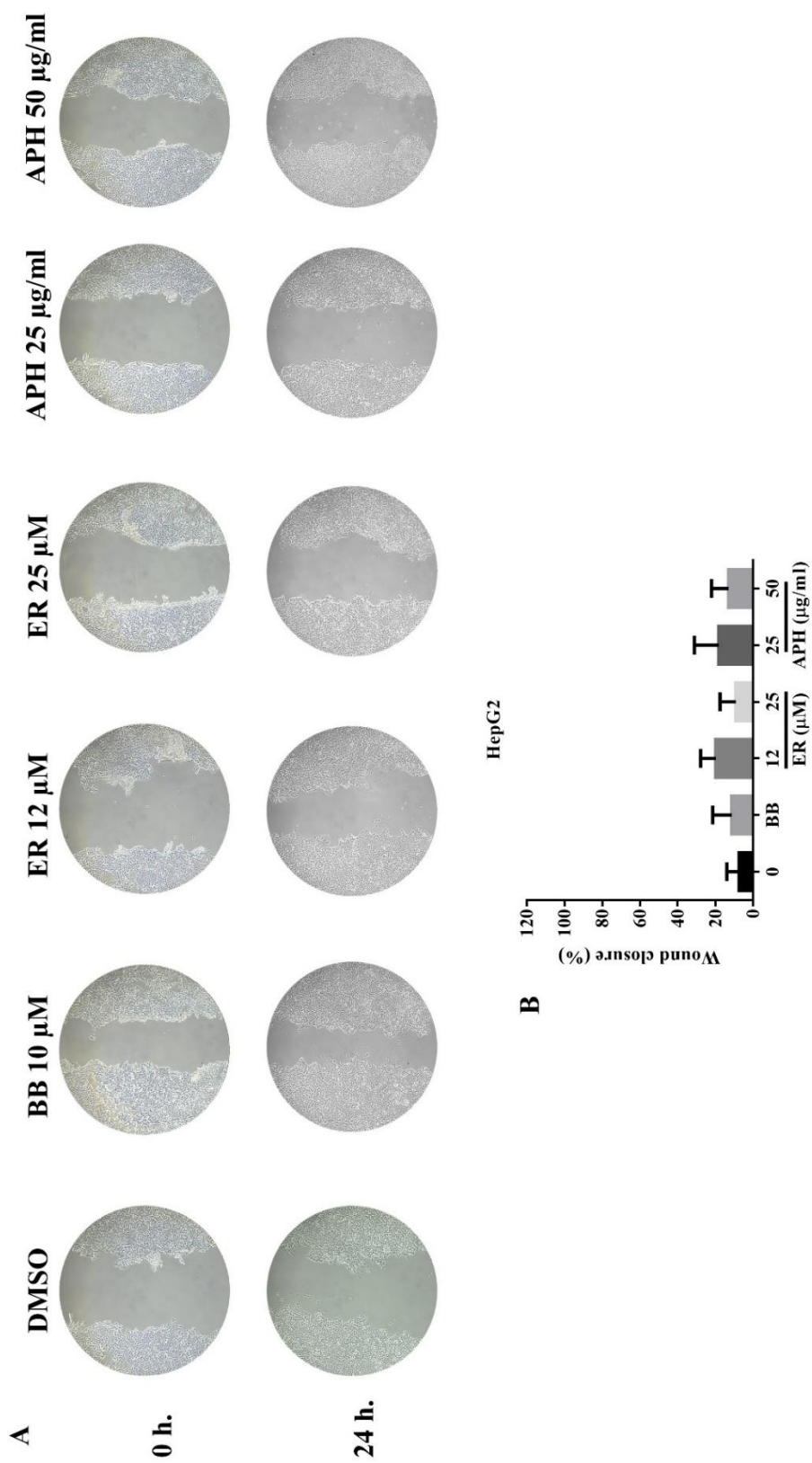
Figure 37   The HepG2 migration assay with APH, ER, and BB treatments.

(A) The photographs of wound at 0 and 24 hours. (B) The wound closure (%) of treatments compared with DMSO control cells.
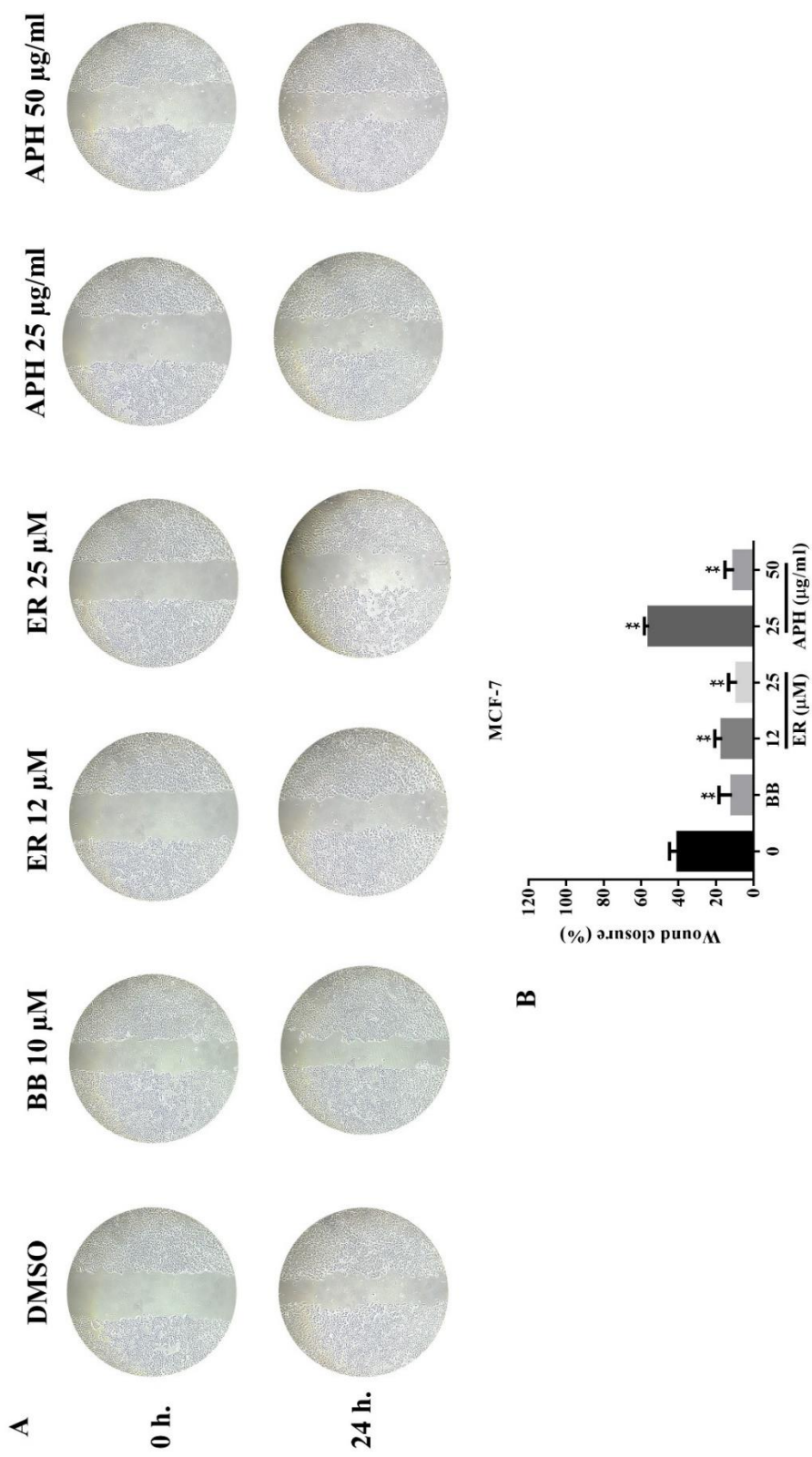
Figure 38 The MCF-7 migration assay with APH, ER, and BB treatments.

(A) The photographs of wound at 0 and 24 hours. (B) The wound closure (%) of treatments compared with DMSO control cells.
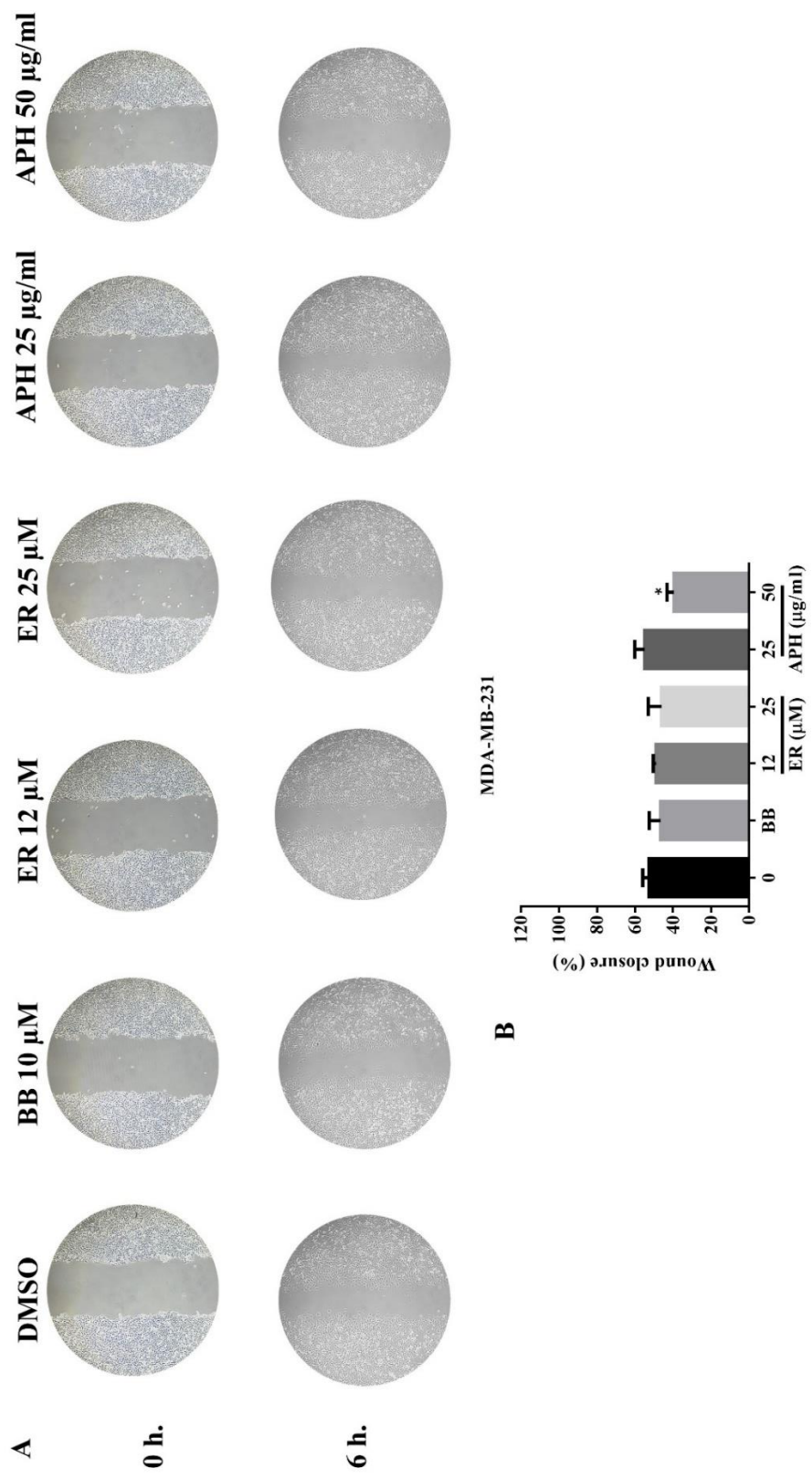
Figure 39   The MDA-MB-231 migration assay with APH, ER, and BB treatments.

(A) The photographs of wound at 0 and 6 hours. (B) The wound closure (%) of treatments compared with DMSO control cells.

4.8   APH and ergosterol inhibits the invasion of MDA-MB-231 cells

The invasion assay was performed on Matrigel-coated transwell inserts with APH, ER, and Batimastat, an anti-MMPs as a positive control for invasion assay, for 24 hours. FBS in the lower compartment of the insert acts as a chemoattractant induced the invasive cells to degrade the Matrigel and penetrate the membrane through the other side of inserts. The invasive cells penetrated through the membrane to the other side of inserts. The results of invasion assay as shown in **Table 18 and Figure 40** after crystal violet staining showed the numbers of invaded cells with APH at 12, 25 and 50 µg/ml were decreased in a dose-dependent manner at 68.93 ± 12.54, 48.60 ± 0.80 and 15.80 ± 3.60 cells per random fields, respectively. Ergosterol (6, 12 and 25 µM) also showed a dose-dependent manner at 43.60 ± 4.60, 32.20 ± 1.60 and 29.13 ± 10.39 cells per random fields, respectively. Whereas, Batimastat at 10 µl showed strong inhibition and resulted in 30.0 ± 8.4 cells per random field of invaded cells of MDA-MB-231 cells. The invasion results were compared to the vehicle control, which showed at 112.60 ± 16.92 invaded cells per random field.

Table 18   The calculated invaded cells per field after APH, ER, and Batimastat treatments on MDA-MB-231 cells.

Treatments	Invaded cells/field
DMSO	112.60 ± 16.92
Batimastat (BB) 10 µM	30.0 ± 8.4[**]
ER 6 µM	43.60 ± 4.60[**]
ER 12 µM	32.20 ± 1.60[**]
ER 25 µM	29.13 ± 10.39[**]
APH 12 µg/ml	68.93 ± 12.54[**]
APH 25 µg/ml	48.60 ± 0.80[**]
APH 50 µg/ml	15.80 ± 3.60[**]
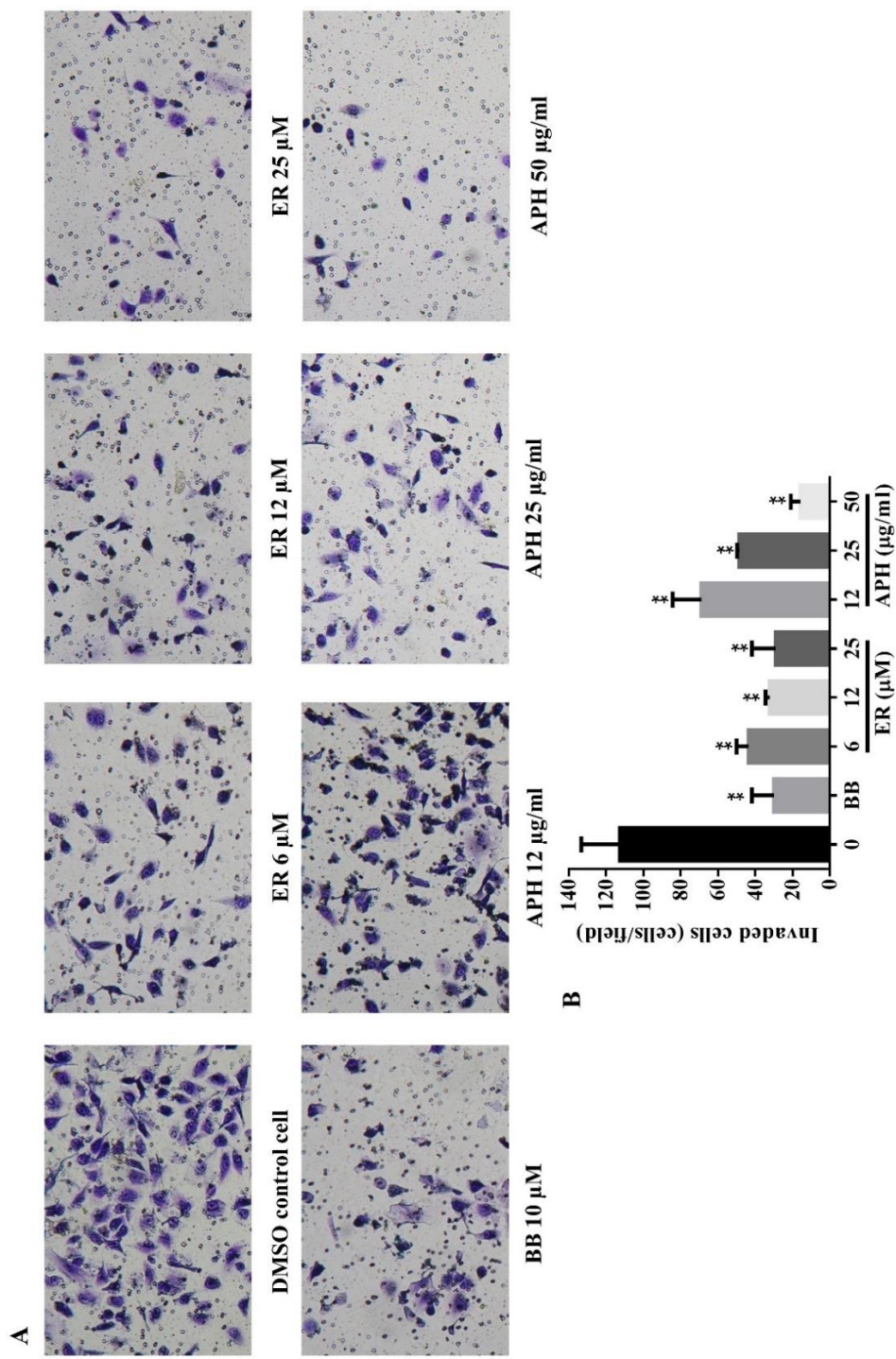
Figure 40 The MDA-MB-231 invaded cells with APH, ER, and BB treatments.

(A) The photographs of inserts after 24 hours. (B) The average of invasive cells after treatments compared with DMSO control cells.

4.9   Molecular modeling study of MMP-2 and ergosterol of APH

4.9.1   Analysis of the MMP-2 binding site in X-ray structure (PDB ID 3AYU)

Matrix metalloproteinases family (MMPs) are zinc-dependent enzymes that involve in many pathologies such as inflammation, tissue remodeling, and cancer progression. In cancer, MMPs subtypes such as gelatinases A (MMP-2) have been correlated to the migration, invasion, and angiogenesis lead to a poor prognosis. Two zinc ions in MMP-2 enzymes. One zinc ion as the structural support of protein and another zinc in the active site as the catalytic ion. The MMP-2 catalytic domain is categorized into the deep S1' pocket type, which is a promising central region of MMPs inhibitors (82).

The S1' pocket is located almost nearest to the right-handed side of zinc-ion in the catalytic domain. In this X-ray structure of the MMP-2 catalytic domain (PDB ID 3AYU) complexed with β-Amyloid precursor protein-derived inhibitory peptide (APP-IP) binds along the surface cleft of MMP-2 catalytic domain in opposite N to C terminus direction of APP-IP (75). The interaction between the APP-IP and MMP-2 catalytic domain from the original structure, including the catalytic domain, which contains zinc ion and the interaction between the HIS120' LEU82, and VAL117 of the MMP-2 and TYR3 and ASP6 of APP-IP in the S1' region, as shown in **Figure 41**.

The interaction of ILE1, ALA7, LEU8, MET9, and PRO10 of APP-IP found to interact with S2'-S3', S2, S3, S4, and S5 subsites, respectively. Moreover, PHE86, VAL92, and ALA87 of MMP-2 at the edge of the substrate-binding cleft interacted with PRO10 of APP-IP in S5 pocket and   PRO140-ILE141-TYR142 region of the MMP-2 interacted with N-terminus of APP-IP and the ALA85-PHE86-ALA87 part of the protease associated with C-terminal of APP-IP. The detailed interaction of MMP-2 and APP-IP showed in the BIOVIA Discovery Studio, as listed in **Table 19 and Figure 42**.

Table 19   the interaction between APP-IP and MMP-2 catalytic domain from PDB ID
3AYU generated by DS 4.5 software.

Subsites	APP-IP residues	Interaction of MMP-2
S1'	TYR3	ZN415, VAL117, HIS120, PRO140
	ASP6	ALA85
S2'-S3'	ILE1	TYR142
S2	ALA7	HIS124, PHE4
S3	LEU8	TYR73, HIS84, ALA85, PHE86
S4	MET9	PHE4, PRO5, ALA87
S5	PRO10	ALA85
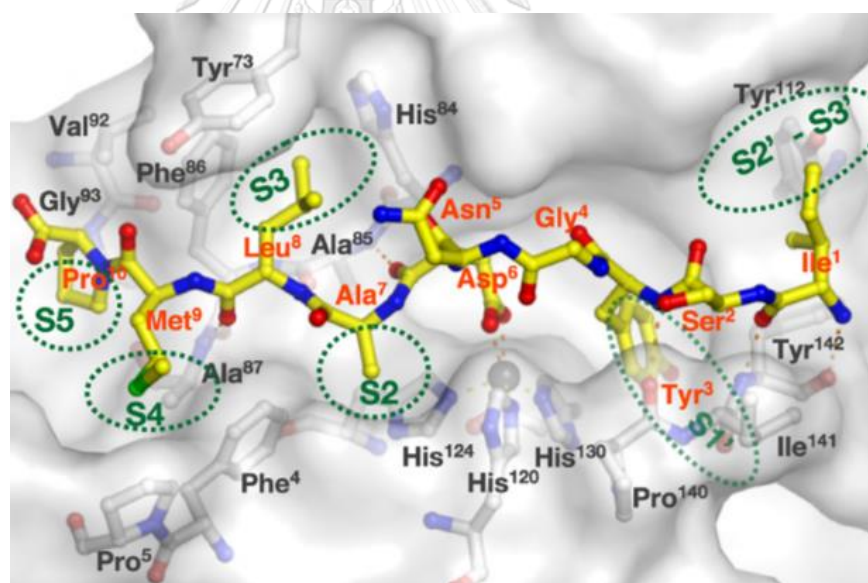
Figure 41   The original 3D structure of MMP-2 protein (PDB ID 3AYU) with APP-IP
in the binding pocket. Showed the S1', S2'-S3', S2, S3, S4 and S5 subsites in the
catalytic domain of MMP-2 in the original structure (1).

Figure 42   The interacting receptor bonds from APP-IP in MMP-2 binding pocket.

4.9.2 Validation of MMP-2

To validate our docking protocol, APP-IP was re-docked into the MMP-2 pocket. In principle, if the interaction found in the re-docking results are compatible to that observed in the original X-ray crystal structure, this would indicate; (i) The protein has maintained its structural integrity; (ii) the bidding pockets (S1-S5) have also maintained their structural integrity (iii) the docking protocol has some validity, in term of mimicking the real interactions between APP-IP and MMP-2 observed in vitro.; . The interactions found in the docking study were compared to those found in the original X-ray structure. The interactions were found to be 85.71 % in common. For instance, the same at ALA85, ALA87, HIS120, HIS124, HIS130, HIS84, PHE86, PRO140, PRO5, TYR142, TYR73 and ZN415 locations as listed in **Table 20**. Furthermore, the binding pose of APP-IP in the docking results adopt the same position and orientation as that found in the X-ray structure in **Figure 43**.

Table 20   The interaction bonds between the MMP-2 and APP-IP.

X-ray	Interactions	X-ray	Interactions
	A: ALA85		A: ALA85
	A: ALA87		A: ALA87
	A: HIS120		A: HIS120
	A: HIS124		A: HIS124
	A: HIS130		A: HIS130
	A: HIS84		A: HIS84
Original	A: PHE4	Validated	A: LEU81
APP-IP	A: PHE86	APP-IP	A: PHE86
	A: PRO140		A: PRO140
	A: PRO5		A: PRO5
	A: TYR142		A: TYR112
	A: TYR73		A: TYR142
	A: VAL117		A: TYR73
	A: ZN415		A: ZN415

	Common interactions	% similarity
S1'	ZN415, ALA85, HIS120	
	HIS130, PRO140	
S2'-S3'	TYR142	
S2	HIS124, PHE4	85.71%
S3	TYR73, HIS84, ALA85, PHE86	
S4	PHE4, PRO5, ALA87	
S5	ALA85	
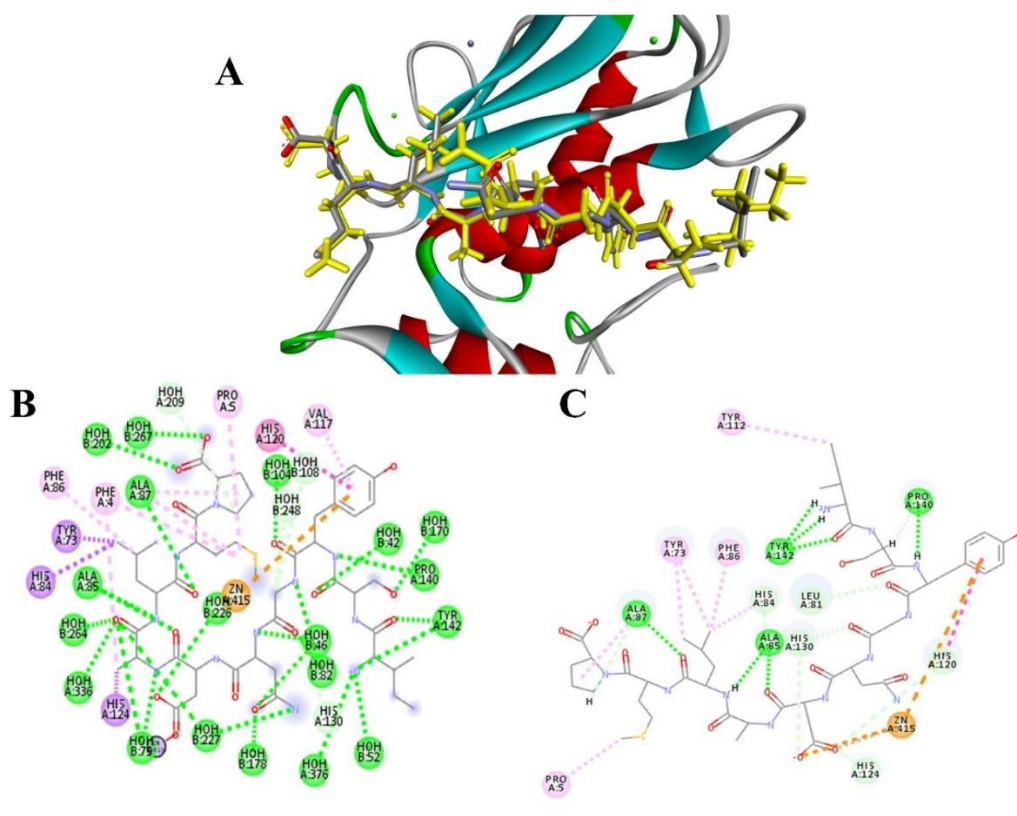
Figure 43 The 3D diagrams of interaction between MMP-2 and APP-IP.

(A) displayed the overlapped pattern between the original APP-IP and MMP-2 complex (grey) and the re-docked APP-IP ligand (yellow), **(B)** the receptor interaction from the original APP-IP and **(C)** The re-docked APP-IP ligand for the method validation.

In conclusion, the prepared MMP-2 protein structure and docking protocol have been validated. They are therefore suitable and can be used to carry -out docking study using other candidate compounds.

4.9.3 Docking results between compounds and MMP-2

From the CDOCKER calculation in **Table 20**, The APP-IP is used as a reference ligand to MMP-2 (IC_{50} of 32 nM), it gave interaction energy at -134.252 kcal/mol, with crucial interactions, as shown in **Table 19**. This binding energy and key interactions are used as the benchmark to compare with the docking results found in candidate compounds.

Compound 49 is a natural derived MMP-2 inhibitor with IC_{50} of 6.6 µM. It is structurally similar to ergosterol was used in the docking study. Compound LY52 is another hydroxamic acid MMP-2 inhibitor with the IC_{50} of 5.6 µM (80). This compound was also used in the docking study. The outcome of the docking study of these two inhibitors would allow for the comparison between docking scores to their report IC_{50} values. This comparative data may provide some insight into the predicted activity IC_{50} of ergosterol at MMP-2.

The docking study of compound 49 showed binding energy at -31.0116 kcal/mol with interactions such as THR145, ASN147, LEU137, ARG149 (listed in **Table 21**), that occupied binding pocket S2'-S3'. Compound LY52 showed the binding energy at -54.921 kcal/mol with interactions at LEU137, THR143, ARG149, ALA136 in S2'-S3' subsite and HIS120 in S1' pocket of the catalytic site. **(Figure 44)** Ergosterol showed the CDOCKER interaction energy at -32.7324 kcal/mol and shared common interactions with the APP-IP reference ligand, which was HIS120 and TYR142 location of MMP-2 which nearby the chelation site of protease in S1' pocket **(Figure 45)**. Moreover, the interaction of ergosterol to MMP-2 at the VAL117 region also shared similar interactions in the original 3AYU complex structure. Besides that, the ergosterol displayed the most interaction in S2'-S3' pocket as same as the Compound 49 **(Figure 46)**. The shared interaction between ergosterol, LY52 and compound 49 was the hydrophobic interaction at LEU137 region of MMP-2. Interestingly, LY52 and Ergosterol, which shared the interaction at HIS120 showed more negative CDOCKER binding energy more than compound 49. Therefore, the ergosterol showed the possibility of binding towards the MMP-2 pocket as the potential MMP-2 inhibitors.

Table 21   Molecular docking results of ligands and MMP-2 proteinase.

X-ray	Ligands	CDOCKER interaction energy (kcal/mol)	Interaction bonds
MMP-2	APP-IP (reference ligand)	-134.252	ZN415
			ALA85
			ALA87
			TYR142
			PRO140
			HIS84
			HIS120
			HIS124
			HIS130
			PRO5
			TYR73
			HIS84
			PHE86
			TYR112
	LY52	-54.9210	LEU137
			THR143
			ARG149
			ALA136
			HIS120
			PRO134
	Compound 49	-31.0116	THR145

X-ray	Ligands	CDOCKER interaction energy (kcal/mol)	Interaction bonds
			ASN147
			LEU137
			ARG149
			VAL117
			LEU116
	Ergosterol	-32.7324	LEU137
			HIS120
			TYR142
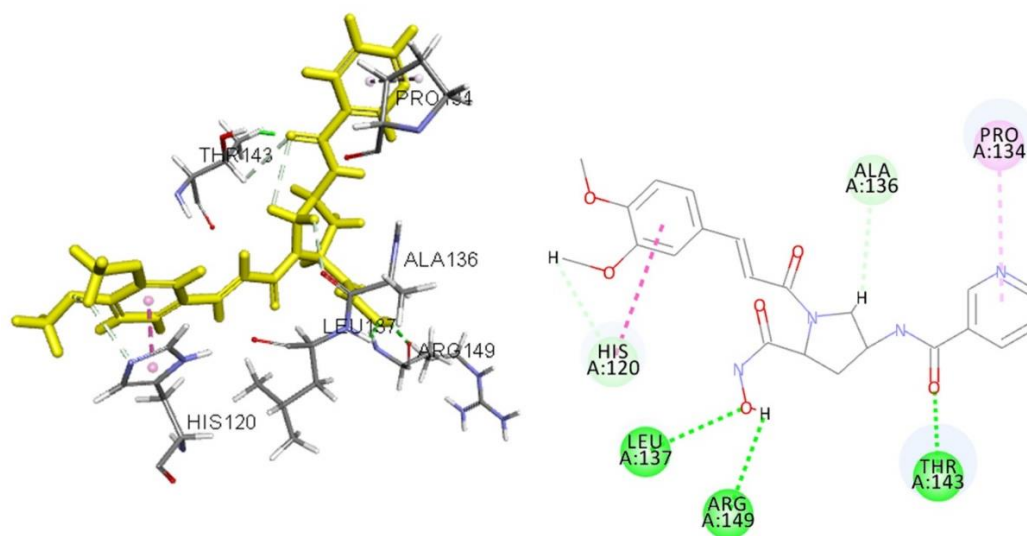
Figure 44   The ligand interaction between the LY52 and MMP-2 enzyme.
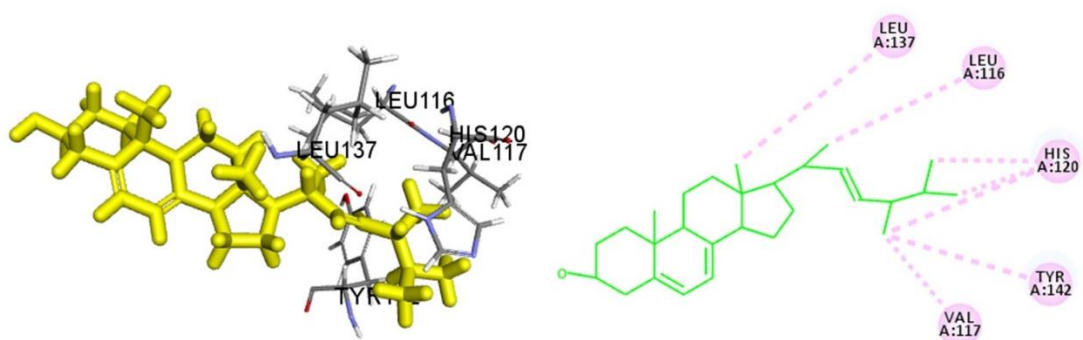
Figure 45   The ligand interaction between the ergosterol and MMP-2 enzyme
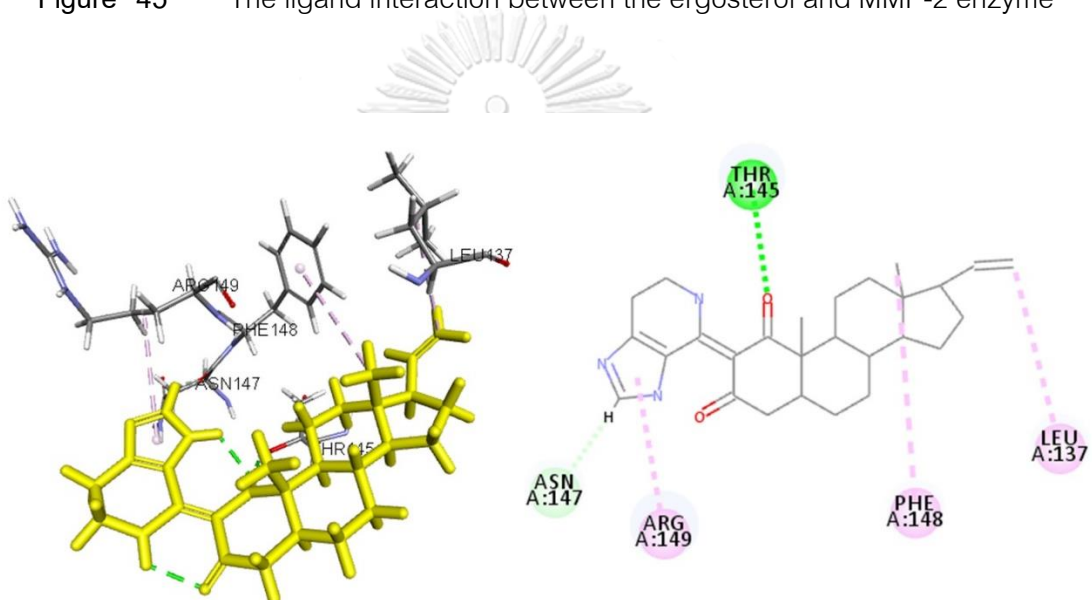
Figure 46   The ligand interaction between compound 49 and MMP-2 protein.

CHAPTER V DISCUSSION

The current cancer drugs often have poor target selectivity, and some were designed to target and disrupt the multifunction of cancer pathways (83). As a consequence, cancer patients suffered from various adverse effects such as pain, fatigue, and peripheral neuropathy (50). Moreover, resistant to cancer drug has been a significant concern because of the cancer heterogeneity, target alteration, and tumor microenvironment promote resistant to medicine (84, 85). Natural product derivatives have been studied for their various activities, including cytotoxicity, apoptosis induction, cell cycle arrest, anti-angiogenesis, anti-metastasis, and immunomodulatory effects. That improves antitumor activity and functional outcomes (86, 87). Besides the potent activity, some natural derivatives showed a very low or non-toxic in healthy cells and a minimal side effect in patients (88).

Mushroom extracts have been gained much attention for their bioactive compounds. For instance, several known mushrooms such as *Ganoderma lucidum* and *Trametes versicolor* have been studied in their polysaccharides fraction PSK and Krestin (15, 18, 75). Likewise, crude extract and active compounds from *Auriculariceae* family such as *Auricularia auricula-judae* and *Auricularia polytricha* also have been explored their crude extracts and active compounds. Polysaccharides such as β-D-glucan, a well-known compound with immunomodulation and antitumor activity, have been observed in the *Auriculariaece* family (20, 60, 64, 89). Therefore, in this study, we aimed to study *Auricularia polytricha* for their antitumor activity against cancer cell lines (HepG2, MCF-7, and MDA-MB-231) by exploring the anticancer activity of the crude ethanol extract in comparison to the crude hexane extract. Anticancer activity of the two extracts was investigated for the first time by our group.

The referring tables and figures in this discussion chapter are from chapter IV. GC/MS analysis of compounds and their compositions of APE were carried out in comparison to that of APH. The results (Table 8 and 9) indicate that both extracts contain common compounds such as palmitic acid, linoleic acid, and stearic acid. However, the composition of these acids was found to be higher in APE (by Soxhlet extraction) than that found in APH (by maceration). The increase in acids composition due to the ability of ethanol, as a polar solvent, to extract out more of polar acids from AP than non-polar solvent such as hexane (14). It is noteworthy that a group of ethyl esters was only found in APE. They are pentadecanoic acid ethyl ester, hexadecenoic acid ethyl ester, 9,12-octadecadienoic acid ethyl ester, ethyl oleate, and octadecanoic acid ethyl ester. These ethyl esters are artifacts which were originated from the esterification of fatty acids and ethanol at elevated temperature to form the corresponding fatty acid ethyl esters (90). In GC/MS analysis, oleic acid was only found in APH extract. From our previous data on GC/MS analysis of APH, we suggested that the high temperature of GC/MS analysis could induce fragmentation of triacylglycerols to form free fatty acids (91, 92). Oleic acid was not extracted product, but it was instead a free fatty acid derived from high temperature-induced fragmentation triacylglycerols of F1 and F2 in the GC-MS analysis (89). On the other hand, the less polar compounds such as 9(11)-Dehydroergosteryl benzoate, Anthiaergostan-5,7,9,16,22-pentane, and Anthiaergostan-5,7,9,22-tetraen-3-ol were only present in APH. Moreover, these three compounds not only found in AP but also have been reported in the GC/MS profile of *Pleurotus cornucopiae* mushroom before (93).

Ergosterol was found in both APE and APH extracts. The composition of ergosterol (36.28%) in APH is much higher than that (14.76%) found in APE. These results suggest that hexane would be a more efficient solvent for the extraction of ergosterol than ethanol. However, ergosterol would be capable of solubilized in either

ethanol or hexane. This unique property is due to the structural design of ergosterol, which contains the polar hydroxy (OH) group as well as the non-polar polycyclic hydrocarbon structure.

Moreover, this solubility nature would make ergosterol being a bioavailable and essential compound in AP. It is, therefore, not surprising to find ergosterol existed in many mushrooms as it is well known to play essential roles in supporting components in the mushroom cell membrane and the metabolic processes in fungus (94-96).

TLC was performed to optimize the mobile system for APH separation in further separation. We found that the Hexane and Ethyl acetate system at 80: 20 ratios were the best condition for four fractions of APH (Table 10). Following by separation of APH crude extract by PREP-LC resulted in several fractions mixture and four main fractions, which further confirmed by TLC (Figures 21 and 22). Four main fractions have been reported in our previous study (92). The identification of all fractions said that F1 and F2 were triacylglycerols, while F3 was identified as linoleic acid, and F4 was identified as ergosterol. This study in HPLC analysis also confirmed the APH-purified ergosterol and commercial ergosterol have an identical characteristic, as shown in Figure 23A-C.

In this work, APE and APH extracts were screened by MTT assay against hepatocellular carcinoma HepG2 cell line and Breast cancer cell lines (MCF-7 and MDA-MB-231) and found that the cell lines are more sensitive toward APH than APE as presented in Table 12 and Figure 24-26. Since the composition of ergosterol is almost twice as much in APH compared to that found APE. Therefore, APH has been prioritized for further study. In the cell viability screening of the control Doxorubicin (DOX) against the three cancer cell lines for 24 hours, one observed its IC_{50} values against MDA-MB-231(> 2 μM) is higher than MCF-7 (0.46 ± 0.07) and HepG2 cell line (0.48 ± 0.06). Results confirm the aggressive nature of the cells against Doxorubicin (97).

The cell viability testing with four fractions have been performed on breast cancer cell lines and HepG2 tested with ergosterol. The results found that ergosterol showed the highest inhibition among four fractions in all three cell lines. (Table 13 and Figure 28-30)

Furthermore, mouse fibroblast cell line 3T3-L1 also used to determine the effect of treatments of APH, ER, DOX, and BB against healthy cells (78, 79). It demonstrated (Table 14 and Figure 30) that the cytotoxicity of APH, DOX, and BB against this cell line are lower than cancer cells. While ER showed IC_{50} values at 13.53 ± 0.51 and 23.54 ± 3.14 µM at 24 and 48 hours, respectively. While at 72 hours incubation time of ER could not determine IC_{50} value. These results suggest that APH and ergosterol are more sensitivity toward cancer cells than 3T3-L1 cells.

The antitumor mechanisms were further assessed via apoptosis, cell cycle, migration, and invasion assays. In apoptosis assay, APE, APH, and DOX were tested in HepG2 cells and resulted in a significantly induced apoptosis at a high dose of APE, APH, and DOX. While, APH, ER, and DOX were treated in MCF-7 and MDA-MB-231 cell lines. Induction of apoptosis cells was observed after the treatment of the cells with APH, DOX, and Ergosterol at increasing doses. These are evidenced by the higher population of annexin V positive cells that indicated the early apoptotic cell population, as shown in Table 16 and Figure 31-33. Moreover, the double strained at the highest dose of APH (50 µg/ml), and Ergosterol (25 µM) showed significantly. Apoptosis induction capacity of AP has been reported with polysaccharides purified compound in A549 cell lines (24).

For the cell cycle arrest of APH and Ergosterol treatment in MCF-7 and MDA-MB-231 cell lines, APH showed no significantly arrest at the cell cycle in MCF-7 and MDA-MB-231 cell lines at higher doses (Figure 34-36). Moreover, the result of ergosterol in

this study was unable to induce cell cycle arrest in these cancer cell lines. Ergosterol found not to affect the G2/M phase in the human promyeloblast cell line (HL-60) cells as well (98).

Next, the migration inhibitory effect of APH and ergosterol have been investigated by wound-healing assay. The wound-healing results showed the migratory effect differently depends on the motility of cell lines as HepG2 and MCF-7 are less invasiveness than MDA-MB-231 cell lines (99), so the migration was observed at 24 hours while MDA-MB-231 cell line exerts the higher invasive behavior so the result at 6 hours was monitored. Refers to the wound closure rate in Table 17 (Figure 37-39), APH (50 µg/ml) and ER (50 µM) showed the inhibitory effect of wound healing better than low doses of APH and ergosterol. In the MCF-7 migration result, APH at 25 µg/ml enhanced the migration, which could be from linoleic acid in APH crude extract, which accounted for about 19% counteracted with ergosterol activity. A broad MMPs inhibitor, batimastat, which has been known to inhibit cell migration, was used as a positive control in these migration and invasion assays (100).

Moreover, the transwell invasion was performed in the high invasive MDA-MB-231 cell line. The invaded cells pass through the Matrigel gel coating, which contained the main component of extracellular matrices such as laminin and collagen IV (101). APH, ER, and BB treatments resulted in the decreased of invaded cells in a dose-dependent manner compared to the vehicle control, as illustrated in Table 18 and Figure 40. Thus, APH and ergosterol can inhibit the invasion in the MDA-MB-231 cell line. Ergosterol also has been reported to the active compound that induced apoptosis in MDA-MB-231 cell by the upregulation of Foxo 3, a tumor suppressor, which resulted in the evaluation of Bim and Fas L in the apoptotic pathway. Also, inhibited the migration and invasion of breast cancer cell lines, B16 cells, and tumor-bearing mice in the study

of *Amauroderma rude* mushroom (102). Moreover, Ergosterol isolated from *Ganoderma lucidum* was reported to inhibit cell viability of various cancers such as human breast carcinoma cells MDA-MB-231, human hepatocellular carcinoma cells HepG2, human lung carcinoma cells A549 as well as human umbilical vein endothelial cells HUVECs, which used for anti-angiogenesis screening. Interestingly, in our work, the apoptosis induction and migration inhibition on HepG2, MCF-7, and MDA-MB-231 cells could be observed from ergosterol treatments since 6 µM and the transwell invasion inhibition in MDA-MB-231 also showed the significant inhibition at the low dose. It should be noted that the invasion step of cancer requires multiple enzymes and growth factors to regulate the mechanism which included Matrix metalloproteinase enzyme (MMPs) especially Gelatinases family (MMP-2 and MMP-9) which have been reported to be associated with poor prognosis in cancer patients (103). The ergosterol effect on MMP-2 enzyme in the antitumor activity via the molecular docking for the first time.

It is hypothesized that MMP-2 may be one of the enzymes targeted by APH or ergosterol. The molecular modeling was performed and compared with a known MMP-2 referenced compound APP-IP and resulted that Ergosterol occupied two interactions to MMP-2 catalytic domain in S1'pocket, which locate at HIS120 and VAL117 region of MMP-2 (Table 20). Most of the ergosterol structure remained outside near to S2'-S3' pocket, but the interaction in S2'-S3' pocket also showed inhibition with less potency to MMP-2. The MMP-2 inhibitors have been studied in many natural derivatives such as Curcumin and Resveratrol (88, 103). The promising target of the MMP-2 domain has been published the criteria for a potential drug as the compound should show the interaction either with interact to a zinc-catalytic ion in binding pocket binds to S1' subsites near Zn-catalytic domain or form the hydrogen bonds in the binding pocket (74, 104). The analysis of the molecular modeling results in comparison to the results

found in invasion assay can only provide some insight into the possibility of MMP-2 being a target. The results should be considered as an indication, which will require further validation by MMP-2 inhibition study in vitro assay.

Ergosterol has shown to have the highest antitumor activity among all isolated compounds from APH, exhibiting via antiproliferation, induced apoptosis, migration, and invasion inhibitions of HepG2, MCF-7, and MDA-MB-231 cancer cells. Interestingly, the APH in crude mixture showed better activity than the isolated ergosterol, which may suggest the combination effect between fractions of APH. Moreover, an in-depth investigation is required to understand the mode of actions in antiproliferation, induced apoptosis, migration, and invasion inhibitions caused by APH and ergosterol. Therefore, both the combination effect and biochemical cascade need further investigation in the future.
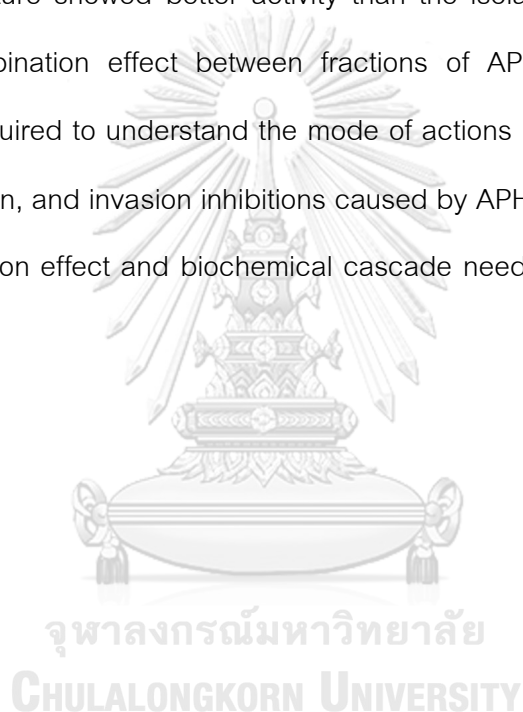
CHAPTER VI CONCLUSION

In summary, we have demonstrated the antitumor activity of *Auricularia polytricha* both in the ethanol extract by Soxhlet extraction and hexane extract by maceration. Ergosterol was found to be the main component in APH. The authentication and purity of isolated ergosterol were tested by HPLC and confirmed to be the same as the commercial product. The APH showed higher inhibition of HepG2, MCF-7, and MDA-MB-231 cancer cells in cell viability screening than APE. APH was found to less cytotoxic against 3T3-L1 healthy cells than the studies cancerous cells. APH crude mixture and ergosterol were the most active in apoptosis induction, migration, and invasion inhibition in cancer cells.

The results from the invasion and migration study suggested that MMP-2 may be a possible target enzyme. Computer-aided molecular modeling study has provided some insight into this hypothesis. In vitro, MMP-2 enzyme inhibition by APH or ergosterol would help in validating the prediction.

Even though, the cytotoxicity test performed in this study with 3T3-L1 cells and resulted in lower toxic than in cancer cells. However, healthy human cell lines should be investigated further for a reliable outcome. The limitation in mechanism investigation on protein targets such as pro-apoptotic regulatory proteins and MMP-2 enzyme activity needs to clarify. The combination effect of F1, F2, F3, and ergosterol in APH is also in our future direction. These allow us to engage in the development of *Auricularia polytricha* as a potential candidate drug or formulation for cancer therapy in the future.

REFERENCES

1.   Clark WH. The Nature of Cancer: Morphogenesis and Progressive (Self)-Disorganization in Neoplastic Development and Progression. Acta Oncologica. 1995;34(1):3-21.

2.   Toporcov TN, Wunsch Filho V. Epidemiological science and cancer control. Clinics (Sao Paulo). 2018;73(suppl 1): e627s.

3.   Momenimovahed Z, Salehiniya H. epidemiological characteristics of and risk factors for breast cancer in the world. Breast Cancer: Targets and Therapy. 2019; 11:151.

4.   Bray F, Ferlay J, Soerjomataram I, Siegel RL, Torre LA, Jemal A. Global cancer statistics 2018: GLOBOCAN estimates of incidence and mortality worldwide for 36 cancers in 185 countries. CA: a cancer journal for clinicians. 2018;68(6):394-424.

5.   Liu Z, Jiang Y, Yuan H, Fang Q, Cai N, Suo C, et al. The trends in incidence of primary liver cancer caused by specific etiologies: Results from the Global Burden of Disease Study 2016 and implications for liver cancer prevention. Journal of hepatology. 2019;70(4):674-83.

6.   Damyanov C, Maslev I, Pavlov V, Avramov L. Conventional treatment of cancer realities and problems. Annals of Complementary and Alternative Medicine. 2018;1(1):1-9.

7.   Arruebo M, Vilaboa N, Sáez-Gutierrez B, Lambea J, Tres A, Valladares M, et al. Assessment of the evolution of cancer treatment therapies. Cancers. 2011;3(3):3279-330.

8.   Housman G, Byler S, Heerboth S, Lapinska K, Longacre M, Snyder N, et al. Drug resistance in cancer: an overview. Cancers (Basel). 2014;6(3):1769-92.

9.   Hasan S, Taha R, Omri HE. Current Opinions on Chemoresistance: An Overview. Bioinformation. 2018;14(2):80-5.

10.   Ogino S, Nowak JA, Hamada T, Phipps AI, Peters U, Milner Jr DA, et al. Integrative analysis of exogenous, endogenous, tumour and immune factors for precision medicine. Gut. 2018;67(6):1168-80.

11.   Chamberlin SR, Blucher A, Wu G, Shinto L, Choonoo G, Kulesz-Martin M, et al. Natural Product Target Network Reveals Potential for Cancer Combination Therapies. Frontiers in Pharmacology. 2019;10.

12.   Thomford NE, Senthebane DA, Rowe A, Munro D, Seele P, Maroyi A, et al. Natural products for drug discovery in the 21st century: innovations for novel drug discovery. International journal of molecular sciences. 2018;19(6):1578.

13.   Valverde ME, Hernández-Pérez T, Paredes-López O. Edible mushrooms: improving human health and promoting quality life. International journal of microbiology. 2015; 376387/1-376387/15.

14.   Elbatrawy EN, Ghonimy EA, Alassar MM, Wu F-S. Medicinal mushroom extracts possess differential antioxidant activity and cytotoxicity to cancer cells. International journal of medicinal mushrooms. 2015;17(5): 471-9.

15.   Hirahara N, Fujioka M, Edamatsu T, Fujieda A, SEKINE F, Wada T, et al. Protein-bound polysaccharide-K (PSK) induces apoptosis and inhibits proliferation of promyelomonocytic leukemia HL-60 cells. Anticancer research. 2011;31(9):2733-8.

16.   Fisher M, Yang L-X. Anticancer effects and mechanisms of polysaccharide-K (PSK): implications of cancer immunotherapy. Anticancer research. 2002;22(3):1737-54.

17.   Torkelson CJ, Sweet E, Martzen MR, Sasagawa M, Wenner CA, Gay J, et al. Phase 1 clinical trial of Trametes versicolor in women with breast cancer. ISRN oncology. 2012;2012: 251632.

18.   Sohretoglu D, Huang S. Ganoderma lucidum polysaccharides as an anti-cancer agent. Anti-Cancer Agents in Medicinal Chemistry (Formerly Current Medicinal Chemistry-Anti-Cancer Agents). 2018;18(5):667-74.

19.   Cao Y, Xu X, Liu S, Huang L, Gu J. Ganoderma: A Cancer Immunotherapy Review. Frontiers in pharmacology. 2018; 9:1217.

20.   Zhao S, Rong C, Liu Y, Xu F, Wang S, Duan C, et al. Extraction of a soluble polysaccharide from Auricularia polytricha and evaluation of its anti-hypercholesterolemic effect in rats. Carbohydrate polymers. 2015; 122:39-45.

21.   Lu J, Tang A. Cellulolytic enzymes and antibacterial activity of Auricularia polytricha. Journal of Food Science. 1986;51(3):668-9.

22.   Muszynska B, Grzywacz-Kisielewska A, Kala K, Gdula-Argasinska J. Anti-inflammatory properties of edible mushrooms: A review. Food Chemistry. 2018; 243:373-81.

23.   Chiu W-C, Yang H-H, Chiang S-C, Chou Y-X, Yang H-T. Auricularia polytricha aqueous extract supplementation decreases hepatic lipid accumulation and improves antioxidative status in animal model of nonalcoholic fatty liver. BioMedicine. 2014;4(2): 12.

24.   Yu J, Sun R, Zhao Z, Wang Y. Auricularia polytricha polysaccharides induce cell cycle arrest and apoptosis in human lung cancer A549 cells. International journal of biological macromolecules. 2014; 68:67-71.

25.   Arora S, Tandon S. Mushroom Extracts Induce Human Colon Cancer Cell (COLO-205) Death by Triggering the Mitochondrial Apoptosis Pathway and Go/G1-Phase Cell Cycle Arrest. Archives of Iranian Medicine (AIM). 2015;18(5): 284-95.

26.   Mahdavifar N, Ghoncheh M, Pakzad R, Momenimovahed Z, Salehiniya H. Epidemiology, incidence and mortality of bladder cancer and their relationship with the development index in the world. Asian Pacific Journal of Cancer Prevention. 2016;17(1):381-6.

27.   Baretta Z, Mocellin S, Goldin E, Olopade OI, Huo D. Effect of BRCA germline mutations on breast cancer prognosis: a systematic review and meta-analysis. Medicine. 2016;95(40): e4975.

28.   Petitjean A, Achatz M, Borresen-Dale A-L, Hainaut P, Olivier M. TP53 mutations in human cancers: functional selection and impact on cancer prognosis and outcomes. Oncogene. 2007;26(15):2157.

29.   Bernstein L, Ross RK. Endogenous hormones and breast cancer risk. Epidemiologic reviews. 1993;15(1):48-65.

30. Dupont WD, Page DL, Rogers LW, Parl FF. Influence of exogenous estrogens, proliferative breast disease, and other variables on breast cancer risk. Cancer. 1989;63(5):948-57.

31. Sloan FA, Gelband H. Cancer causes and risk factors and the elements of cancer control. Cancer Control Opportunities in Low-and Middle-Income Countries: National Academies Press (US); 2007.

32. Perz JF, Armstrong GL, Farrington LA, Hutin YJ, Bell BP. The contributions of hepatitis B virus and hepatitis C virus infections to cirrhosis and primary liver cancer worldwide. Journal of hepatology. 2006;45(4):529-38.

33. Zur Hausen H. Papillomavirus infections—a major cause of human cancers. Biochimica et biophysica acta (BBA)-reviews on cancer. 1996;1288(2):F55-F78.

34. Kuper H, Adami HO, Trichopoulos D. Infections as a major preventable cause of human cancer. Journal of internal medicine. 2000;248(3):171-83.

35. Kelsey JL, Gammon MD, John EM. Reproductive factors and breast cancer. Epidemiologic reviews. 1993;15(1):36.

36. Phipps AI, Buist DS, Malone KE, Barlow WE, Porter PL, Kerlikowske K, et al. Family history of breast cancer in first-degree relatives and triple-negative breast cancer risk. Breast cancer research and treatment. 2011;126(3):671-8.

37. Bremnes RM, Dønnem T, Al-Saad S, Al-Shibli K, Andersen S, Sirera R, et al. The Role of Tumor Stroma in Cancer Progression and Prognosis: Emphasis on Carcinoma-Associated Fibroblasts and Non-small Cell Lung Cancer. Journal of Thoracic Oncology. 2011;6(1):209-17.

38. Quail DF, Joyce JA. Microenvironmental regulation of tumor progression and metastasis. Nature Medicine. 2013; 19:1423.

39. Hanahan D, Weinberg RA. The hallmarks of cancer. Cell. 2000;100(1):57-70.

40. Dhillon AS, Hagan S, Rath O, Kolch W. MAP kinase signalling pathways in cancer. Oncogene. 2007;26(22):3279.

41. Atkins MB, Yasothan U, Kirkpatrick P. Everolimus. Nature Reviews Drug Discovery. 2009;8(7):535-6.

42.   Dickson M, Schwartz G. Development of cell-cycle inhibitors for cancer therapy. Current Oncology. 2009;16(2):36.

43.   Wong RS. Apoptosis in cancer: from pathogenesis to treatment. Journal of experimental and clinical cancer research. 2011;30(1):87.

44.   Sankari SL, Masthan K, Babu NA, Bhattacharjee T, Elumalai M. Apoptosis in cancer-an update. Asian Pacific Journal of Cancer Prevention. 2012;13(10):4873-8.

45.   Hanahan D, Weinberg RA. Hallmarks of cancer: the next generation. Cell. 2011;144(5):646-74.

46.   Yaswen P, MacKenzie KL, Keith WN, Hentosh P, Rodier F, Zhu J, et al., editors. Therapeutic targeting of replicative immortality. Seminars in cancer biology; 2015: Elsevier.

47.   Jiang WG, Sanders AJ, Katoh M, Ungefroren H, Gieseler F, Prince M, et al., editors. Tissue invasion and metastasis: Molecular, biological and clinical perspectives. Seminars in cancer biology; 2015: Elsevier.

48.   Miller A, Hoogstraten B, Staquet M, Winkler A. Reporting results of cancer treatment. Cancer. 1981;47(1):207-14.

49.   Nurgali K, Jagoe RT, Abalo R. Adverse effects of cancer chemotherapy: Anything new to improve tolerance and reduce sequelae? Frontiers in pharmacology. 2018; 9:245.

50.   Pearce A, Haas M, Viney R, Pearson S-A, Haywood P, Brown C, et al. Incidence and severity of self-reported chemotherapy side effects in routine care: A prospective cohort study. Plos one. 2017;12(10):e0184360.

51.   Harvey AL. Natural products in drug discovery. Drug discovery today. 2008;13(19-20):894-901.

52.   Mondal S, Bandyopadhyay S, K Ghosh M, Mukhopadhyay S, Roy S, Mandal C. Natural products: promising resources for cancer drug discovery. Anti-Cancer Agents in Medicinal Chemistry (Formerly Current Medicinal Chemistry-Anti-Cancer Agents). 2012;12(1):49-75.

53.   Hsu Y-L, Kuo P-L, Cho C-Y, Ni W-C, Tzeng T-F, Ng L-T, et al. Antrodia cinnamomea fruiting bodies extract suppresses the invasive potential of human liver cancer cell line PLC/PRF/5 through inhibition of nuclear factor кB pathway. Food and Chemical Toxicology. 2007;45(7):1249-57.

54.   Eroğlu C, Seçme M, Atmaca P, Kaygusuz O, Gezer K, Bağcı G, et al. Extract of Calvatia gigantea inhibits proliferation of A549 human lung cancer cells. Cytotechnology. 2016;68(5):2075-81.

55.   Sarup Singh R, Preet Kaur H, Rakesh Kanwar J. Mushroom lectins as promising anticancer substances. Current Protein and Peptide Science. 2016;17(8):797-807.

56.   Gao Y, Gao H, Chan E, Tang W, Xu A, Yang H, et al. Antitumor activity and underlying mechanisms of ganopoly, the refined polysaccharides extracted from Ganoderma lucidum, in mice. Immunological Investigations. 2005;34(2):171-98.

57.   Ning X, Luo Q, Li C, Ding Z, Pang J, Zhao C. Inhibitory effects of a polysaccharide extract from the Chaga medicinal mushroom, Inonotus obliquus (higher Basidiomycetes), on the proliferation of human neurogliocytoma cells. International Journal of Mdicinal Mushrooms. 2014;16(1): 29-36.

58.   Lin YW, Pan JH, Liu RH, Kuo YH, Sheen LY, Chiang BH. The 4‐acetylantroquinonol B isolated from mycelium of Antrodia cinnamomea inhibits proliferation of hepatoma cells. Journal of the Science of Food and Agriculture. 2010;90(10):1739-44.

59.   Finimundy TC, Dillon AJP, Henriques JAP, Ely MR. A review on general nutritional compounds and pharmacological properties of the Lentinula edodes mushroom. Food and Nutrition Sciences. 2014;5(12):1095.

60.   Reza MA, Hossain MA, Lee S-J, Yohannes SB, Damte D, Rhee M-h, et al. Dichlormethane extract of the jelly ear mushroom Auricularia auricula-judae (higher Basidiomycetes) inhibits tumor cell growth in vitro. International Journal of Medicinal Mushrooms. 2014;16(1): 37-47.

61.   Panthong S, Boonsathorn N, Chuchawankul S. Antioxidant activity, anti-proliferative activity, and amino acid profiles of ethanolic extracts of edible mushrooms. Genetics and Molecular Research. 2016;15(4).

62.   Reza MA, Jo W-S, Park S-C. Comparative antitumor activity of jelly ear culinary-medicinal mushroom, Auricularia auricula-judae (Bull.) J. Schrot.(Higher Basidiomycetes) extracts against tumor cells in vitro. International Journal of Medicinal Mushrooms. 2012;14(4): 403-9.

63.   Arora S, Goyal S, Balani J, Tandon S. Enhanced antiproliferative effects of aqueous extracts of some medicinal mushrooms on colon cancer cells. International Journal of Medicinal Mushrooms. 2013;15(3): 301-314.

64.   Qiu J, Zhang H, Wang Z, Liu D, Liu S, Han W, et al. The antitumor effect of folic acid conjugated-Auricularia auricular polysaccharide-cisplatin complex on cervical carcinoma cells in nude mice. International Journal of Biological Macromolecules. 2018; 107:2180-9.

65.   Zhou Y, Chen L, Fan X, Bian Y. De novo assembly of Auricularia polytricha transcriptome using Illumina sequencing for gene discovery and SSR marker identification. PloS one. 2014;9(3):e91740-e.

66.   De Silva DD, Rapior S, Fons F, Bahkali AH, Hyde KD. Medicinal mushrooms in supportive cancer therapies: an approach to anti-cancer effects and putative mechanisms of action. Fungal Diversity. 2012;55(1):1-35.

67.   K Chellappan D, Ganasen S, Batumalai S, Candasamy M, Krishnappa P, Dua K, et al. The protective action of the aqueous extract of Auricularia polytricha in paracetamol induced hepatotoxicity in rats. Recent Patents on Drug Delivery and Formulation. 2016;10(1):72-6.

68.   Sliwoski G, Kothiwale S, Meiler J, Lowe EW. Computational Methods in Drug Discovery. Pharmacological Reviews. 2014;66(1):334-95.

69.   Burley SK, Berman HM, Bhikadiya C, Bi C, Chen L, Di Costanzo L, et al. RCSB Protein Data Bank: biological macromolecular structures enabling research and

education in fundamental biology, biomedicine, biotechnology and energy. Nucleic Acids Research. 2019;47(D1): D464-D74.

70.   Aminpour M, Montemagno C, Tuszynski JA. An Overview of Molecular Modeling for Drug Discovery with Specific Illustrative Examples of Applications. Molecules. 2019;24(9):1693.

71.   Shim J, Mackerell AD, Jr. Computational ligand-based rational design: Role of conformational sampling and force fields in model development. MedChemComm. 2011;2(5):356-70.

72.   Ferreira LG, Dos Santos RN, Oliva G, Andricopulo AD. Molecular docking and structure-based drug design strategies. Molecules. 2015;20(7):13384-421.

73.   Wu G, Robertson DH, Brooks CL, 3rd, Vieth M. Detailed analysis of grid-based molecular docking: A case study of CDOCKER-A CHARMm-based MD docking algorithm. Journal of Computational Chemistry. 2003;24(13):1549-62.

74.   Dhanaraj V, Ye QZ, Johnson LL, Hupe DJ, Ortwine DF, Dunbar JJB, et al. X-ray structure of a hydroxamate inhibitor complex of stromelysin catalytic domain and its comparison with members of the zinc metalloproteinase superfamily. Structure. 1996;4(4):375-86.

75.   Hashimoto H, Takeuchi T, Komatsu K, Miyazaki K, Sato M, Higashi S. Structural basis for matrix metalloproteinase-2 (MMP-2)-selective inhibitory action of beta-amyloid precursor protein-derived inhibitor. Journal of Biological Chemistry. 2011;286(38):33236-43.

76.   Horwitz KB, Costlow ME, McGuire WL. MCF-7; a human breast cancer cell line with estrogen, androgen, progesterone, and glucocorticoid receptors. Steroids. 1975;26(6):785-95.

77.   Li H, Qiu Z, Li F, Wang C. The relationship between MMP-2 and MMP-9 expression levels with breast cancer incidence and prognosis. Oncology Letters. 2017;14(5):5865-70.

78. Capella V, Rivero RE, Liaudat AC, Ibarra LE, Roma DA, Alustiza F, et al. Cytotoxicity and bioadhesive properties of poly-N-isopropylacrylamide hydrogel. Heliyon. 2019;5(4):e01474-e.

79. Ng WK, Saiful Yazan L, Yap LH, Wan Nor Hafiza WAG, How CW, Abdullah R. Thymoquinone-loaded nanostructured lipid carrier exhibited cytotoxicity towards breast cancer cell lines (MDA-MB-231 and MCF-7) and cervical cancer cell lines (HeLa and SiHa). Biomed Res Int. 2015; 2015:263131-.

80. Zhong Y, Lu Y-T, Sun Y, Shi Z-H, Li N-G, Tang Y-P, et al. Recent opportunities in matrix metalloproteinase inhibitor drug design for cancer. Expert opinion on drug discovery. 2018;13(1):75-87.

81. Adhikari N, Amin SA, Saha A, Jha T. Structural exploration for the refinement of anticancer matrix metalloproteinase-2 inhibitor designing approaches through robust validated multi-QSARs. Journal of Molecular Structure. 2018; 1156:501-15.

82. Gupta SP, Patil VM. Specificity of binding with matrix metalloproteinases. Matrix metalloproteinase inhibitors: Springer; 2012. p. 35-56.

83. Herranz-López M, Losada-Echeberría M, Barrajón-Catalán E. The multitarget activity of natural extracts on cancer: Synergy and xenohormesis. Medicines. 2019;6(1):6.

84. Holohan C, Van Schaeybroeck S, Longley DB, Johnston PG. Cancer drug resistance: an evolving paradigm. Nature Reviews Cancer. 2013;13(10):714-26.

85. Gottesman MM. Mechanisms of cancer drug resistance. Annual Review of Medicine. 2002; 53:615-27.

86. Song Y-h, Sun H, Zhang A-h, Yan G-l, Han Y, Wang X-j. Plant-derived natural products as leads to anti-cancer drugs. Journal of Medicinal Plant and Herbal Therapy Research. 2014; 2:6-15.

87. Ling T, Lang WH, Maier J, Quintana Centurion M, Rivas F. Cytostatic and Cytotoxic Natural Products against Cancer Cell Models. Molecules. 2019;24(10):2012.

88.   Panda AK, Chakraborty D, Sarkar I, Khan T, Sa G. New insights into therapeutic activity and anticancer properties of curcumin. Journal of Experimental Pharmacology. 2017; 9:31-45.

89.   Abdolshahi A, Majd MH, Rad JS, Taheri M, Shabani A, Da Silva JAT. Choice of solvent extraction technique affects fatty acid composition of pistachio (Pistacia vera L.) oil. Journal of Food Science and Technology. 2015;52(4):2422-7.

90.   Tyagi T, Agarwal M. Phytochemical screening and GC-MS analysis of bioactive constituents in the ethanolic extract of Pistia stratiotes L. and Eichhornia crassipes (Mart.) solms. Journal of Pharmacognosy and Phytochemistry. 2017;6(1):195-206.

91.   Aparamarta HW, Anggraini D, Istianingsih D, Susanto DF, Widjaja A, Ju Y-H, et al., editors. Fatty acid fragmentation of triacylglycerol isolated from crude nyamplung oil. AIP Conference Proceedings; 2017: AIP Publishing.

92.   Sillapachaiyaporn C, Nilkhet S, Ung AT, Chuchawankul S. Anti-HIV-1 protease activity of the crude extracts and isolated compounds from Auricularia polytricha. BMC Complement Altern Med. 2019;19(1):351.

93.   Parmar R, Kumar D, editors. Study of chemical composition in wild edible mushroom Pleurotus cornucopiae (Paulet) from Himachal Pradesh, India by using Fourier transforms infrared spectrometry (FTIR), Gas chromatography-mass spectrometry (GCMS) and X-ray fluorescence (XRF). Biological Forum; 2015: Research Trend.

94.   Lee NK, Aan B-Y. Optimization of ergosterol to vitamin D 2 synthesis in Agaricus bisporus powder using ultraviolet-B radiation. Food Science and Biotechnology. 2016;25(6):1627-31.

95.   Huang G, Cai W, Xu B. Vitamin D2, ergosterol, and vitamin B2 content in commercially dried mushrooms marketed in China and increased vitamin D2 content following UV-C irradiation. International Journal for Vitamin and Nutrition Research. 2016;1(1):1-10.

96.   Gąsecka M, Siwulski M, Magdziak Z, Budzyńska S, Stuper-Szablewska K, Niedzielski P, et al. The effect of drying temperature on bioactive compounds and

antioxidant activity of Leccinum scabrum (Bull.) Gray and Hericium erinaceus (Bull.) Pers. Journal of Food Science and Technology. 2019; 1-13.

97.   Smith L, Watson MB, O'Kane SL, Drew PJ, Lind MJ, Cawkwell L. The analysis of doxorubicin resistance in human breast cancer cells using antibody microarrays. Molecular Cancer Therapeutics. 2006;5(8):2115-20.

98.   Suárez Y, Fernández C, Ledo B, Ferruelo AJ, Martín M, Vega MA, et al. Differential effects of ergosterol and cholesterol on Cdk1 activation and SRE‐driven transcription: Sterol stringency for cell cycle progression in human cells. European Journal of Biochemistry. 2002;269(6):1761-71.

99.   Pijuan J, Barceló C, Maiques O, Moreno DF, Sisó P, Marti RM, et al. In vitro cell migration, invasion and adhesion assays: from cell imaging to data analysis. Frontiers in Cell and Developmental Biology. 2019; 7:107.

100.   Jayatilaka H, Umanzor FG, Shah V, Meirson T, Russo G, Starich B, et al. Tumor cell density regulates matrix metalloproteinases for enhanced migration. Oncotarget. 2018;9(66):32556.

101.   Kumar GB, Nair BG, Perry JJP, Martin DB. Recent insights into natural product inhibitors of matrix metalloproteinases. MedChemComm. 2019 Ahead of Print.

102.   Li X, Wu Q, Xie Y, Ding Y, Du WW, Sdiri M, et al. Ergosterol purified from medicinal mushroom Amauroderma rude inhibits cancer growth in vitro and in vivo by up-regulating multiple tumor suppressors. Oncotarget. 2015;6(19):17832.

103.   Pavan AR, Silva GDBd, Jornada DH, Chiba DE, Fernandes GFDS, Man Chin C, et al. Unraveling the Anticancer Effect of Curcumin and Resveratrol. Nutrients. 2016;8(11):628.

104.   Gimeno A, Beltrán-Debón R, Mulero M, Pujadas G, Garcia-Vallvé S. Understanding the variability of the S1′ pocket to improve matrix metalloproteinase inhibitor selectivity profiles. Drug Discovery Today. 9 September 2019

VITA

NAME	Sunita Nilkhet
DATE OF BIRTH	11 October 1994
PLACE OF BIRTH	Bangkok
INSTITUTIONS ATTENDED	2014 - Bachelor of Sciences (Medical Technology), Faculty of Allied Health Sciences, Thammasat University
HOME ADDRESS	56/78 M.10 Phahonyothin 66 Road, Kukot, Lumlookka, Pathumthani, Thailand 12130
PUBLICATION	Sillapachaiyaporn C, Nilkhet S, Ung AT, Chuchawankul S. Anti-HIV-1 protease activity of the crude extracts and isolated compounds from Auricularia polytricha. BMC Complement Altern Med. 2019;19(1):351.

จุฬาลงกรณ์มหาวิทยาลัย

CHULALONGKORN UNIVERSITY